Determination of the Forces in X-Frames in Curved Girder Bridges

Final Report
April 2021

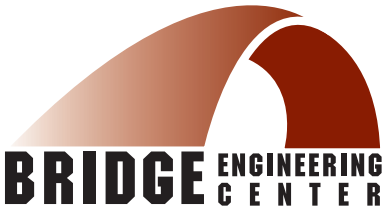

IOWA STATE UNIVERSITY
Institute for Transportation

Sponsored by
Iowa Department of Transportation
(InTrans Project 16-594)

About the Bridge Engineering Center

The mission of the Bridge Engineering Center (BEC) is to conduct research on bridge technologies to help bridge designers/owners design, build, and maintain long-lasting bridges.

About the Institute for Transportation

The mission of the Institute for Transportation (InTrans) at Iowa State University is to save lives and improve economic vitality through discovery, research innovation, outreach, and the implementation of bold ideas.

Iowa State University Nondiscrimination Statement

Iowa State University does not discriminate on the basis of race, color, age, ethnicity, religion, national origin, pregnancy, sexual orientation, gender identity, genetic information, sex, marital status, disability, or status as a US veteran. Inquiries regarding nondiscrimination policies may be directed to the Office of Equal Opportunity, 3410 Beardshear Hall, 515 Morrill Road, Ames, Iowa 50011, telephone: 515-294-7612, hotline: 515-294-1222, email: eooffice@iastate.edu.

Disclaimer Notice

The contents of this report reflect the views of the authors, who are responsible for the facts and the accuracy of the information presented herein. The opinions, findings and conclusions expressed in this publication are those of the authors and not necessarily those of the sponsors.

The sponsors assume no liability for the contents or use of the information contained in this document. This report does not constitute a standard, specification, or regulation.

The sponsors do not endorse products or manufacturers. Trademarks or manufacturers' names appear in this report only because they are considered essential to the objective of the document.

Iowa DOT Statements

Federal and state laws prohibit employment and/or public accommodation discrimination on the basis of age, color, creed, disability, gender identity, national origin, pregnancy, race, religion, sex, sexual orientation or veteran's status. If you believe you have been discriminated against, please contact the Iowa Civil Rights Commission at 800-457-4416 or Iowa Department of Transportation's affirmative action officer. If you need accommodations because of a disability to access the Iowa Department of Transportation's services, contact the agency's affirmative action officer at 800-262-0003.

The preparation of this report was financed in part through funds provided by the Iowa Department of Transportation through its "Second Revised Agreement for the Management of Research Conducted by Iowa State University for the Iowa Department of Transportation" and its amendments.

The opinions, findings, and conclusions expressed in this publication are those of the authors and not necessarily those of the Iowa Department of Transportation.

1. Report No.	2. Government Accession No.	3. Recipient's Catalog No.
InTrans Project 16-594		

4. Title	5. Report Date
Determination of the Forces in X-Frames in Curved Girder Bridges	April 2021
	6. Performing Organization Code

7. Authors	8. Performing Organization Report No.
Behrouz Shafei (orcid.org/0000-0001-5677-6324), Brent Phares (orcid.org/0000-0001-5894-4774), Abhijit Kulkarni (orcid.org/0000-0002-7657-5586), and Weizhuo Shi (orcid.org/0000-0001-8193-0098)	InTrans Project 16-594

9. Performing Organization Name and Address	10. Work Unit No. (TRAIS)
Bridge Engineering Center Iowa State University 2711 South Loop Drive, Suite 4700 Ames, IA 50010-8664	**11. Contract or Grant No.**

12. Sponsoring Organization Name and Address	13. Type of Report and Period Covered
Iowa Department of Transportation 800 Lincoln Way Ames, IA 50010	Final Report
	14. Sponsoring Agency Code 17-SPR0-019

15. Supplementary Notes

Visit https://bec.iastate.edu/ for color pdfs of this and other research reports.

16. Abstract

While for decades horizontally curved steel girder bridges have been a solution for constructing interchanges between state and Interstate highways, concerns remain regarding their design and construction. The cross-frames in these bridges are especially critical because, unlike in straight bridges, they are major load carrying elements.

The design and analysis of cross-frames in curved bridges is complex due to complexities in how loads are transmitted throughout these types of bridges. However, a unique opportunity exists to improve the design of these components using modern computer software and short- and long-term monitoring.

This project investigated a horizontally curved bridge located in Story County near Ames, Iowa, to understand the behavior of cross-frames during construction and over the service life of the bridge. The project involved a numerical investigation using finite element modeling and short-term and long-term monitoring in the field to (1) identify sections of the bridge to instrument under dead, live, and temperature loading; (2) evaluate the performance of cross-frames through long-term monitoring; (3) evaluate the performance of cross-frames using live load tests; and (4) provide recommendations for practice.

The research results suggest that the cross-frames close to supports may experience high stress levels, and therefore special attention is required for their design compared to the other cross-frames. The cross-frames within the interior bays were also found to carry higher forces than those in the outer bays. This situation requires additional analysis during design to ensure the safety and performance of curved girder bridges.

17. Key Words	18. Distribution Statement
cross-frames—field testing—finite element modeling—horizontally curved bridges—long-term monitoring—steel girders	No restrictions.

19. Security Classification (of this report)	20. Security Classification (of this page)	21. No. of Pages	22. Price
Unclassified.	Unclassified.	120	NA

DETERMINATION OF THE FORCES IN X-FRAMES IN CURVED GIRDER BRIDGES

Final Report
April 2021

Principal Investigator
Behrouz Shafei, Associate Professor
Bridge Engineering Center, Iowa State University

Co-Principal Investigator
Brent Phares, Bridge Research Engineer
Bridge Engineering Center, Iowa State University

Research Assistants
Abhijit Kulkarni and Weizhuo Shi

Authors
Behrouz Shafei, Brent Phares, Abhijit Kulkarni, and Weizhuo Shi

Sponsored by
Iowa Department of Transportation

Preparation of this report was financed in part
through funds provided by the Iowa Department of Transportation
through its Research Management Agreement with the
Institute for Transportation
(InTrans Project 16-594)

A report from
Bridge Engineering Center
Iowa State University
2711 South Loop Drive, Suite 4700
Ames, IA 50010-8664
Phone: 515-294-8103 / Fax: 515-294-0467
https://bec.iastate.edu

TABLE OF CONTENTS

LIST OF FIGURES

LIST OF TABLES

ACKNOWLEDGMENTS

The authors would like to acknowledge the Iowa Department of Transportation (DOT) for sponsoring this project using Federal State Planning and Research (SPR) Part II, CFDA 20.205, funds.

The authors would also like to thank the members of the technical advisory committee (TAC) for their input and guidance:

- Michael Nop, Bridge Project Development Engineer, Iowa DOT
- Curtis Carter, Senior Structures Engineer, Iowa DOT
- David Evans, Final Design Unit Leader, Iowa DOT

EXECUTIVE SUMMARY

While for decades horizontally curved steel girder bridges have been a solution for constructing interchanges between state and Interstate highways, concerns remain regarding their design and construction. The cross-frames in these bridges are especially critical because, unlike in straight bridges, they are major load carrying elements.

The design and analysis of cross-frames in curved bridges is complex due to complexities in how loads are transmitted throughout these types of bridges. The configuration of cross-frames has generally been based on standard designs that have depended principally on gross geometries, slenderness limits for tension and compression members, and other minimum requirements. As such, a unique opportunity exists to improve the design of these components using modern computer software and short- and long-term monitoring. The reconstruction of the Interstate system in western Iowa offers a unique opportunity to monitor the behavior of several yet-to-be-constructed horizontally curved steel girder bridges.

To estimate the forces in the cross-frames of horizontally curved bridges, this project investigated a horizontally curved bridge located in Story County near Ames, Iowa, on northbound I-35 and westbound US 30. The goal of this research project was to understand the behavior of cross-frames during various stages of construction and over the service life of the bridge. Special consideration was given to identifying critical locations for instrumentation on such components of the bridge superstructure as the main girders, cross-frames, and diaphragms as part of data collection efforts to evaluate the long-term performance of the cross-frames.

This project involved a numerical investigation using finite element modeling and short-term and long-term monitoring of the cross-frames in the field to achieve the following objectives:

- Identify the sections of the bridge to instrument under dead, live, and temperature loading
- Evaluate the performance of cross-frames through long-term monitoring
- Evaluate the performance of cross-frames using live load tests

The following general conclusions were made based on the results of this study:

- From the finite element analysis (FEA) carried out for this project, the following conclusions can be drawn: The maximum and minimum forces in the cross-frames were found within the third and fourth span of the bridge and near the interior supports. The girders were subjected to forces vertically as well as radially. This bidirectional translation confirmed that the displacement of girders does not follow a particular path.

- From the FEA, it was confirmed that the load within the top chord of the cross-frame varies significantly at the two ends of each connection. The cross-frames in the interior bays were found to carry higher forces than those in the exterior bays. The observations from the FEAs led the research team to identify the cross-frames that are critical for instrumentation. In addition, considering all the contributing load combinations, it was concluded that attention

is required for the design of the top chords of the cross-frames, especially at the support locations.

- From the long-term monitoring data, the maximum compressive stress level, 11 ksi, was found in the diagonal strut during the minimum temperature period. As also determined from the FEA, a stress difference of about 6 to 8 ksi is present within the top chord member in the cross-frame located near the middle of the span. Top chords and their connections may become vulnerable to higher stress differences during extreme sustained and fluctuating temperatures.

- From the field tests carried out for this analysis, the girder flanges' maximum responses were as follows: In the longitudinal direction, the maximum response was 80 microstrain (2.4 ksi), measured in the bottom flange of Girder 5 during load case (LC) 12 (i.e., one semi-truck). In the transverse direction, the maximum response was -20 microstrain (-0.6 ksi), measured in the bottom flange of Girder 5 during LC 12. As for the cross-frames' responses, for the interior bay, both diagonal members and the bottom chord showed higher response values than the other members, with maximum stresses of 0.6 ksi; for the exterior bay, the two diagonal members showed higher response values than the top and bottom chords. The maximum stresses were recorded during LC 12, with values of 0.9 ksi (tension) and -0.9 ksi (compression).

Overall, the research results suggest that the cross-frames close to supports may experience high stress levels, and therefore special attention is required for their design compared to the other cross-frames. The cross-frames within the interior bays were also found to carry higher forces than those in the outer bays. This situation requires additional analysis during design to ensure the safety and performance of curved girder bridges.

INTRODUCTION

Background

Horizontally curved bridges are generally constructed to ease the layout of roadways at interchanges on state and Interstate highways. As a result of the difficult geometries of interchanges, limited right of ways, and the need for uninterrupted traffic flow, horizontally curved bridges have become popular in the bridge industry since the 1960s (Itani and Reno 2000). According to a 1991 survey, 20% to 25% of the bridge inventory in the United States consists of curved steel bridges, and the use of curved steel bridges is likely to increase as time progresses (Hall et al. 1999).

A limited number of studies have been conducted on horizontally curved bridges. In the late 1980s and early 1990s, the American Association of State Highway and Transportation Officials (AASHTO) and the Federal Highway Administration (FHWA) recognized the need to formulate guidelines and specifications for horizontally curved steel girder bridges. The efforts of these organizations and others resulted in the publication of the AASHTO *Guide Specifications for Horizontally Curved Bridges* in 1980. These specifications were based on work performed by research groups collectively known as the Consortium of University Research Teams (CURT) and were written in allowable stress design (ASD) format. In 1993, the guide specifications were updated and written in ASD as well as load factor design (LFD) format.

However, the portions of the AASHTO guide specifications addressing the design and construction of horizontally curved steel bridges demonstrated major deficiencies (Hall et al. 1999). In 1999, a multiyear research program conducted under National Cooperative Highway Research Program (NCHRP) Project 12-38 resulted in a report, *Improved Design Specifications for Horizontally Curved Steel Girder Highway Bridges*, that updated the guide specifications for horizontally curved highway bridges. The report provided recommended load factor design and construction specifications that addressed many of the problems associated with the design and construction of horizontally curved bridges.

AASHTO, FHWA, and NCHRP have since significantly increased their efforts to understand the behavior of horizontally curved bridges through a number of analytical and experimental studies. NCHRP Project 12-52 was initiated to develop design specifications for curved bridges in AASHTO load resistance factor design (LRFD) format. The provisions specified in the report for NCHRP Project 12-52 were published in AASHTO's 2006 interim revisions to the guide specifications. The revisions significantly improved the AASHTO specifications related to horizontally curved steel bridges, yet a few issues remained unanswered, in large part because the behavior of curved bridges is more complex than that of straight girder bridges. In 2012, NCHRP Report 725 (White et al. 2012a) provided guidelines for the construction and analysis of curved and skewed steel girder bridges that included many aspects of three-dimensional (3D) finite element modeling (FEM), as well as one-dimensional (1D) and two-dimensional (2D) analysis methods that can be used in place of 3D analysis and require less computational time and cost.

Around the same time as NCHRP Project 12-38 was underway, the FHWA in cooperation with AASHTO began a multiyear research program on horizontally curved steel I-girder highway bridges. Research conducted by Grubb and Hall (2019) under this FHWA project focused on experimental testing as well as an elastic analysis of a three-girder simple span curved bridge using commercially available software packages such as the BSDI 3D system, GTSTRUDL, MDX, and VANCK. MDX and VANCK are software applications that mainly use grid analysis and V-load analysis, respectively, while the BSDI 3D system and GTSTRUDL are 3D analysis programs. A comparison of the results from the different software applications showed reasonably good agreement among all programs except VANCK. Vertical deflections computed in VANCK were significantly lower than those computed in the other three programs. The research comprehensively focused on the behavior of all bridge components and the overall behavior of full-scale curved I-girder bridges in laboratory conditions. The cross-frames of the bridges were designed based on the forces estimated from the elastic analyses using 3D computer models. The researchers also presented the philosophy of the component bending tests used in the study and a detailed description of the experimental design for the curved steel bridge research project.

Nationally, concerns remain regarding the design and construction of horizontally curved steel girder bridges due to difficult-to-predict girder displacements, fit-up issues, and locked-in stresses. Some of the more complicated components to analyze and design in these bridges are the cross-frames due to complexities associated with how loads are transmitted throughout the bridges.

In steel bridges, cross-frames provide lateral load resistance, distribute traffic loads throughout the system, and reduce the buckling length of compression flanges. During the construction process, and in the absence of a hardened concrete deck, cross-frames provide lateral support to steel girders against wind loads along with overall stability. In the case of horizontally curved bridges, the radial forces in the top and bottom flanges of the girders cause the girders to twist about their horizontal axis. Therefore, due to the interaction between bending and torsion in horizontally curved bridges, the cross-frames become major load carrying elements.

The importance of cross-frames in horizontally curved steel girder bridges is very well known to the bridge industry. However, while research on the behavior of curved bridges has progressed over the past few decades, little research has been conducted on the behavior of cross-frames, and the analysis and design of cross-frames is still a vague, poorly understood area.

The configuration of cross-frames has generally been based on standard designs that have depended principally on gross geometries, slenderness limits for tension and compression members specified in the American Association of State Highway and Transportation Officials (AASHTO) *LRFD Bridge Design Specifications*, and meeting minimum requirements. As such, a unique opportunity exists to improve the design of these components. Using modern computer software, the forces in cross-frames due to common loads on curved bridges can be accurately determined and sized accordingly. Additionally, including the effects of field-recorded temperature loads on cross-frames can expand our understanding of the overall behavior of cross-frames under a combination of dead, live, and temperature loads.

A recent study conducted on six curved girder bridges in Iowa revealed that, for modest amounts of curvature, the primary girders can be designed using design principles used for noncurved girders (Greimann et al. 2014). However, that study focused on bridges with steel diaphragms and primarily focused on the main bridge girders. Furthermore, the project focused on the influence of integral abutments, thermal expansion/contraction, and response under live loads. As a result, many questions remain about how cross-frames behave, including during various phases of construction.

The reconstruction of the Interstate system in western Iowa offers a unique opportunity to monitor the behavior of several yet-to-be-constructed curved girder bridges. The opportunity to collect data on a yet-to-be-constructed bridge could provide a better understanding of the ways cross-frames participate in the global response of a horizontally curved bridge. Additionally, the data collected from such bridges will form a strong baseline from which our understanding of the whole-life forces acting on horizontally curved steel girder bridges can be expanded.

Research Objective and Scope

To address the issue of estimating the forces in the cross-frames of horizontally curved bridges, this project investigated a horizontally curved bridge located in Story County near Ames, Iowa, on northbound I-35 and westbound US 30. The goal of this research project was to understand the behavior of cross-frames during various stages of construction and over the service life of the bridge. Special consideration was given to identifying critical locations for instrumentation on such components of the bridge superstructure as the main girders, cross-frames, and diaphragms as part of data collection efforts to evaluate the long-term performance of the cross-frames. This project involved a numerical investigation using a well-known computer application and short-term and long-term monitoring of the cross-frames to achieve the following objectives:

- Identify the sections of the bridge to instrument under dead, live, and temperature loading
- Evaluate the performance of cross-frames through long-term monitoring
- Evaluate the performance of cross-frames using live load tests

Report Organization

The remainder of this report is organized as follows:

- The second chapter provides a review of the literature related to the behavior of horizontally curved bridges, particularly focusing on cross-frames.
- The third chapter provides the details of a numerical modeling study that used computer software to identify critical locations in the bridge under consideration for live load tests and long-term monitoring of the cross-frames.
- The fourth chapter provides the details of long-term monitoring efforts of the cross-frames in the Story County bridge and field-observed data.
- The fifth chapter provides the details of live load tests that were carried out on the Story County bridge.

- The final chapter provides recommendations and conclusions drawn from the results of the numerical modeling, long-term monitoring, and live load testing.

LITERATURE REVIEW

Horizontally Curved Steel Girder Bridges and Cross-Frames

Previous research undertaken at Iowa State University (Greimann et al. 2014) focused primarily on the behavior of horizontally curved bridges (with integral and semi-integral abutments) specifically to understand their behavior under varying thermal loading. Over the years, a number of studies on the behavior of curved bridges have been undertaken. However, few research studies and/or guidelines have focused specifically on the behavior of cross-frames in horizontally curved bridges.

Helwig and Wang (2003) focused on the behavior of cross-frames and diaphragms in skewed bridges. The primary focus of the research was on the bracing requirements of skewed bridges. The outcome of this research lead to the introduction of the lean-on bracing system, which is aimed at reducing the number of cross-frame members in the intermediate cross-frames. However, the sizing and design of the cross-frames was mainly based on the bracing stiffness requirement.

Out of the handful of research studies focused on the cross-frames of horizontally curved bridges, Maneetes and Linzell (2003) carried out studies on the influence of cross-frames and lateral bracing on the free vibration response of horizontally curved steel bridges. The study found that providing bracing in the exterior bays of curved bridges led to a reduction in dynamic stresses and hence was more effective than not bracing. However, bracing all bays did not lead to an appreciable reduction in dynamic stresses. The behaviors of K-type and X-type braces were identical. McConell et al. (2014) investigated the cross-frame forces in skewed bridges. The findings from the field investigation indicated that a significant amount of bending was present in some cross-frames. Sharafbayani and Linzell (2014) investigated cross-frame optimization to enhance the performance of horizontally curved steel bridges. The study evaluated the orientation, spacing, and framing combinations of the cross-frames. Keating et al. (1997) performed an investigation of cross-frame diaphragm fatigue and load distribution behavior in steel highway bridges. The findings from this investigation suggested that sizing individual members for maximum design load conditions results in an increase in member sizes. The increased member sizes then lead to an increase in the overall stiffness of the diaphragms, increasing their load carrying contribution to the structure and resulting in even larger member sizes. Therefore, the authors suggested that diaphragm members be the minimum size necessary to provide girder stability.

Yoo and Littrell (1986) investigated the response of horizontally curved girders connected by slabs and cross-frames under dead and live loads using a set of finite element analysis (FEA) models. The investigation found that the cross-sections of the plate girders deform (warp) excessively under a combination of dead and live loads if they are not adequately braced and that warping stresses are sensitive to bracing spacing. The authors recommended that warping stresses to be included in design methodologies.

A study by White et al. (2012a) conducted under NCHRP Project 12-79 provided a set of detailed analytical methods for designing and evaluating curved and skewed steel girder bridges. The authors argued that engineers practically never consider the effects of lack of fit in the initial analysis and design phases and noted that locked-in forces can significantly influence the girder layovers, cross-frame forces, and girder major-axis bending and/or flange lateral bending stresses. Davidson et al. (1996) investigated different parameters, such as degree of curvature, span length, and flange width, that affect the behavior of cross-frame bracing systems. A nonlinear statistical equation was developed to determine the preliminary design limit for the cross-frame spacing interval. The study was primarily focused on the warping and bending stresses induced in the girder flanges and their effects on cross-frame spacing. Of the parameters investigated in the research, span length, radius of curvature, flange width, and cross-frame spacing were found to have the greatest effect on the warping-to-bending stress ratio. Greimann et al. (2014) and Hoffman (2013) investigated the performance of horizontally curved integral abutment bridges that were part of the reconstruction of the Northeast Mixmaster, an intersection between I-35, I-80, and I-235 near Des Moines, Iowa. The findings from the research related to thermal stresses in horizontally curved girders were not alarming, but the research emphasizes the importance of thermal loading in the design of horizontally curved bridges that incorporate restrained supports with increasing degrees of curvature.

According to the Hanshin Guidelines (Nakai and Yoo 1988), in horizontally curved girder bridges the resisting normal stresses due to load effects have four basic components, as shown in Figure 1.

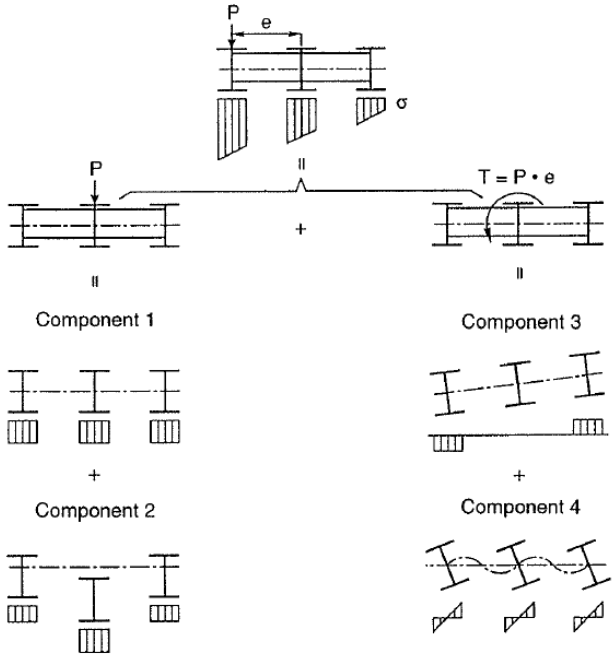

Hall et al. 1999, NCHRP

Figure 1. Four normal stress components described in the Hanshin Guidelines

The figure includes the normal stresses due to bending in the first three components and stresses caused by nonuniform torsion effects in the fourth component. The comprehensive effects of loading on curved steel bridges are summarized in the next section. However, for further reading, the handbook on bridges published by U.S. Steel (1984) can be referenced. For I-girder curved steel bridges, the Hanshin Guidelines uses a linear interaction equation that includes the effects due to vertical bending stress and lateral bending stress, as shown in the following equation (Hall et al. 1999, Nakai and Yoo 1988):

$$\frac{f_b}{F_b} + \frac{f_l}{F_l} \leq 1.0$$

where f_b= vertical bending stress, f_l = lateral flange bending stress, F_b = allowable vertical bending stress, and F_l = allowable lateral flange bending stress.

1D Line Analysis

Before computing power was used in the analysis of curved bridges, the 1D line girder method was the most basic method used in the engineering of bridges. The V-load method presented in Fiechtl et al. (1987) and U.S. Steel (1984) was used to extend the 1D line girder method to curved bridges by including the effects due to horizontal curvature. As the use of computers and computing software increased, soon the place of V-load analysis was taken by more advanced 2D and 3D computer models. However, for the purposes of a literature review, it is important to summarize the classical method used for the analysis of curved bridges. The V-load method for approximate analysis of horizontally curved bridges is summarized in this section.

The method has some limitations that are pointed out in various sources. Some of the limitations are summarized in this section. This method assumes that approximate forces on horizontally curved girders connected with radial diaphragms can be determined from equilibrium. In the case of curved bridges, the outer girder experiences an increase in load due to curvature while the inner girder experiences a decrease in load. Figure 2 shows the details of a curved bridge unit with two girders spaced at distance *D*.

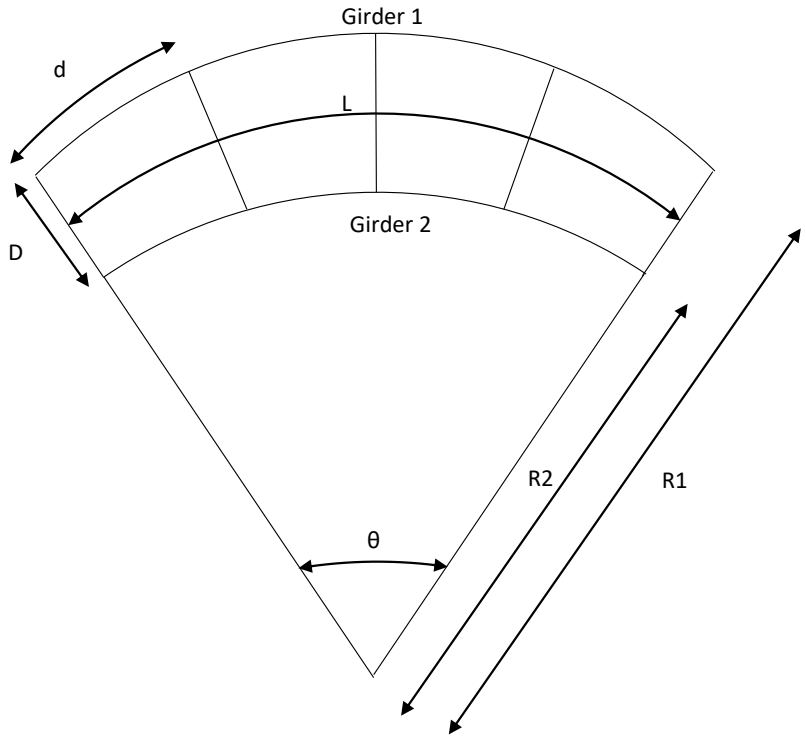

Fiechtl et al. 1987, Center for Transportation Research, University of Texas at Austin

Figure 2. Two-girder horizontally curved bridge unit

In this configuration, the angle of curvature of the bridge is θ, the radius of the outside girder (Girder 1) is R_1, and the arclength is L_1. The radius of the inside girder (Girder 2) is R_2, and the arclength is L_2. The radial cross-frames/diaphragms are spaced at distance *d*.

In this configuration, assuming the bending moment M_1 generated in the outer curved steel I-girder (Girder 1) is resisted by the longitudinal forces in the flanges, the flange force in each flange of the girder is M_1/h_1, where h_1 is the depth of Girder 1. Similarly, if the bending moment M_2 generated in the inner curved steel I-girder (Girder 2) is resisted by the longitudinal forces in the flanges, the flange force in each flange of the girder is M_2/h_2, where h_2 is the depth of Girder 2. Due to the curvature of the flanges, the longitudinal forces due to bending are not collinear. Thus, the chord of the diaphragm develops a radial force to maintain the radial equilibrium of the flange. The top and bottom flanges develop equal and opposite radial forces with respect to the compressive and tensile forces in the flanges of the curved steel girder. Figure 3 shows a free body diagram of the cross-section of a bridge and the cross-frame location.

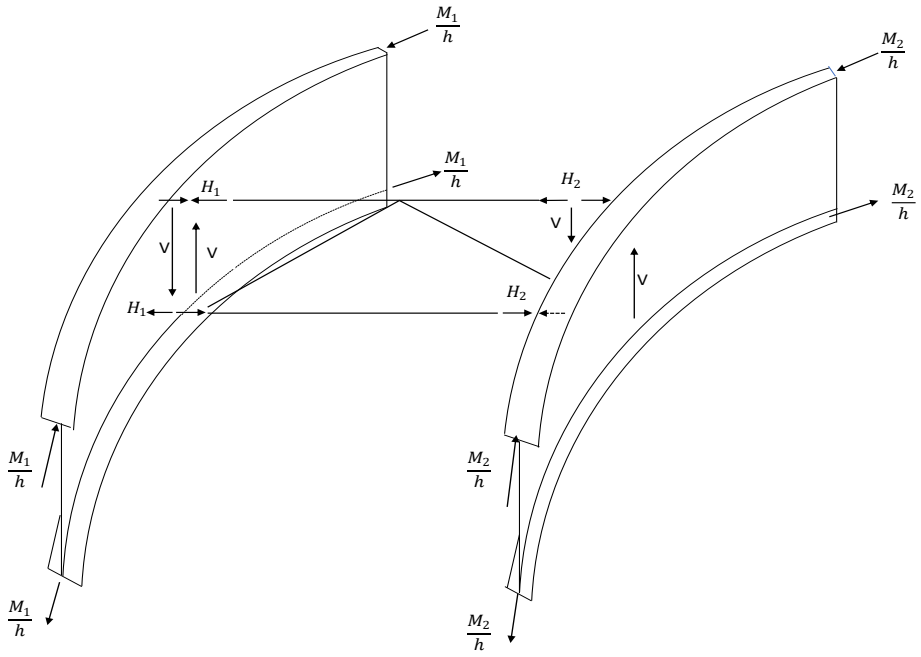

(a) Horizontally curved twin girder system

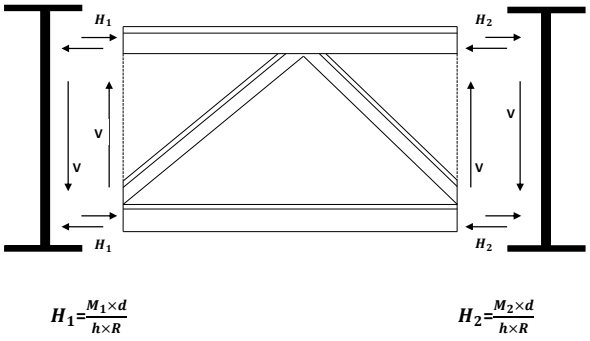

(b) Force action on the cross-frames

Fiechtl et al. 1987, Center for Transportation Research, University of Texas at Austin

Figure 3. Horizontally curved twin girders

The horizontal radial forces developed in the cross-frame of Girder 1 and Girder 2 are given as

$$H_1 = \frac{M_1 d_1}{h_1 R_1} \text{ and } H_2 = \frac{M_2 d_2}{h_2 R_2} \quad (1)$$

The moment equilibrium of the diaphragm when the two girders are of the same depth, the vertical shear, then becomes

$$V = (H_1 + H_2)\frac{h}{D} \quad (2)$$

After substituting the expressions of H_1 and H_2 and, from geometry, $d_1/R_1 = d_2/R_2 = d/R$, the expression of shear force in the diaphragm becomes

$$V = \frac{M_1+M_2}{R\frac{D}{d}} \tag{3}$$

The bending moments of Girders 1 and 2 in equation (3) are due to the applied loads and the additional forces due to the curvature and are calculated as

$$M_1 = M_{1p} + M_{1v} \tag{4}$$

$$M_2 = M_{2p} + M_{2v} \tag{5}$$

The V-load moments are assumed to be proportional to their respective girder lengths (U.S. Steel 1984), which can be further expressed as

$$\frac{M_{2v}}{L_2} = -\frac{M_{1v}}{L_1} \tag{6}$$

The equation then may take the form

$$M_1 + M_2 = M_{1p} + M_{2p} + M_{1v}\left(1 - \frac{L_2}{L_1}\right) \tag{7}$$

Neglecting the term $(1 - L_2/L_1)$ because it is small, the equation becomes

$$M_1 + M_2 = M_{1p} + M_{2p} \tag{8}$$

Thus, substituting this in the equation leads to

$$V = \frac{M_{1p}+M_{2p}}{R\frac{D}{d}} \tag{9}$$

In the summary, the V-load method involves analyzing the girder system twice. The first analysis provides the response of the P-loads, which are applied loads. After analyzing the V-loads, the moments due to the V-loads are once again calculated and added to the total moment M_1 and M_2, and then the overall shear forces at the diaphragm panels or cross-frames are calculated. This method is easily extended to multi-girder bridges, as shown in Figure 4.

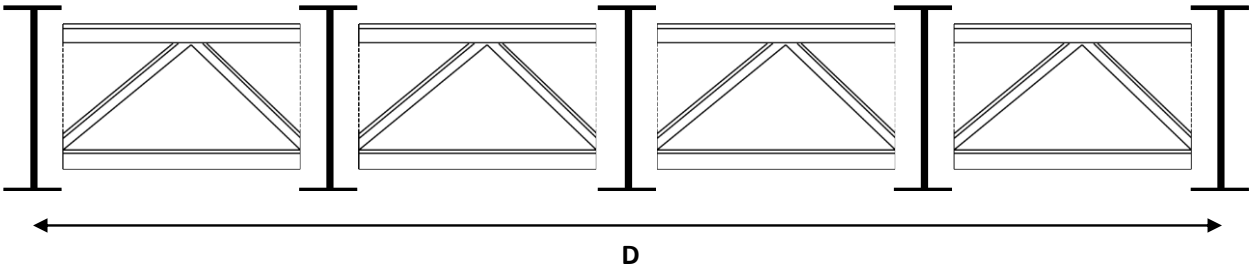

Fiechtl et al. 1987, Center for Transportation Research, University of Texas at Austin

Figure 4. Typical cross-section of a horizontally curved bridge

For a bridge with N_g girders, where *D* is the distance between the outer and inner girders, the shear force in the diaphragm panel is given as

$$\sum_{i=1}^{N_g} H_i = \sum_{i=1}^{N} V_i' \left(\frac{D}{Nh}\right) \tag{10}$$

V_i' is the shear in diaphragm or cross-frame *i*, *h* is the depth of the girder, *N* is the number of diaphragm panels in cross-section $N = N_g - 1$, and *d* and *R* are the cross-frame spacing and radius of curvature of the girder, respectively.

H_i, the lateral force in girder *i*, is given by $H_i = \frac{M_i d}{hR}$.

After substituting H_i in equation (10), equation (10) becomes

$$\sum_{i=1}^{N_g} M_i \frac{dN}{RD} = \sum_{i=1}^{N} V_j' \tag{11}$$

The shear in any panel *j*, which is equal to the sum of the shear forces on Girder 1 to *j*, is given as

$$V_j' = \sum_{i=1}^{j} V_i \tag{12}$$

Due to the horizontal curvature of the bridge, the girders must resist torsional forces. The shear forces on an individual girder are calculated as

$$V_i = V\left[1 - \frac{2(i-1)}{N}\right] \tag{13}$$

where *V* is the shear force on the outer girder.

Substituting equation (13) in equation (12) and equation (12) in equation (11) yields equation (14) and equation (15), respectively:

$$V_j' = \sum_{i=1}^{j} V\left[1 - \frac{2(i-1)}{N}\right] \tag{14}$$

$$C'V = \sum_{i=1}^{N_g} M_i \left(\frac{dN}{RD}\right) \tag{15}$$

Where $C' = \sum_{i=1}^{N} \sum_{i=1}^{j} \left[1 - \frac{2(i-1)}{N}\right]$ (16)

Rearranging equation (15), we get

$$V = \frac{\sum_{i=1}^{N_g} M_i}{c'(RD/dN)} \tag{17}$$

Solving equation (16), the coefficient C' in terms of *N* is given as

$$C' = \frac{1}{2}(N+1)^2 - \frac{1}{6}(N+1)(2N+1) \tag{18}$$

Defining $C = \frac{C'}{N}$ and substituting that into equation (17), we get

$$V = \frac{\sum_{i=1}^{N_g} M_i}{C(RD/d)} \tag{19}$$

Where $C = \frac{1}{6}\frac{N_g(N_g+1)}{N_g} - 1$ (20)

For multiple girders, the coefficient *C* is shown in Table 1 (U.S. Steel 1984).

Table 1. Values of coefficient C

No. of girders in system	Coefficient, C
2	1
3	1
4	10/9
5	5/4
6	7/5
7	14/9
8	12/7
9	15/8
10	165/81

The V-load acting on the outer girder at the cross-frame location is given by

$$V = \frac{\sum_{i=1}^{N_g} M_{pi}}{C(RD/d)} \tag{21}$$

Thus, to calculate the total forces in V-load analysis, the analysis procedure is performed twice. The first analysis gives the P-load moments, shear, and reactions. Based on the P-load responses, self-equilibrating V-load forces are calculated. The moments and shear forces due to the self-equilibrating V-load forces are then added into the P-load responses to get the total forces acting on the cross-frames.

The V-load method assumes that the internal torsional load on the bridge is resisted by the shears that develops in the diaphragms or cross-frames. Any additional torsion is resisted internally by the girders. The horizontal girders in curved bridges are required to resist the torsional forces on the entire cross-section of the bridge as a single unit. The I-shaped steel girder has two types of torsional resistances: St. Venants torsion stiffness and warping torsional stiffness. When both torsional effects, shown in Figure 5 (a), (b), and (c), are combined, they cause additional bending stress and shear stress on the girder sections and must be accounted for in the design.

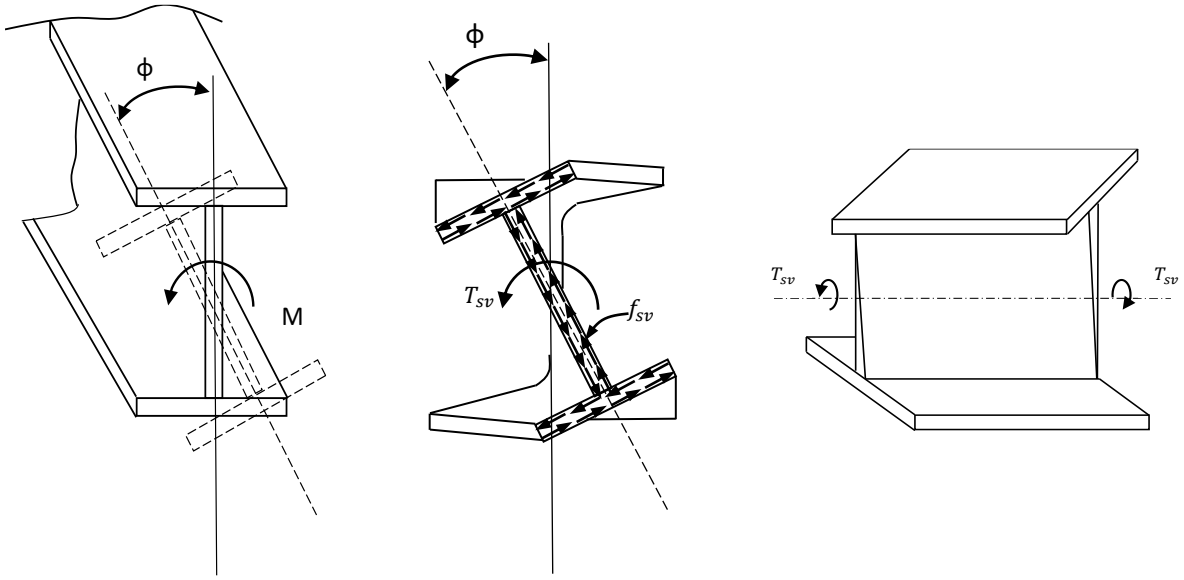

(a) I-girder subjected to torsion (b) St. Venants torsion (c) Warping of cross-section

U.S. Steel 1984

Figure 5. I-girder subjected to torsion and warping

In bridges, the bottom flange of each curved I-girder is not braced in its plane, and as a result the St. Venants stiffness in each I-girder is less than its warping stiffness. Thus, the St. Venants torsional stresses are generally less than the warping stresses, and St. Venants torsion is neglected in the approximate analysis of curved girder units for which bracing is not provided in the plane of the bottom flange. For this reason, warping torsion is important in the approximate

analysis of curved I-girders. The effects of warping torsion can be included by applying lateral forces to a straight model of the girder. The lateral force F_r on the flange changes along the length of the girder and is proportional to the bending moment as required for radial equilibrium:

$$F_r = \frac{M}{hR} \tag{22}$$

Where M is the total bending moment in the girder at the location of interest, h is the distance between the flanges, and R is the radius of the girder. The lateral bending moments resulting from such loading are the flange warping moments M_f. The flange warping moments also change along the length of the girder. The warping stress σ_w at the tip of the flange is given by

$$\sigma_w = \frac{M_f}{S_f} \tag{23}$$

Where S_f is the section modulus of the bottom flange for lateral bending. The warping stresses alone are usually in the range of 5 to 10 ksi and should not be ignored (U.S. Steel 1984). The warping stress is combined with the longitudinal bending stress in order to determine the maximum total flange stress, as shown in Figure 6.

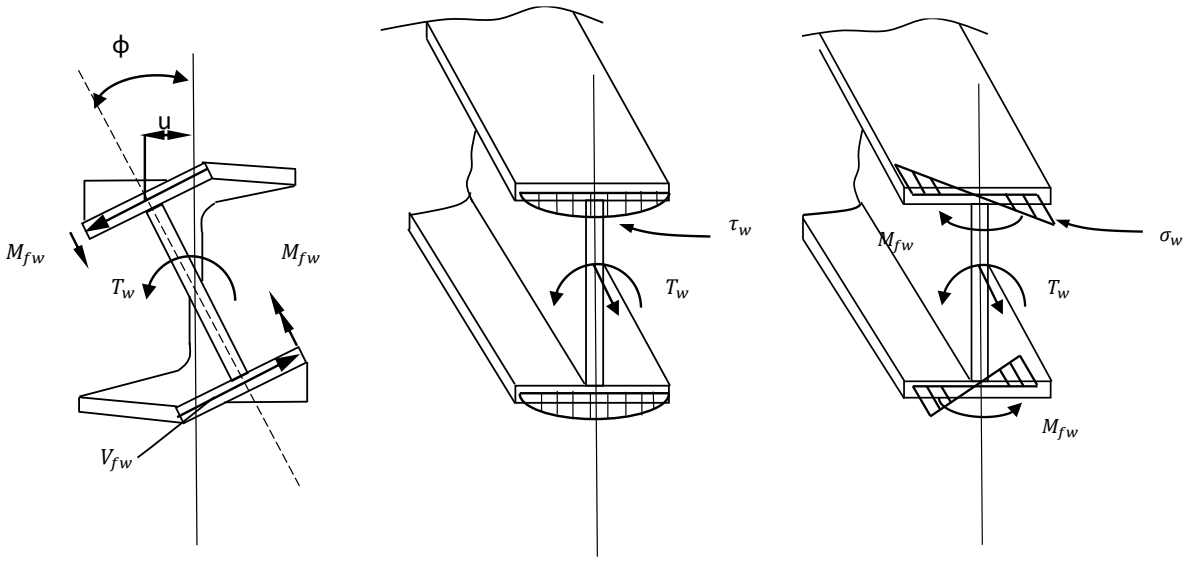

(a) warping torsion (b) Warping shear stress (c) warping normal stress

U.S. Steel 1984

Figure 6. Stress distribution in an I-girder

2D Analysis

The 2D grid method is an approximate analysis usually employed in the analysis and design of steel I- and tub-girder bridges. In this approach, the girders and cross-frames are modeled as line

elements that have three degrees of freedom (DOFs) per node, two rotational and one translational, as shown in Figure 7.

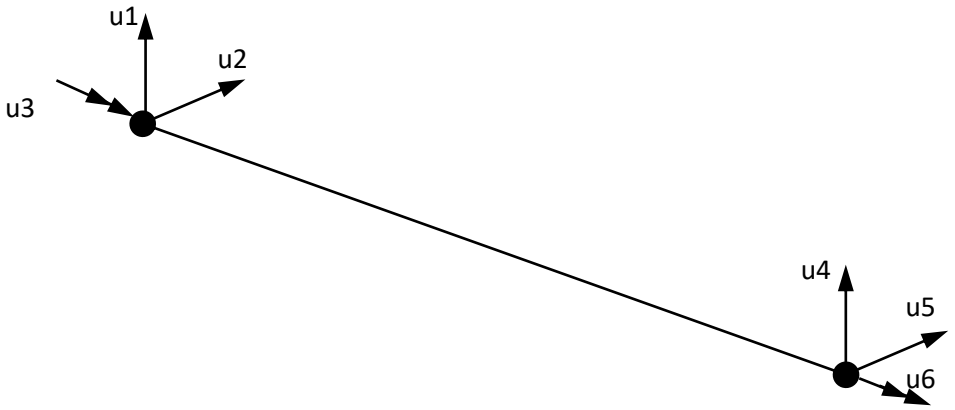

White et al. 2012b, NCHRP

Figure 7. Beam element in 2D analysis

The vertical depth of the superstructure is not included in a 2D grid model. The girders and their cross-frames or diaphragms are theoretically connected together at one common elevation; internally, it is taken as the centroidal axes of the girders (White et al. 2012a). All of the bearings, supports, diaphragms, and cross-frames theoretically are located at this same elevation in the model. The analysis software calculates only the vertical displacements and the rotations within the plan of the bridge. In addition to 2D grid analysis, steel bridges are also analyzed using the 2D frame method. In the 2D frame method, each node has six DOFs. Unlike the elements in Figure 7, these elements have three translational and three rotational DOFs at each node. The additional DOFs are translation in the X and Y direction and rotation about the Z direction. However, the 2D frame method does not provide additional information beyond that resulting from 2D grid analysis.

3D Analysis

According to the guidelines presented in White et al. (2012a), any matrix analysis software in which the structure is modeled in three dimensions may be considered three-dimensional finite element analysis (3D FEA) software. According to the G13.1 guidelines developed by AASHTO and the National Steel Bridge Alliance (2014), an analysis method is classified as a 3D FEA if all of the following are true:

- The superstructure is modeled fully in three dimensions.
- The individual girder flanges are modeled using beam, shell, or solid type elements.
- The girder webs are modeled using shell or solid type elements.
- The cross-frames or diaphragms are modeled using truss, beam, shell, or solid type elements as appropriate.

- The concrete deck is modeled using shell or solid elements (when considering the response of the composite structure).

Discussion of Analysis Methods

Each of the methods have limitations. In line girder models, the girders are analyzed separately without considering their interactions with other framing. The dead loads applied to the individual girders are based on their tributary areas, and the interactions between the cross-frames and girders are neglected. Therefore, line girder analyses do not predict any torsion of the girders. The V-load method is required to extend the line-girder method to include the effects due to curvature. Additionally, the line-girder method does not include any information about the bridge's skew and therefore cannot accurately represent the effects due to skewed supports.

2D grid models are generally sufficient to represent the behavior of cross-frames, girders, and diaphragms. However, the components are generally modeled using elements that are based on Euler-Bernoulli or Timoshenko beam theory, and these elements are not sufficient to represent the physical behavior of the structural components (White et al. 2012a). The cross-frame forces cause lateral bending in the girder flanges, and it is necessary to have an accurate prediction of the cross-frame forces to compute the expected levels of girder flange stress. Conventional 2D grid models are not able to predict the lateral bending responses of flanges with reasonable accuracy.

More information about a structure's behavior is provided when the structure is modeled fully in three dimensions. The 3D analysis method is deemed the most accurate analysis method among the bridge engineering community but is time consuming and complicated and is deemed most appropriate for complicated bridges (AASHTO and NSBA 2014). There are fewer concerns associated with 3D analysis methods than with the other methods described above. However, when and how to use refined 3D FEM analysis methods in engineering design is an issue of debate. Detailed guidelines about 3D analysis have not been incorporated into AASHTO specifications as of March 2021.

NUMERICAL ANALYSIS

Introduction

As previously discussed, the objective of this research was to gather information that will assist in the design and construction of cross-frames in horizontally curved bridges. For this purpose, this project investigated a horizontally curved bridge located in Story County, Iowa, on the southeastern edge of Ames.

This chapter describes a finite element model developed to identify critical areas of the bridge for instrumentation. A preliminary analysis of the bridge was carried out to ensure that the moments in the girders were similar to those reported in the analysis and design of the bridge. The analysis was established using the commercial finite FEM analysis software package CSIBridge (Computers & Structures, Inc. 2017).

The Story County bridge serves as a ramp from northbound I-35 to westbound US 30 with a total span of 1,970 ft and a radius of curvature of 1,100 ft. The bridge layout is shown in Figure 8, and a cross-section is shown in Figure 9.

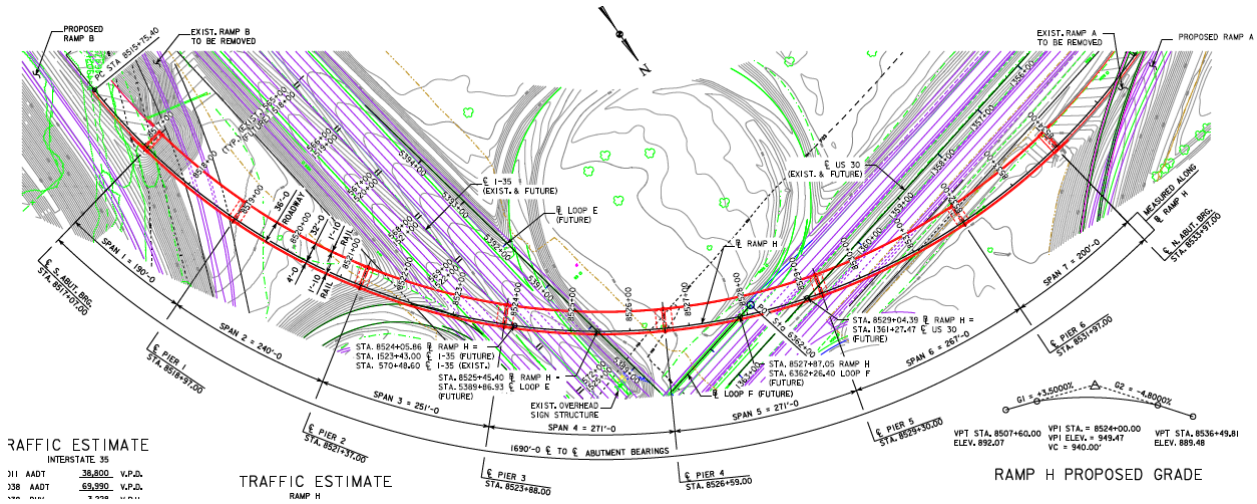

Figure 8. Layout of Story County bridge

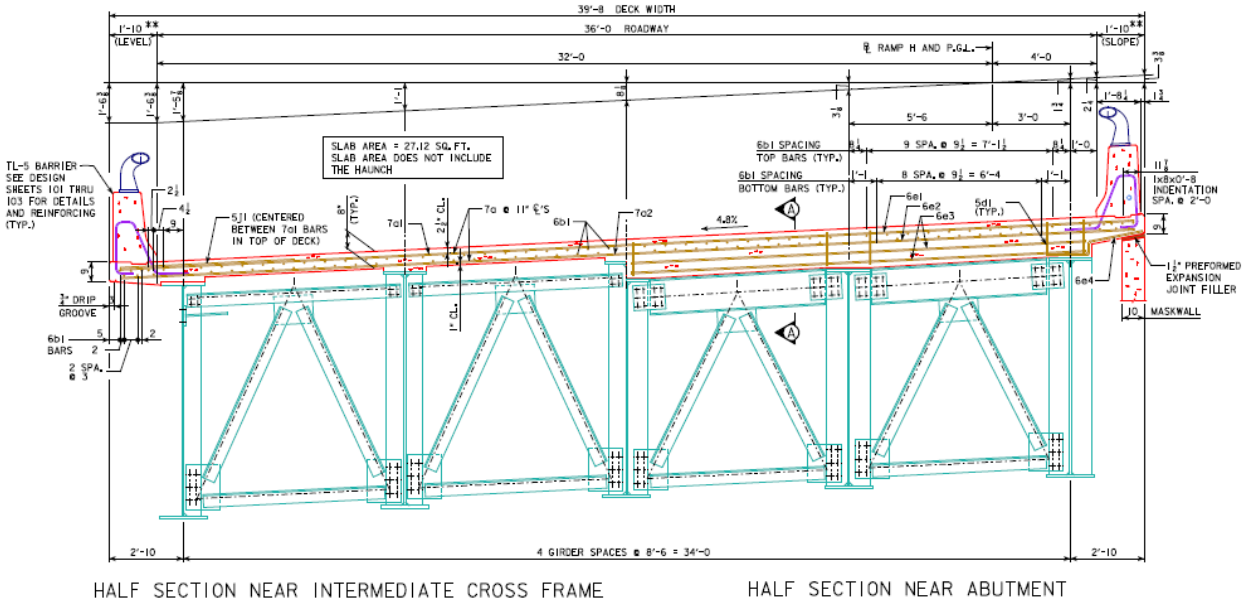

Figure 9. Cross-section of Story County bridge

The bridge has six spans and span lengths of 190, 240, 251, 271, 271, and 200 ft, respectively. It consists of an 8 in. composite deck supported by five curved I-girders. The bridge is braced at the abutments, pier, and intermediate cross-bracing by the use of L 6 X 6 X 5/8, W 16 X 67, and plate girder diaphragms. At the abutments, W 16 X 67 is used as the top chord and L 6 X 6 X 5/8 is used as inverted V bracing and the bottom chord. For the intermediate cross-bracing, L 6 X 6 X 5/8 is used as the top chord, inverted V bracing, and bottom chord. At pier locations, plate girders consisting of 80 X 1 for the web and 20 X 1 1/8 for the top and bottom flanges are used as diaphragms. The girders are spliced at different locations along the length of the bridge and have different cross-sections. The smallest cross-section (for Girders A, B, and C) consists of 1 X 18 for the bottom flange, 7/8 X 18 for the top flange, and 3/4 X 106 for the web; Girders D and E consist of 1 X 22 for the bottom flange, 7/8 X 20 for the top flange, and 3/4 X 106 for the web.

Bridge Geometry, Loads, and Assumptions in the Analysis

A bridge model was prepared using FEM guidelines specified in various guidance documents and reports (AASHTO and NSBA 2014, White et al. 2012a, White et al. 2012b, AASHTO 2017). To account for cross-sectional warping, girders were modeled with a combination of a shell element and two separate beam/frame elements. The top and bottom flanges were modeled using frame elements, whereas the web of the girders was modeled as a shell element. Cross-frames, diaphragms, and lateral bracing at the top flanges in the inner girders near the pier were modeled using frame elements. In the preliminary analysis phase, two analysis models of the same bridge were prepared. In the first model, moment releases at the ends of cross-frames were assigned. In the second model, no moment releases were assigned.

The bridge geometry was prepared using existing information from Iowa DOT drawings. For example, the horizontal and vertical layout of the bridge, the heights of the columns, and the start and end elevations of the abutments were modeled in CSIBridge using existing information. At the abutments and at Piers 1, 2, 5, and 6, a free bearing was modeled, and at Piers 3 and 4 a fixed bearing was modeled. The concrete deck was estimated to be about 8 in., and the haunch was assumed to be a constant 2 in. along the length of the bridge. The bent properties were modeled as specified in the engineering drawings provided by the Iowa DOT. A 4.8% superelevation was included in the model for this bridge.

The bridge model is shown in Figure 10, and a closer look at one of the spans is shown in Figure 11.

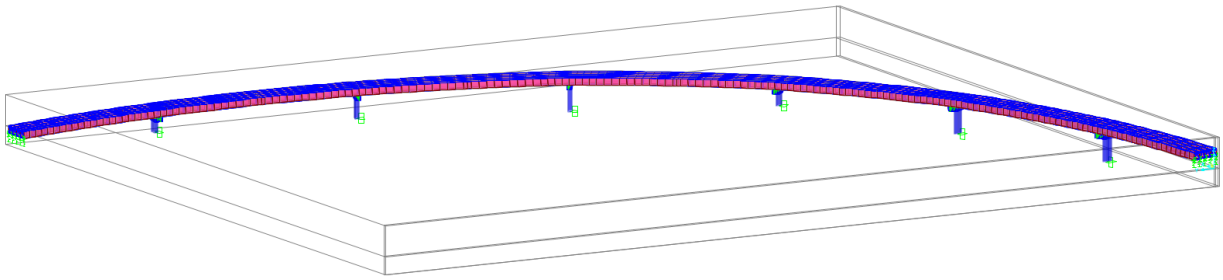

Figure 10. Bridge model in CSIBridge

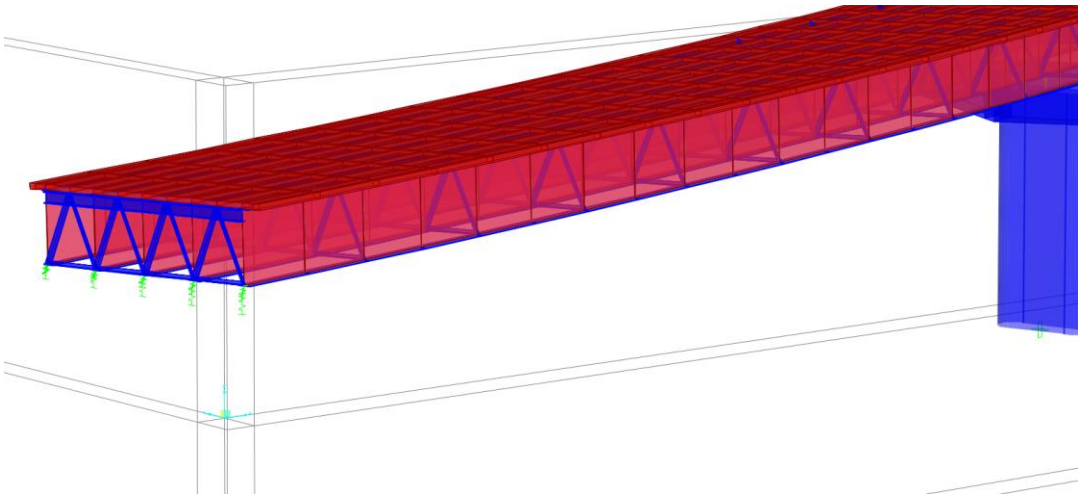

Figure 11. Closer look at Span 1

The noncomposite uniform dead load for the entire bridge section was 1.186 kips/ft on the internal girders and 1.21 kips/ft on the external girders. The DC2 load was estimated to be about 0.52 kips/ft and was applied on both edges of the concrete deck. The DW load was about 0.02 kips/ft^2 and was applied as a surface/area load directly on the concrete deck. The HL-93 load was considered to be a governing case based on observation. The load placements for the positive and negative moments are shown in Figures 12 and 13, respectively.

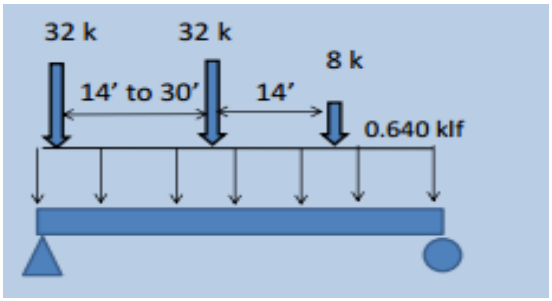

Figure 12. Load placement for positive moment

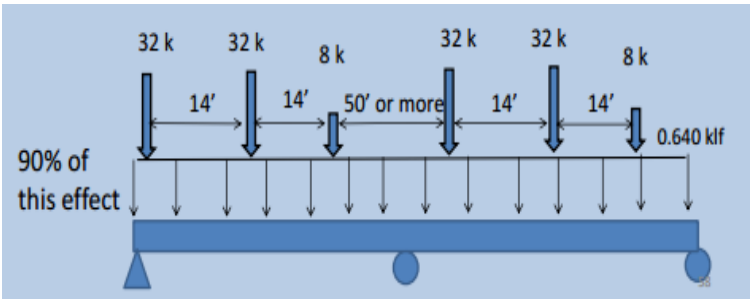

Figure 13. Load placement for negative moment

The following configurations were used to determine the maximum negative and positive moment effects. For a uniform temperature, a temperature range of 150°F was considered. A load case (LC) consisting of positive and negative temperature gradients was considered in the analysis of the bridge. To reflect Iowa's climate, the positive temperature gradient was considered to be 46°F for T1 and 12°F for T2, whereas for the superstructure below the thickness of the slab a constant temperature linearly interpolated between 0°F and 12°F was considered.

Temperature Loading for the Bridge

In the field, bridges are exposed to temperature variations throughout their service life. The temperature variations induce movement in bridges. Due to temperature fluctuations, the steel members in steel girder bridges expand and contract. Generally, in continuous steel girder bridges, restraints on movement are provided by means of fixed and free bearings. These restraints can cause internal forces in the steel girders. In bridges with expansion joints, bearings have been observed to produce limited displacement because of corrosion and general wear and tear. In such cases, the bridge's movement solely depends on the deformation of the bridge's piers and abutments. The free bearings are typically oriented on tangents or on chord. (For the bridge investigated in the present study, the free bearings were oriented on chord.) Using too many fixed bearings can over-constrain the structure, whereas using too many free bearings can lead to stability issues. Thermal deformation can occur in multiple directions, such as tangentially, on chord, or radially, and therefore guided bearings that allow unidirectional translation are used in almost all horizontally curved bridges.

The remainder of this chapter reviews current AASHTO provisions for considering design loads in light of thermal effects, describes the analysis in CSIBridge, and presents the results of the analysis.

Thermal loading on horizontally curved steel girder bridges has not been studied comprehensively. The current AASHTO specifications provide minimal guidelines on the behavior of steel bridges in the presence of thermal effects. The AASHTO specifications also fail to provide guidelines on the behavior of cross-frames in horizontally curved bridges for different types of loads, including temperature loads. The orientation of bearings and bearing movement is extremely important in the case of horizontally curved bridges. In the case of horizontally curved bridges, curvature can induce lateral thermal forces at the supports when only tangential movement is allowed. In a tangential movement system, a particular path is imposed on the structure. In such systems, excessive transverse forces are generated. To minimize the thermal forces, a chordal system uses guided bearings that allow unidirectional translation; these are used on most horizontally curved bridges. Restraints at the supports can cause internal forces within the structure, and these forces can damage the components of the bridge in terms of irregular bending, warping of the cross-section, and damage to the bearing devices, which may lead to costly repairs.

In addition to irregular deformation and other damage, thermal loading has been found to negatively affect the structural capacity of steel girders. Previous experiments by Moorty and Roeder (1992) and field investigations by Reynolds (1972) and Beckett (2013) have shown that thermal movement does not follow a particular path. Field observations have shown that in horizontally curved bridges, thermal movements do not only occur in the tangential direction or on chord. Radial movements can result in the same amount of movement as tangential or on chord movements.

In the present analysis, the focus was on the behavior of the cross-frames. In order to understand the effects of temperature loading on the cross-frames, it is necessary to observe the behavior of the curved steel girders because, as described in Hall et al. (1999), U.S. Steel (1984), and Fiechtl et al. (1987), the forces in the cross-frames depend on the behavior of the curved steel girders.

AASHTO (2017) Temperature Loading Guidelines

AASHTO design specifications require that temperature loading be considered in the analysis of steel girder bridges. However, engineers tend to neglect temperature loading effects when designing structural members. AASHTO (2014) provides two load cases for temperature loading: uniform temperature and temperature gradient. The temperature changes in a bridge do not occur uniformly; rather, bridges are designed for an assumed temperature range for maximum movement. According to the current AASHTO design guide as of the writing of this report, a uniform temperature range is assumed to design for the movement of the bridge, while in reality bridges experience a temperature gradient. The free bearings are designed in consideration of the maximum movement due to the temperature range. AASHTO (2014) provides temperature ranges for different types of superstructure such as steel or aluminum, concrete, or wood (Table 2).

Table 2. AASHTO 3.12.2.1-1 Procedure A temperature ranges

Climate	Steel or Aluminum	Concrete	Wood
Moderate	0°F to 120°F	10°F to 80°F	10°F to 75°F
Cold	−30°F to 120°F	0°F to 80°F	0°F to 75°F

The United States is divided into two climate zones: moderate and cold. For steel or aluminum, the temperature range varies from 0°F to 120°F in moderate climates, whereas in cold climates the range varies from -30°F to 120°F. Concrete bridges are categorized in terms of the same climate zones; in moderate climates, the range varies from 10°F to 80°F, and in cold climates it varies from 0°F to 80°F. Concrete bridges have a greater thermal mass and a slower rate of heat transfer than steel bridges.

Because of continuous temperature variations, bridges are always in a state of heat transfer. The heat transfer takes place via three mechanisms: direct radiation from the sun, convection of heat between the surface and the ambient air, and re-radiation of the surface to or from the surrounding environment. The bridge deck is directly exposed to solar radiation, whereas the temperature in the rest of the superstructure below remains less exposed to that heat. Thus, a nonlinear temperature loading situation takes place. The four solar radiation zones in the United States are shown in Figure 14, and the temperature gradients for the zones are listed in Table 3.

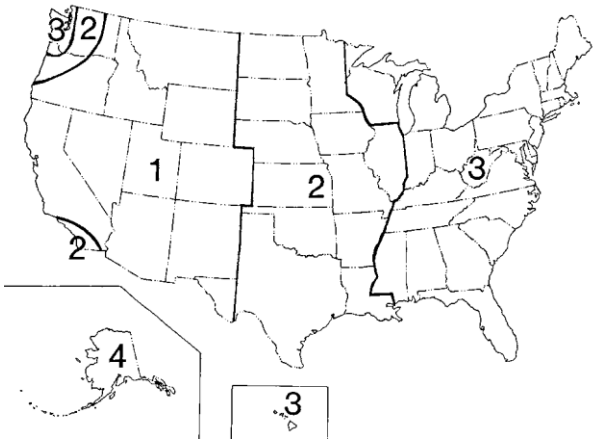

Figure 14. Solar radiation zones in the United States

Table 3. Temperature gradients for the solar radiation zones in the United States

Zone	T1 (°F)	T2 (°F)
1	54	14
2	46	12
3	41	11
4	38	9

AASHTO provides guidelines for considering positive and negative temperature gradients. For steel superstructures, the temperature below the concrete is taken as a constant. The value of A in Figure 15 is taken to be 12.0 in.

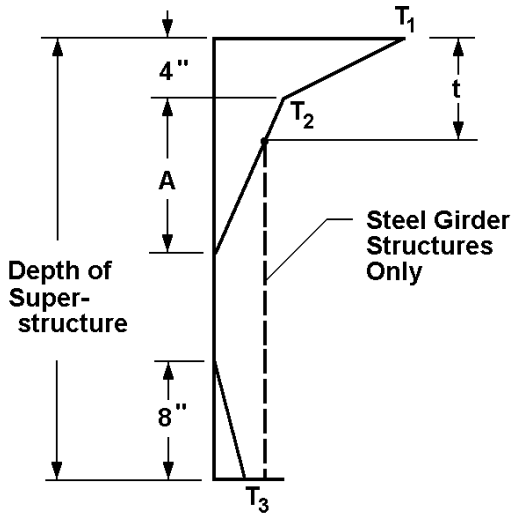

Figure 15. Temperature gradient for concrete and steel superstructures

Verification of CSIBridge Thermal Load Applications

Three-dimensional analysis tools can facilitate the process of analysis and design; however, it is of utmost importance that the load application that the engineer chooses provides accurate results. The application of temperature gradients within the environment of CSIBridge required the research team to verify the automatic application of temperature to elements of the bridge such as the deck, girder web (shell elements), girder flanges (beam elements), and so on. Application of incorrect temperature gradient values may result in incorrect calculation of moments and forces, which may lead to erroneous selection of critical locations for long-term health monitoring. The stress distribution of a temperature gradient is calculated as $E\alpha T$. The temperature gradient is specified initially and applied to the transformed section, and then the axial forces (P) and moment (M3) are calculated. After the calculation of said parameters, an equivalent temperature distribution (constant + linear) is applied over the depth of the section. It is possible to solve for the axial force by integrating this equation over the depth of the section that accounts the web and flange areas.

Results

The axial forces and moments in the individual members of the exterior cross-frames of the first four spans are reported in this section. It was determined during the analysis phase that a limited number of braces would be instrumented to ensure the efficiency of the instrumentation plan. Therefore, during the analysis phase the exterior cross-frames were analyzed in detail to identify the most critical members.

The overall results for the girder moments and shear values were compared with the data provided in the Iowa DOT design documents to confirm the validity of the structural model prepared by the ISU research team, with the following results:

- The results were found to be in accordance with the data provided by the Iowa DOT. The observed difference was about 5% to 10%.
- The inner girders experienced fewer loads than the outer girders. In the case of the inner girders, the values resulting from the CSIBridge modeling were less than those provided by the Iowa DOT, but the results for the outer girders were relatively close, with a difference of 2% to 5%.
- Effects like torsion and moment about the vertical axis due to radial forces are significantly influenced by cross-frames.

Summary of Results

The effects due to the temperature and gravity load cases are discussed in this section, and the forces predicted by the numerical analysis are presented. Three cases of temperature loading are discussed: uniform temperature, positive temperature gradient, and negative temperature gradient. The effects of uniform temperature loading are certainly the largest when the three load cases are compared. In reality, however, uniform temperature loading does not occur. Therefore, temperature gradient was included in the analysis to capture any irregularities in the behavior of the steel girders, cross-frames, or diaphragms. The nomenclature used for the cross-bracings is shown in Figure 16.

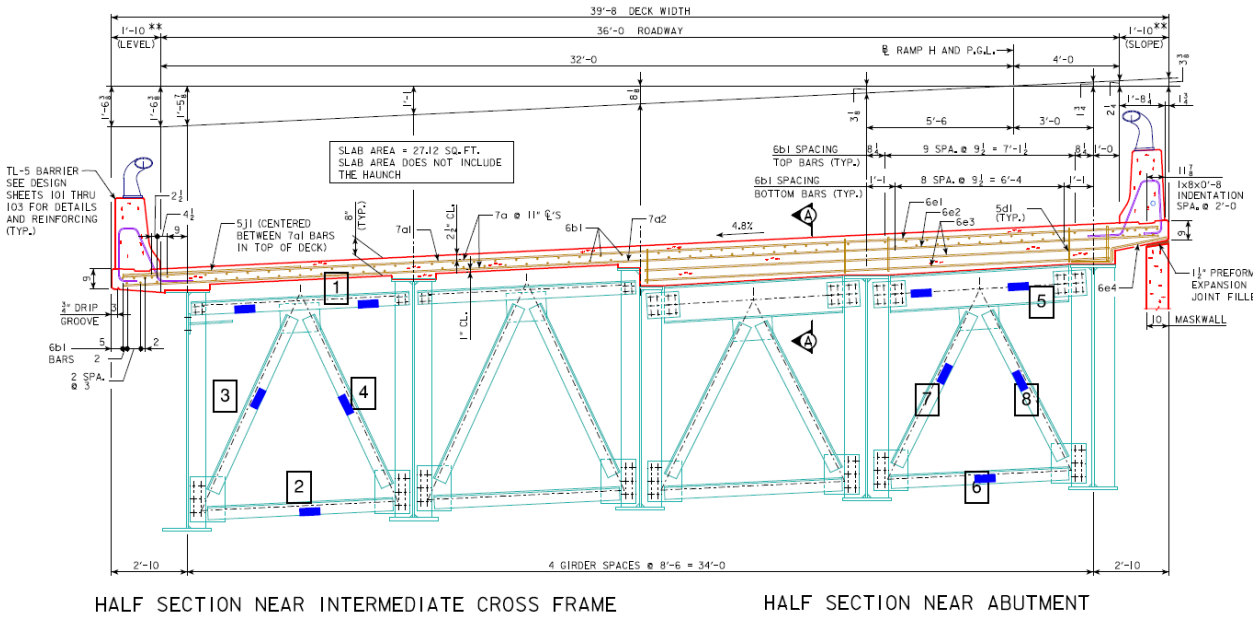

Figure 16. Nomenclature of the cross-bracings

Starting from an axial load distribution, uniform temperature loading induced a compressive force within the section near the support and a positive tensile force within the spans. This trend is visible in the axial force diagram for each individual girder. The negative force was at maximum at the location of the fixed bearings, whose purpose is to prevent translation in any direction. Hence, a high restraining force was generated. Similarly, at the location of the free bearings, a comparatively low negative force (axial compression) was seen. This low axial compression was due to a combination of the presence of the full depth of the diaphragm and a relatively low stiffness due to the free bearings.

As the bridge expanded, the right exterior portion (the right exterior girder and the third interior girder) of the second, fourth, and sixth spans experienced an upward deflection. The upward deflection was significant in the fourth span. In contrast, when the bridge contracted, the exterior portion of the first, third, fifth, and seventh spans experienced an upward deflection, although this upward deflection was not as significant as the upward deflection in the fourth span when the superstructure underwent expansion. It is important to highlight that the girders were forced to translate both vertically as well as radially. This bidirectional translation confirmed that the displacement of girders does not follow a particular path. As a result, there is a high likelihood of high lateral forces acting on the bridge piers in both directions.

It should be noted that the observations from the three load cases that focused on temperature (i.e., uniform temperature, positive temperature gradient, and negative temperature gradient) do not include other gravity-based load components. The investigations covered this separate set of individual load cases because the primary focus of this research project was on identifying the critical cross-frames where the loading demands are highest.

From the simulation results, it was found that when the bridge expands under the uniform temperature case, the right exterior girder and the third interior girder move up (in Span 2, 4, and 6). Because both of its ends are fixed, Span 4 experiences forces higher than those in the other spans (due to the uniform temperature). As reported in the literature, bridges do not follow one particular movement pattern when subjected to temperature loads, as they may move tangentially as well as radially. As a result of the upward moving demand and due to the curved nature of the bridge under consideration in this research project, the girder system was forced to translate vertically and radially. Under a positive temperature gradient, for example, an upward deflection was recorded for Span 1 and 7.

It is important to highlight that these observations are purely based on the numerical simulation results and do not include deflections due to gravity-based load components, which counteract upward deflections. The field investigations did not cover the deflection profile of the girders, although that can be a topic of interest that may complement the findings of the current research project on cross-frames.

For the moment about the vertical axis (M2), the cross-frames influenced M2, especially near the supports for the left exterior and first interior girders. The temperature loading caused alternating twisting of the steel girders at different cross-frames and between cross-frames. This resulted in a zigzag pattern of torsional forces. The forces in this zigzag pattern were generally higher than

those witnessed within the spans. At the fixed supports, the bottom portion of the web was found to deflect. For the positive temperature gradient, no significant twisting was seen in the first and seventh spans, but all other spans twisted. The direction of twisting was such that the girders (the entire system) within the supports rotated in a clockwise direction. The negative temperature gradient had the exact opposite effect on the system, where the twisting direction was in a counterclockwise direction. The first and last spans were observed to be sagging.

Forces in the Members of the Left Brace

Figures 17 through 32 show the axial forces and moments in the individual members of the exterior cross-frames of the first four spans in the left brace.

Span 1

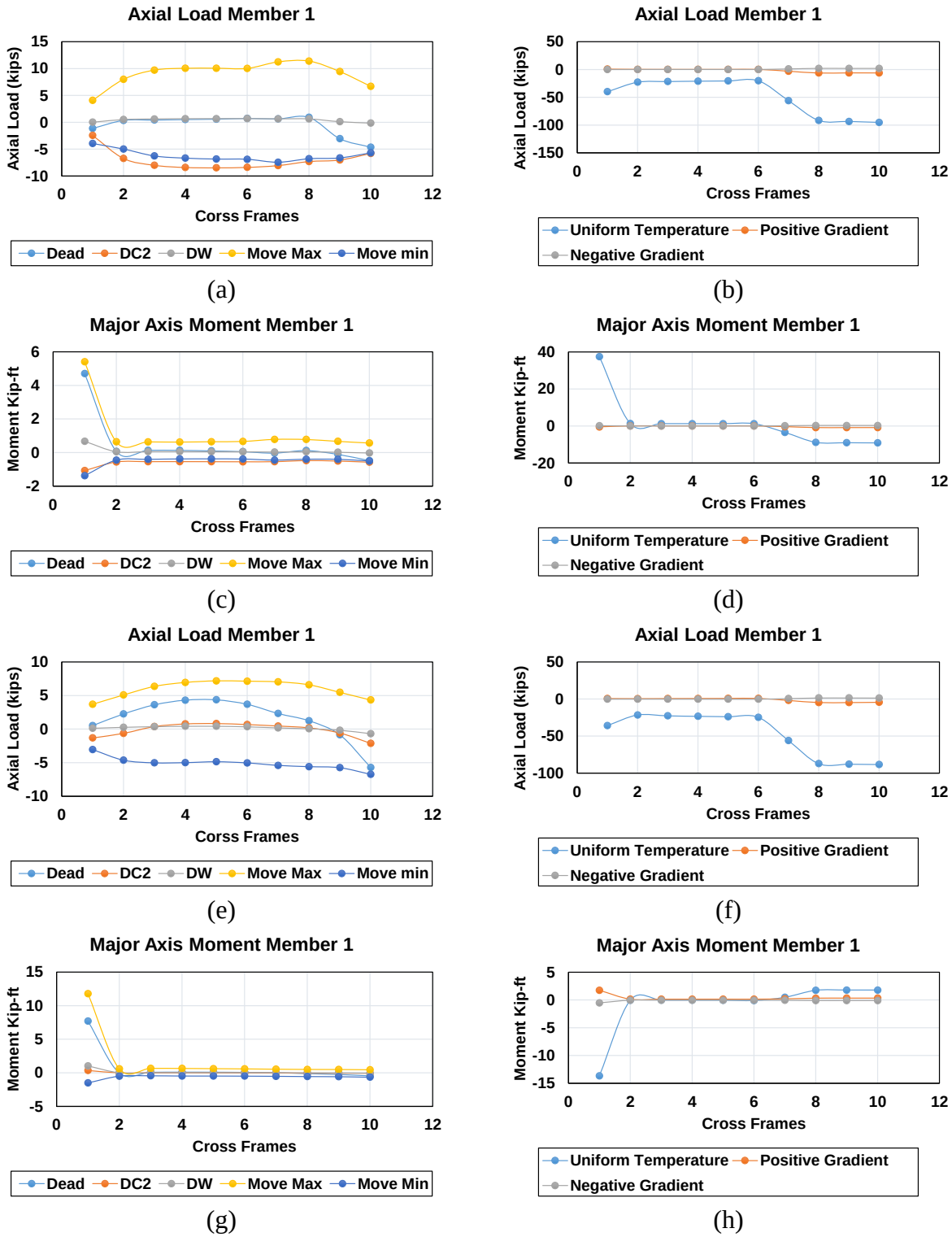

Figure 17. Forces in Member 1 within Span 1, left brace

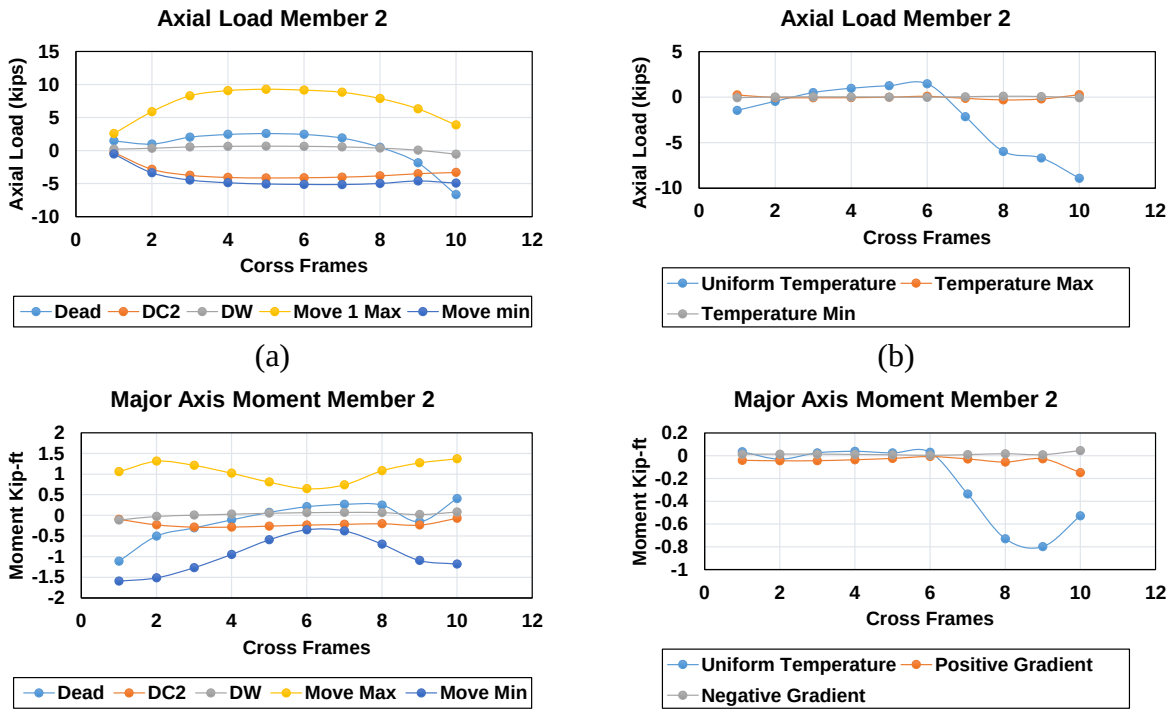

Figure 18. Forces in Member 2 within Span 1, left brace

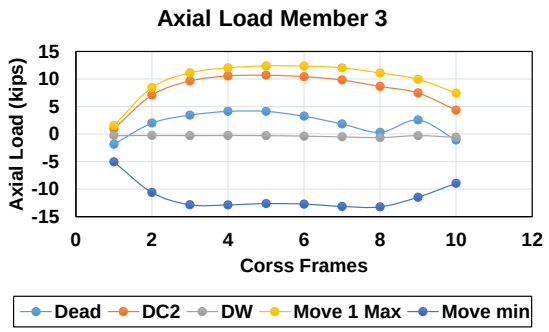

(a)

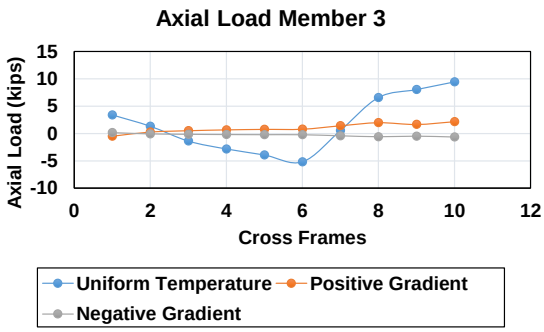

(b)

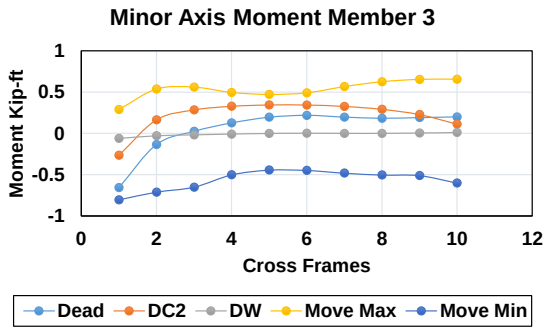

(c)

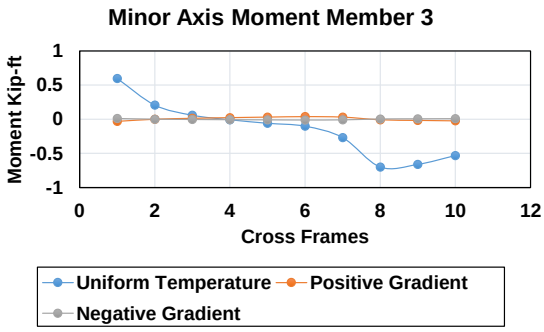

(d)

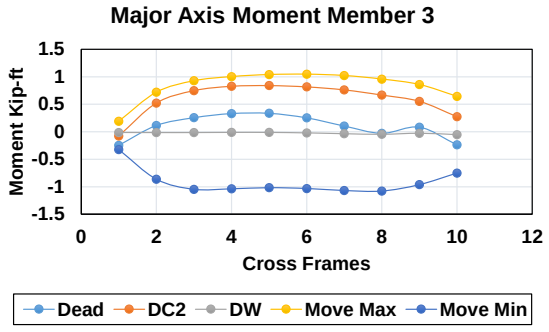

(e)

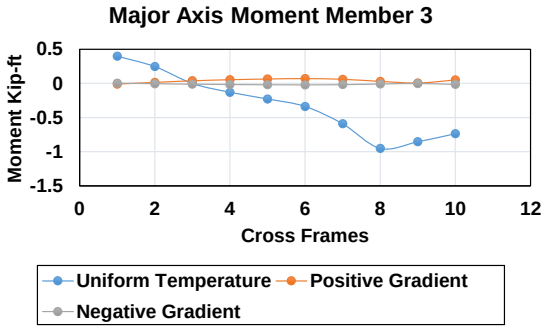

(f)

Figure 19. Forces in Member 3 within Span 1, left brace

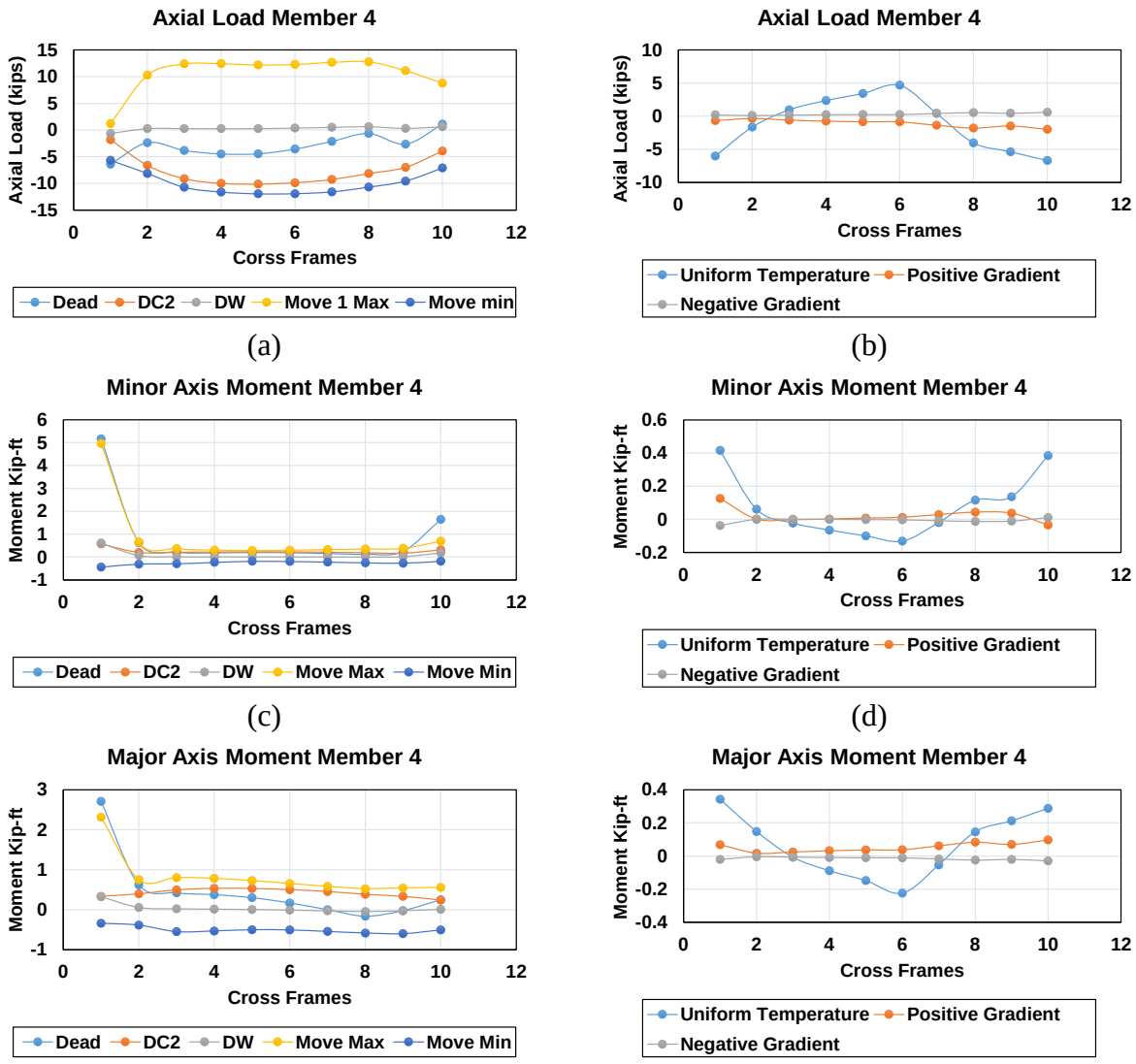

Figure 20. Forces in Member 4 within Span 1, left brace

Span 2

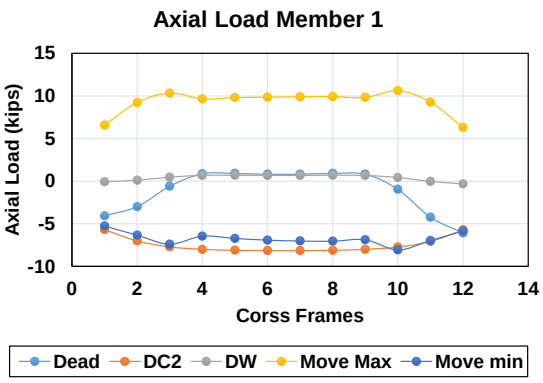

(a)

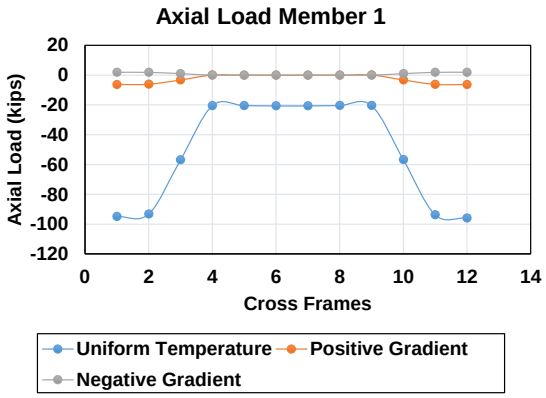

(b)

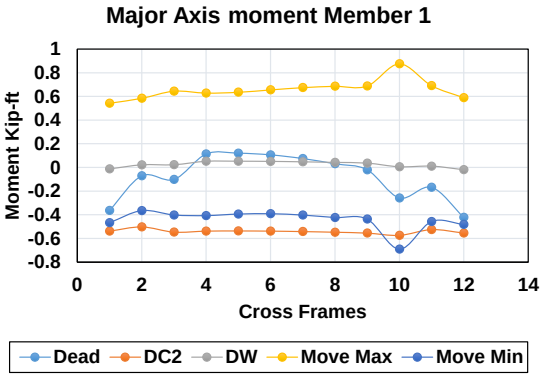

(c)

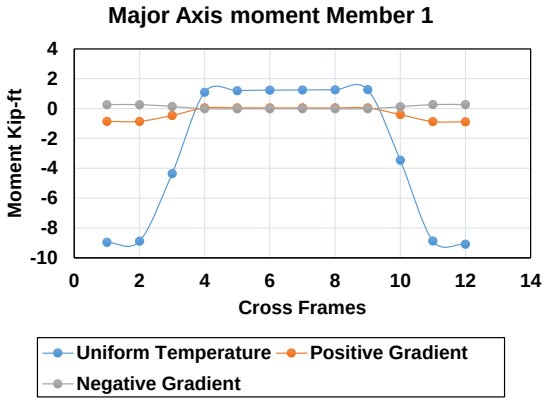

(d)

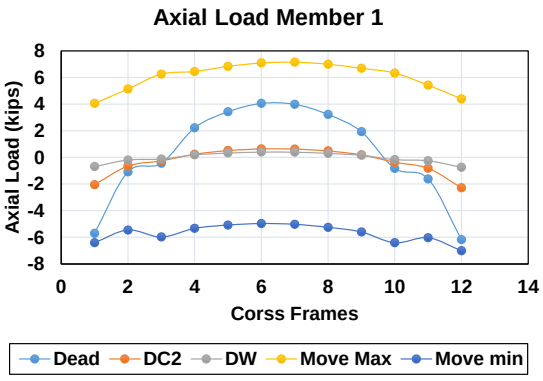

(e)

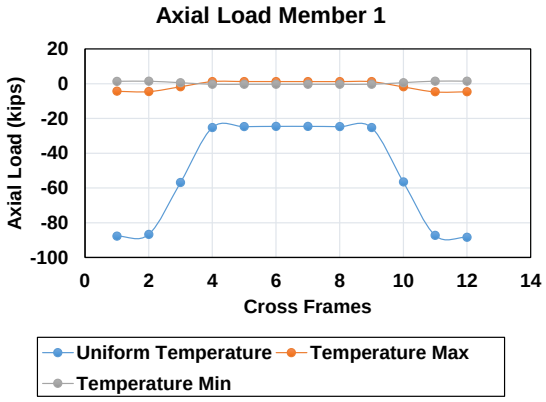

(f)

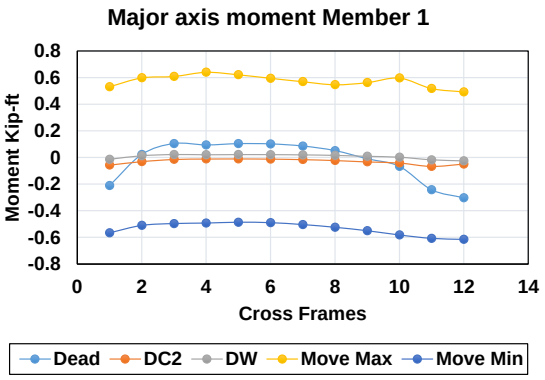

(g)

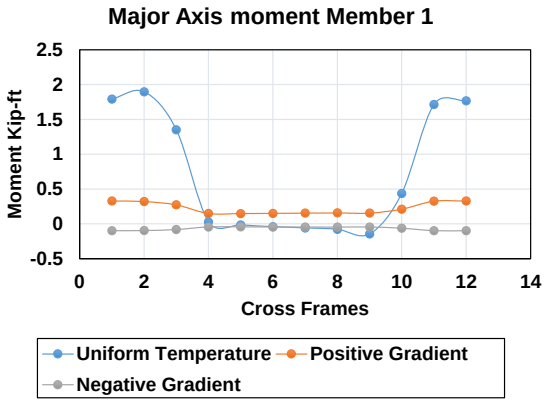

(h)

Figure 21. Forces in Member 1 within Span 2, left brace

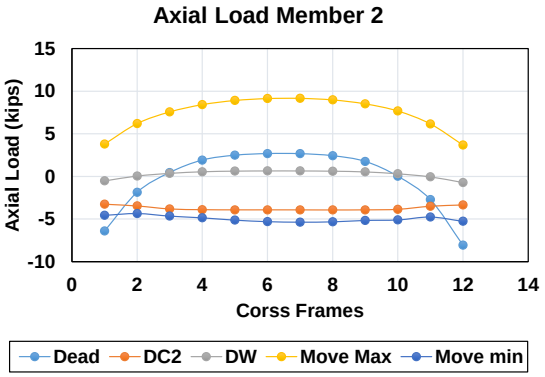

(a)

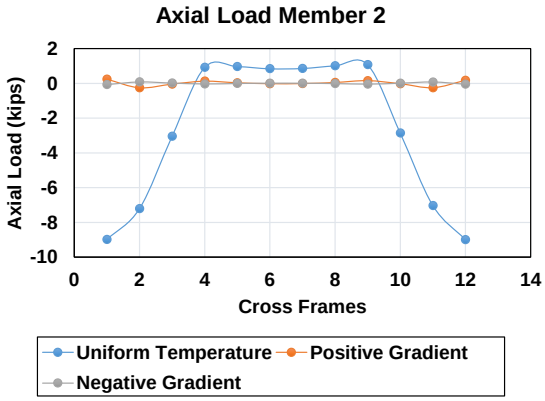

(b)

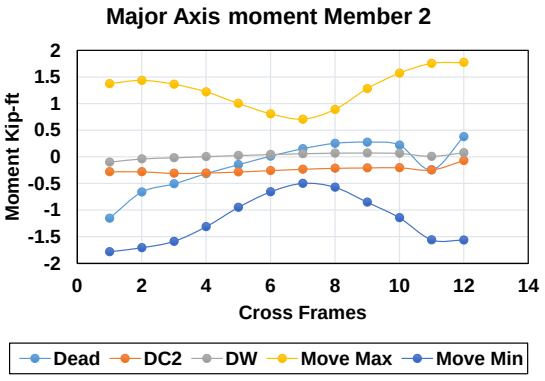

(c)

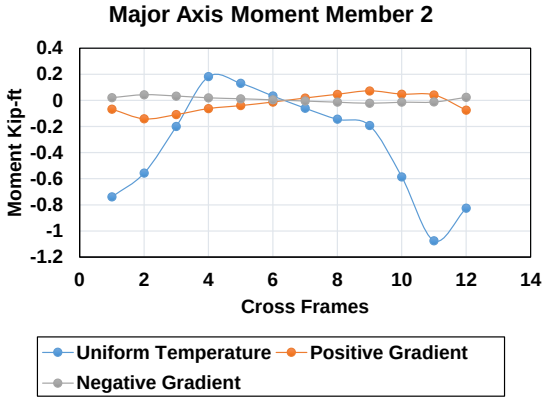

(d)

Figure 22. Forces in Member 2 within Span 2, left brace

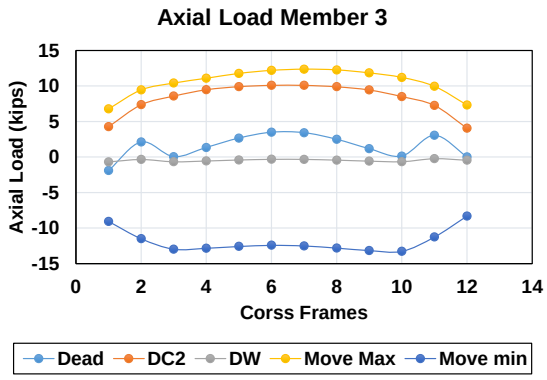

(a)

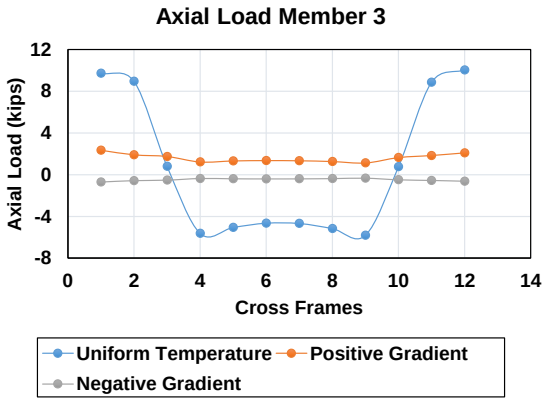

(b)

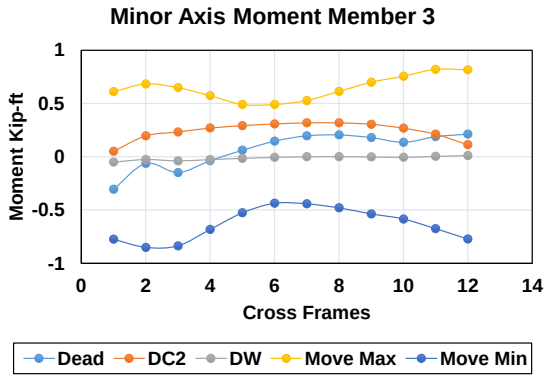

(c)

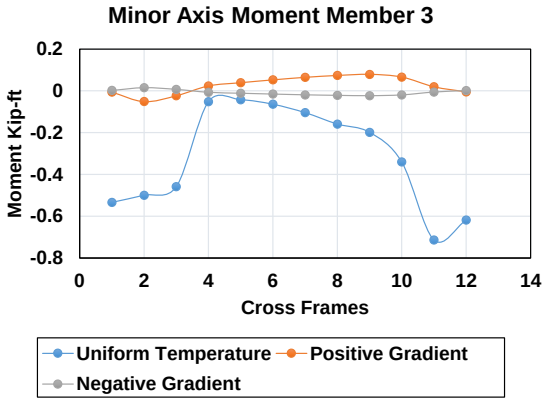

(d)

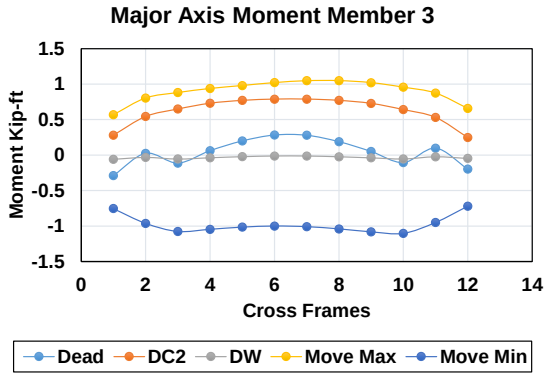

(e)

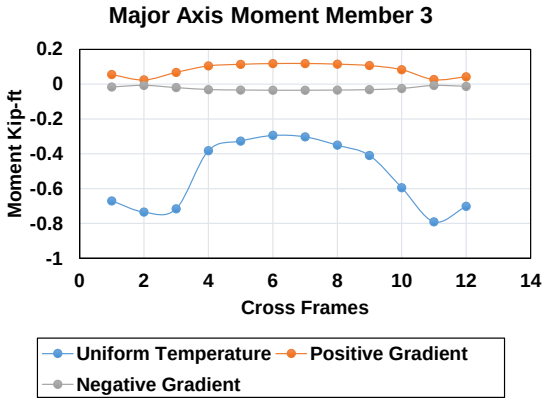

(f)

Figure 23. Forces in Member 3 within Span 2, left brace

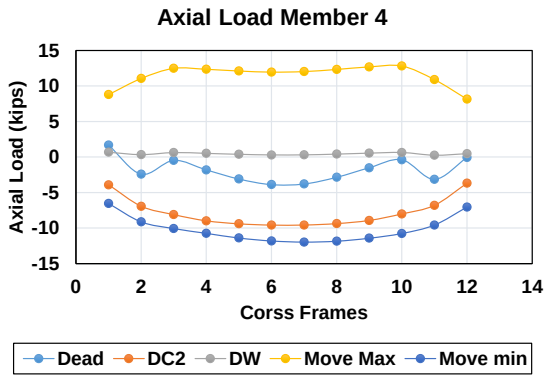

(a)

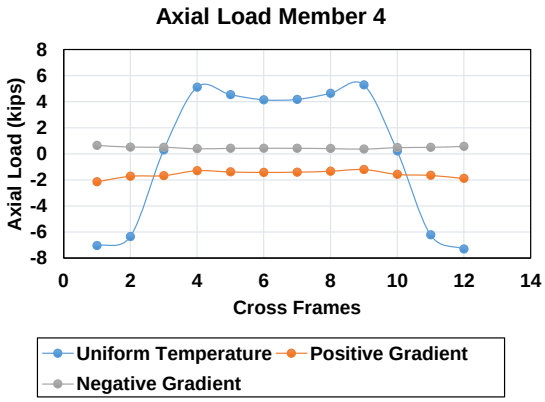

(b)

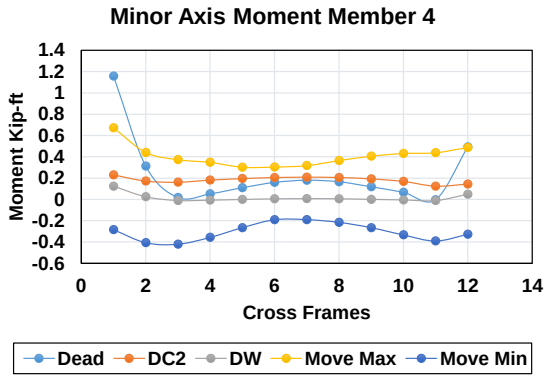

(c)

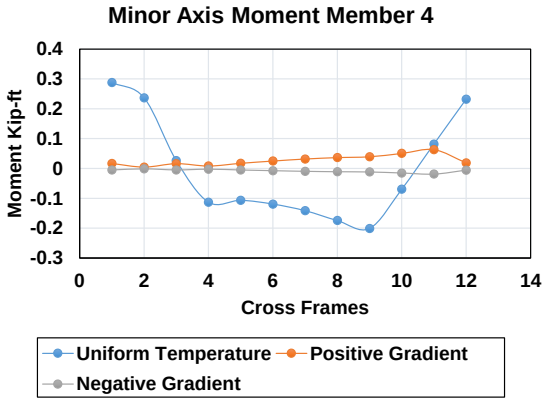

(d)

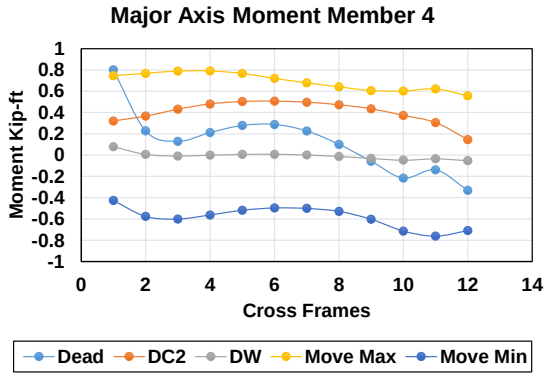

(e)

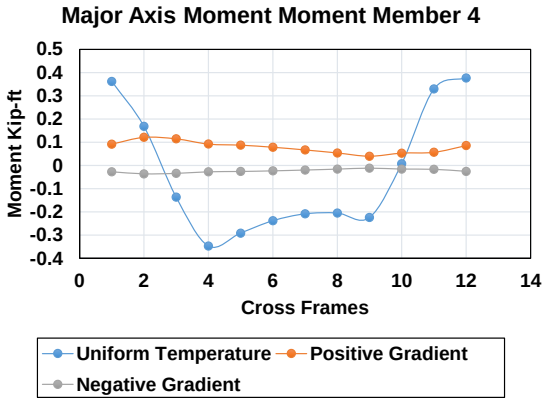

(f)

Figure 24. Forces in Member 4 within Span 2, left brace

Span 3

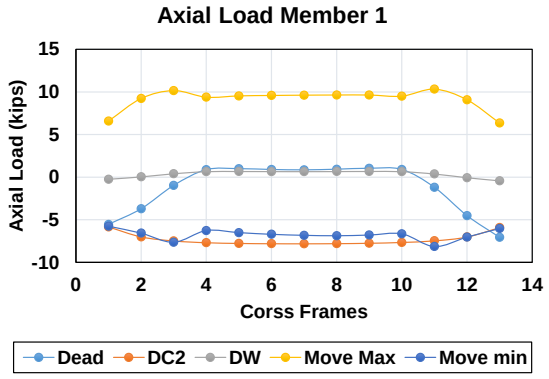

(a)

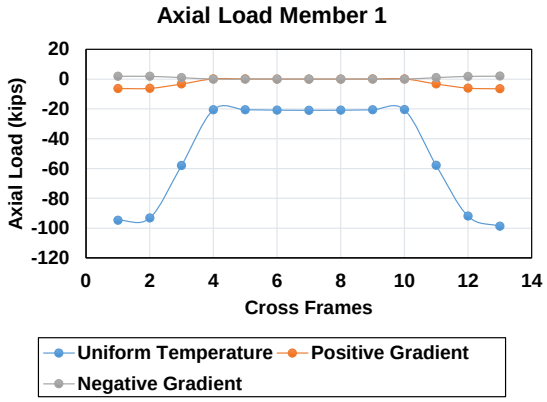

(b)

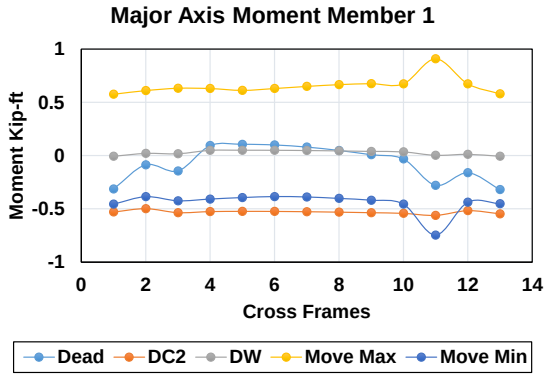

(c)

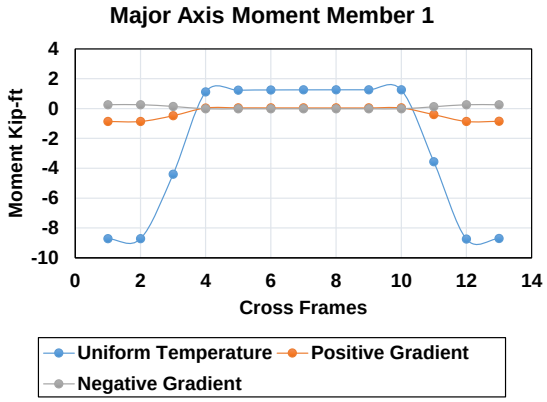

(d)

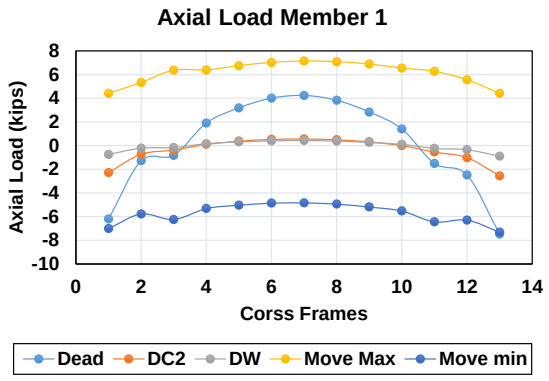

(e)

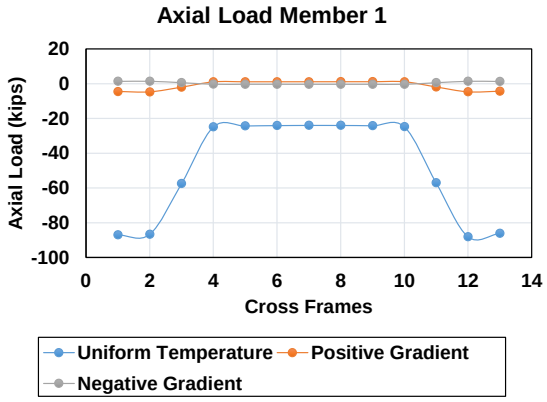

(f)

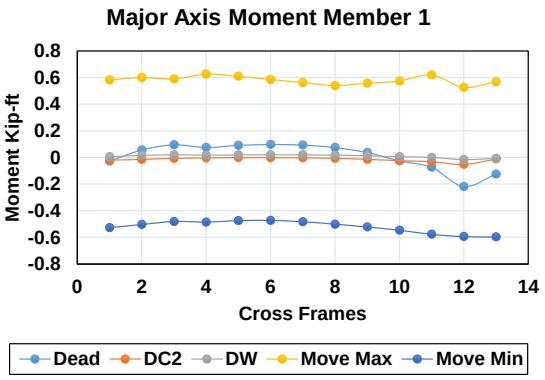

(g)

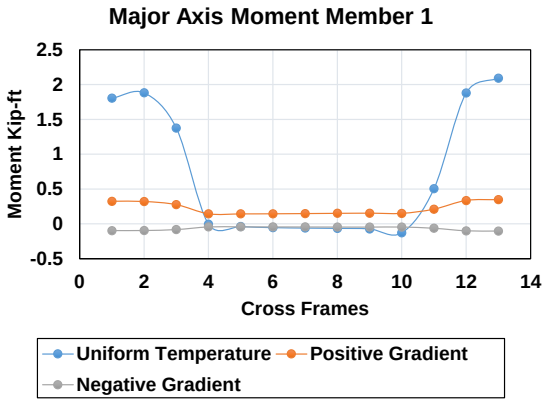

(h)

Figure 25. Forces in Member 1 within Span 3, left brace

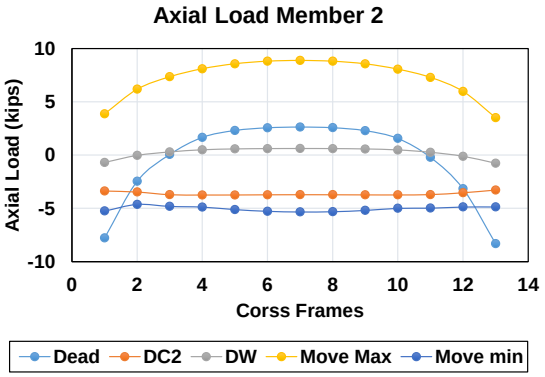

(a)

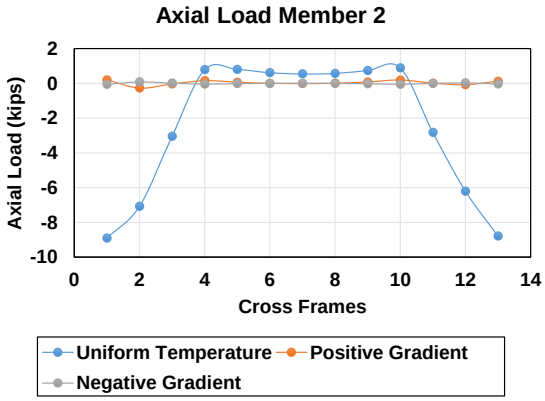

(b)

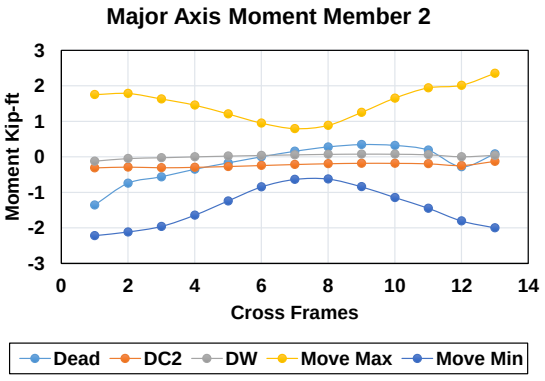

(c)

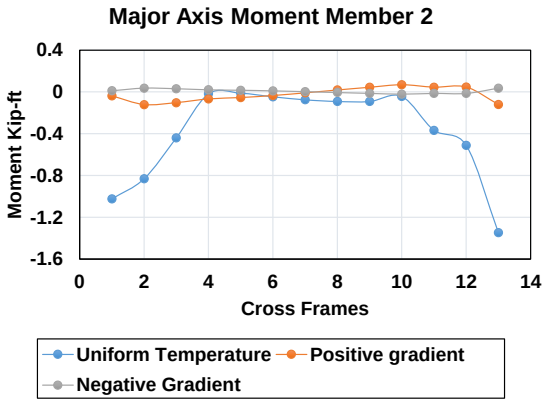

(d)

Figure 26. Forces in Member 2 within Span 3, left brace

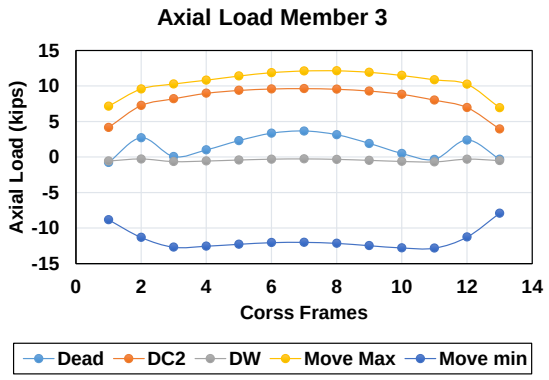

(a)

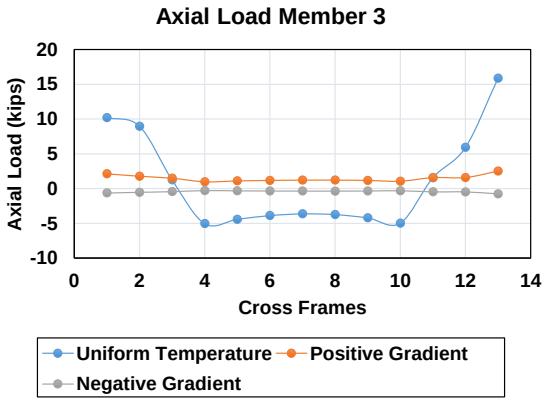

(b)

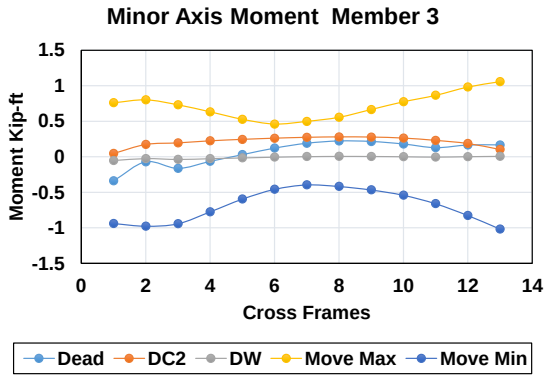

(c)

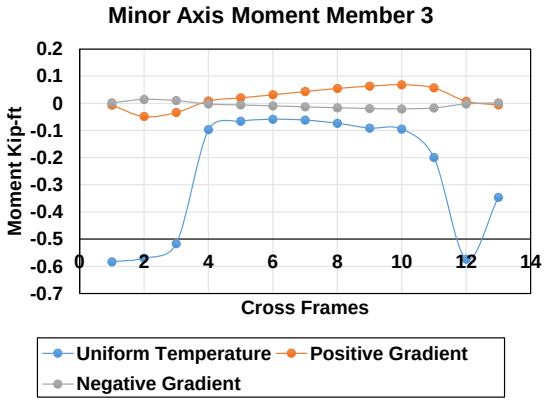

(d)

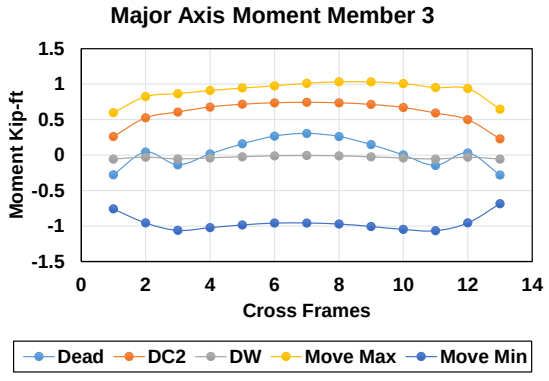

(e)

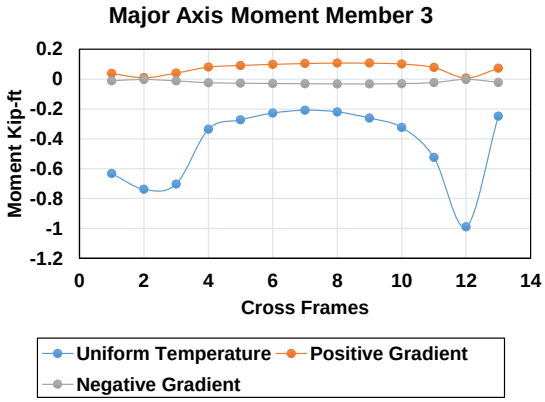

(f)

Figure 27. Forces in Member 3 within Span 3, left brace

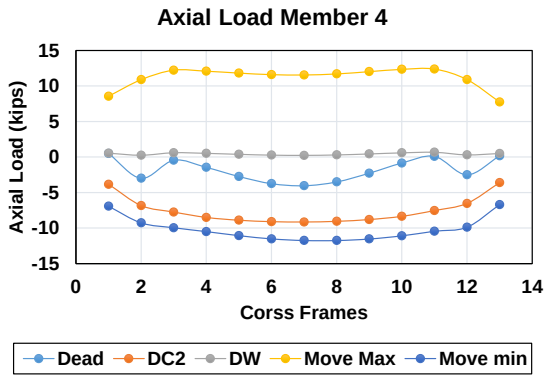

(a)

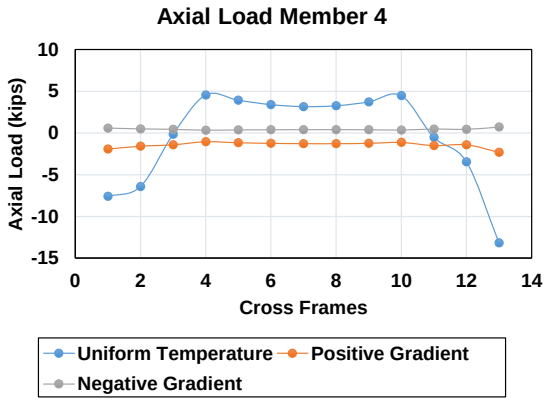

(b)

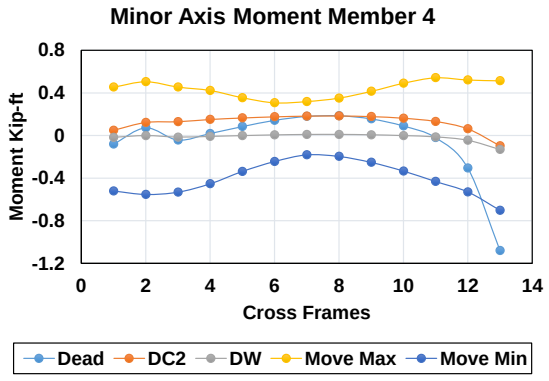

(c)

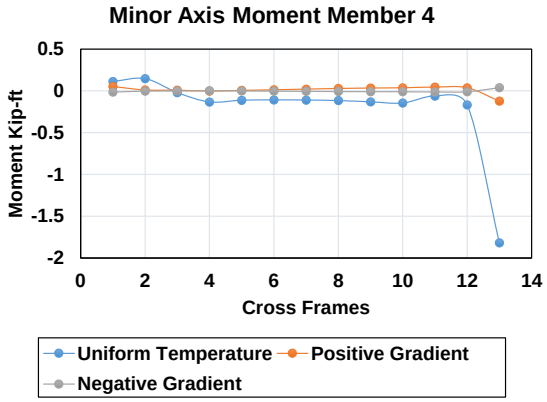

(d)

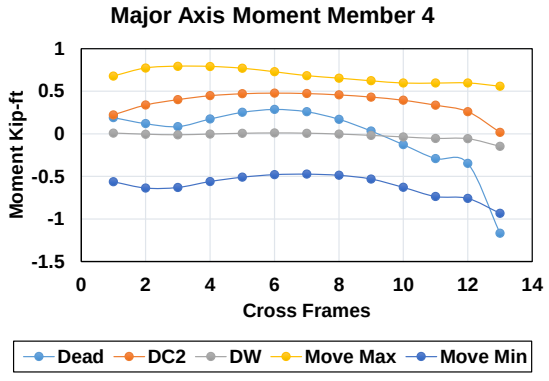

(e)

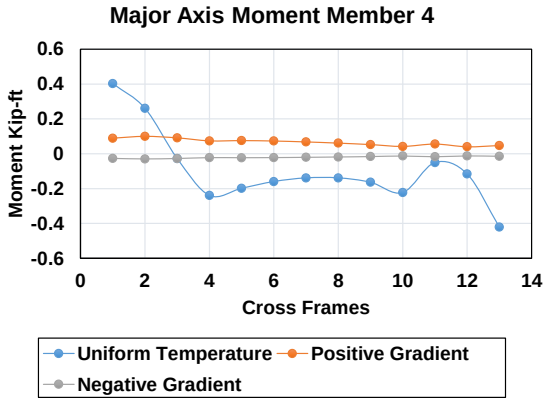

(f)

Figure 28. Forces in Member 4 within Span 3, left brace

Span 4

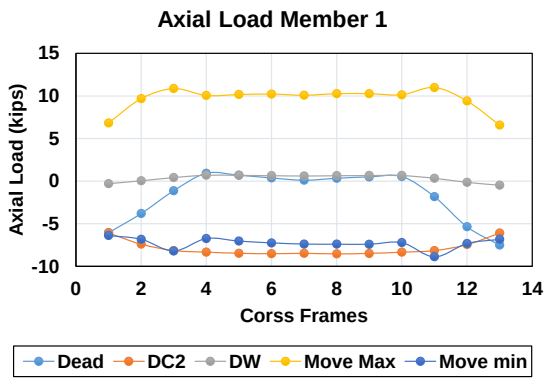

(a)

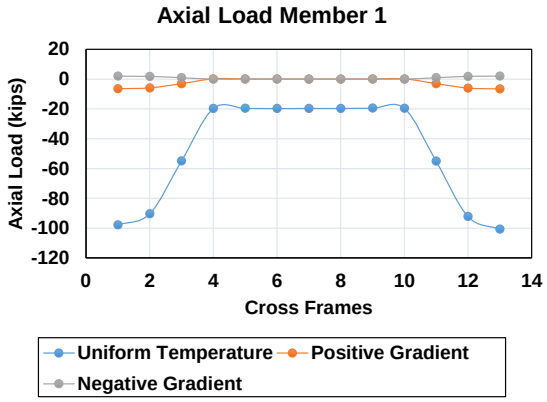

(b)

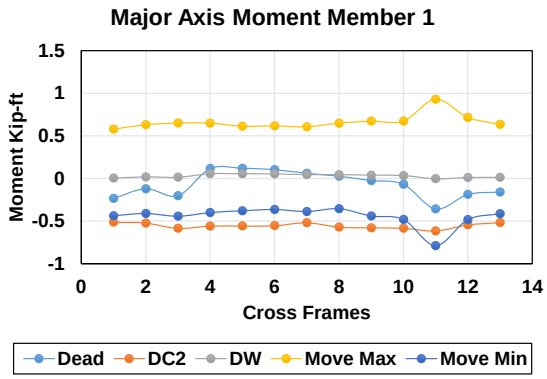

(c)

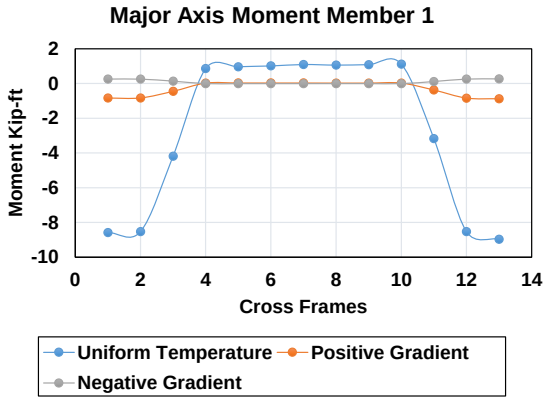

(d)

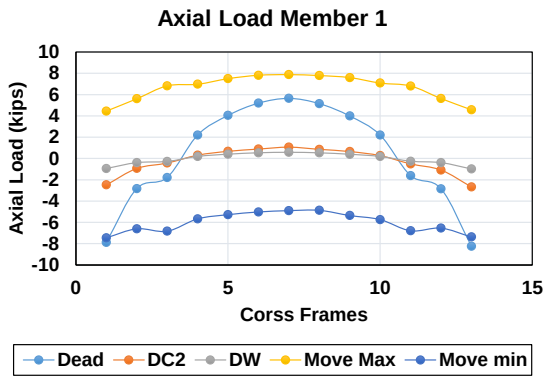

(e)

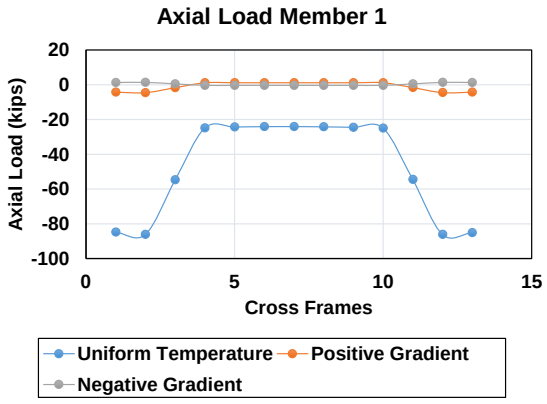

(f)

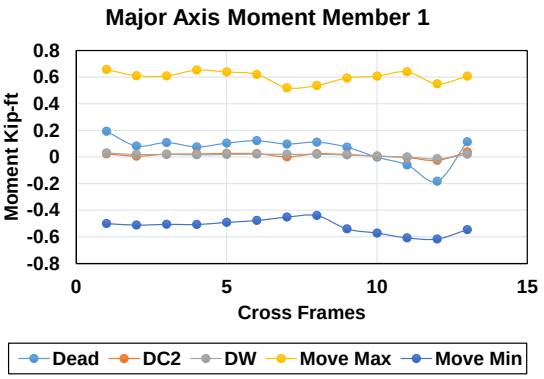

(g)

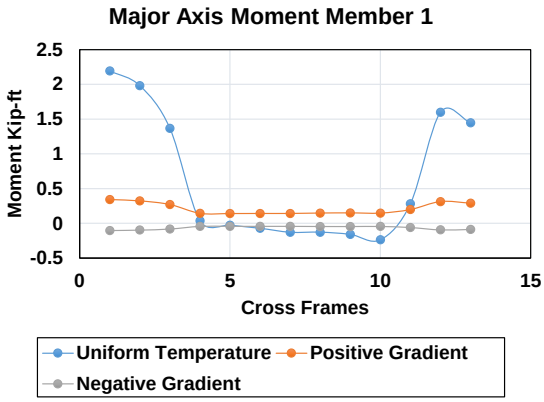

(h)

Figure 29. Forces in Member 1 within Span 4, left brace

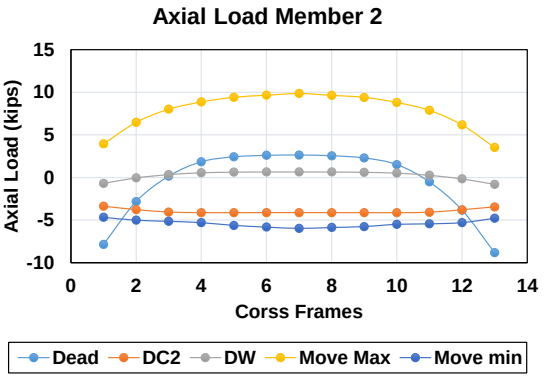

(a)

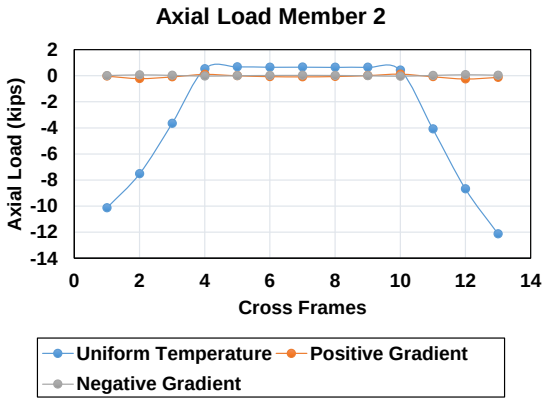

(b)

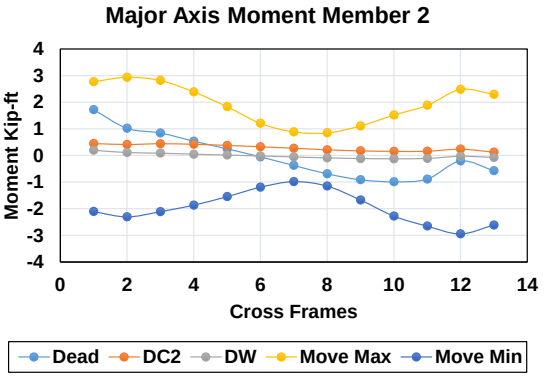

(c)

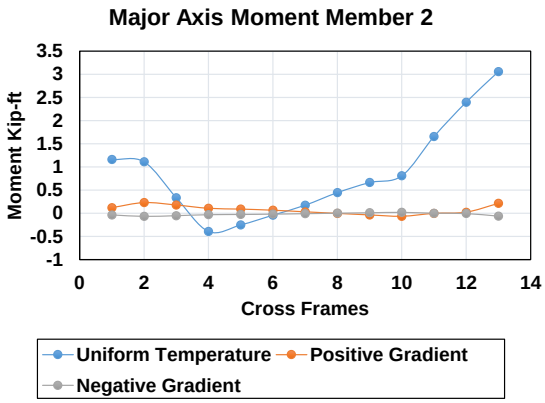

(d)

Figure 30. Forces in Member 2 within Span 4, left brace

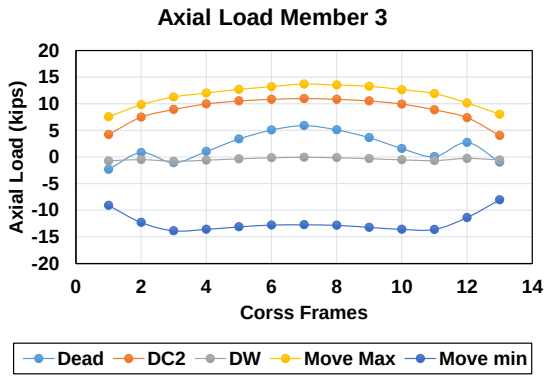

(a)

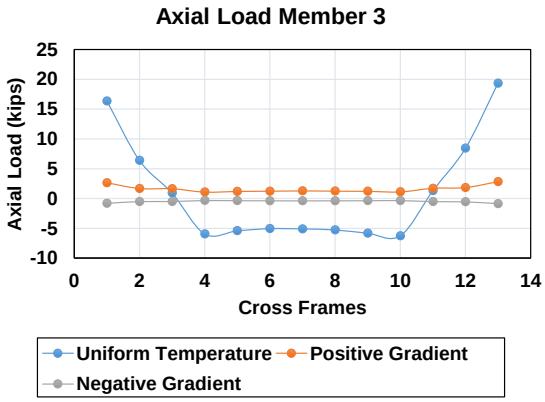

(b)

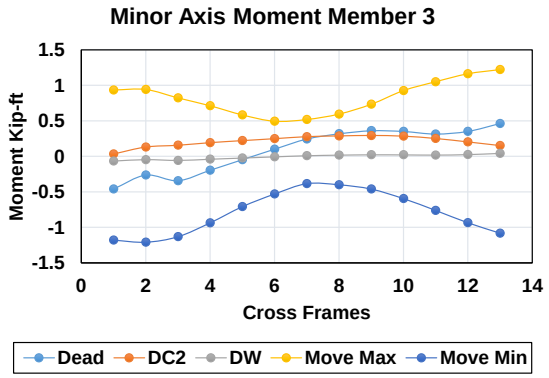

(c)

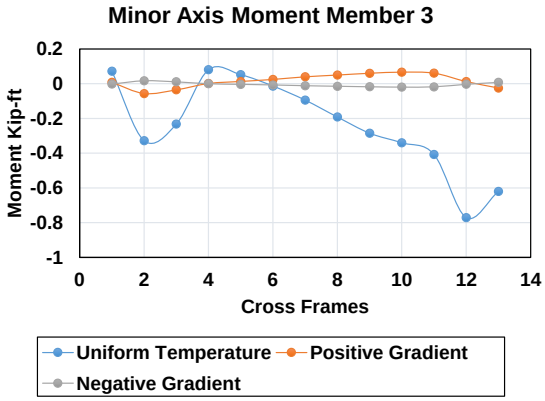

(d)

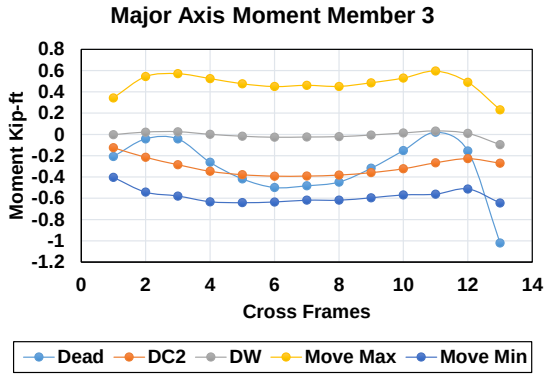

(e)

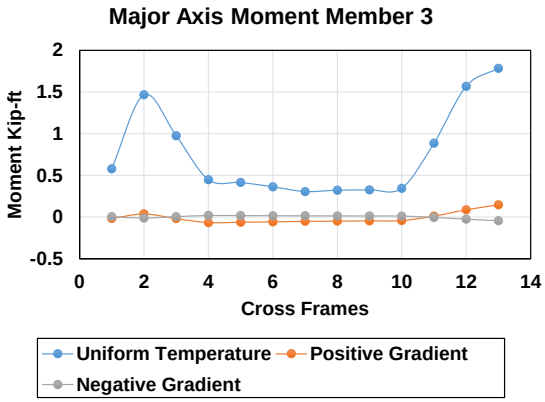

(f)

Figure 31. Forces in Member 3 within Span 4, left brace

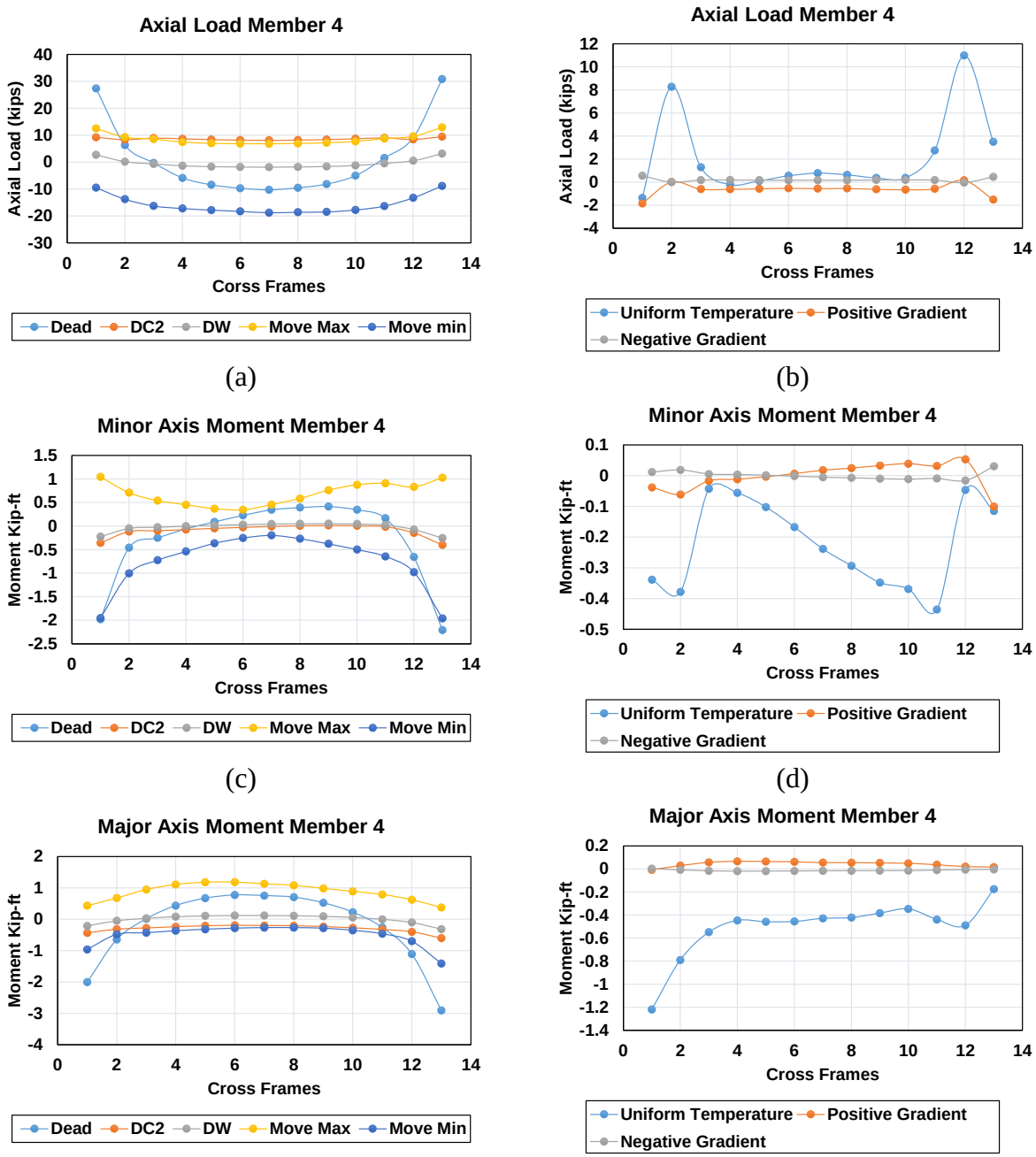

Figure 32. Forces in Member 4 within Span 4, left brace

Forces in the Members of Right Brace

Figures 33 through 48 show the axial forces and moments in the individual members of the exterior cross-frames of the first four spans in the left brace.

Span 1

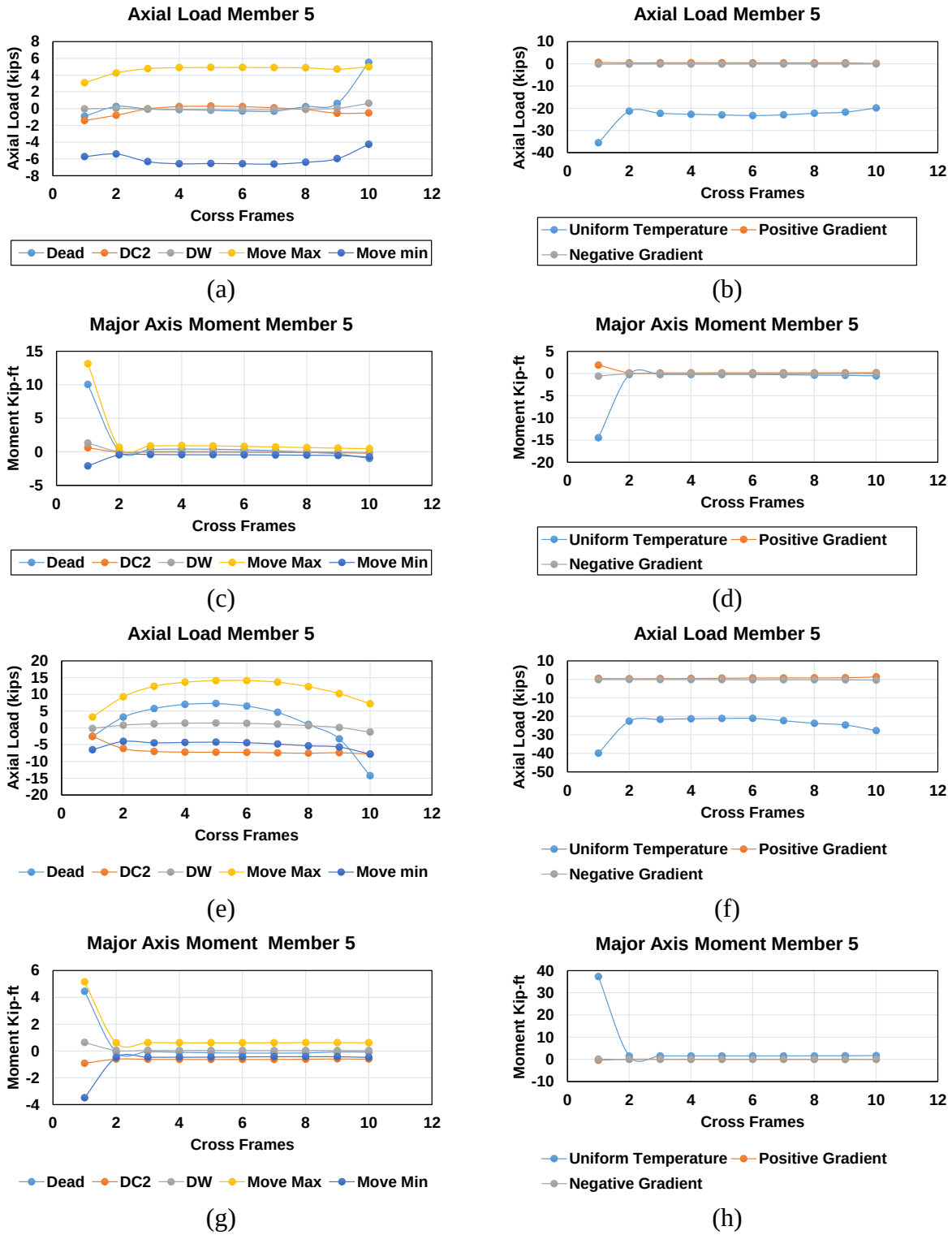

Figure 33. Forces in Member 5 within Span 1, right brace

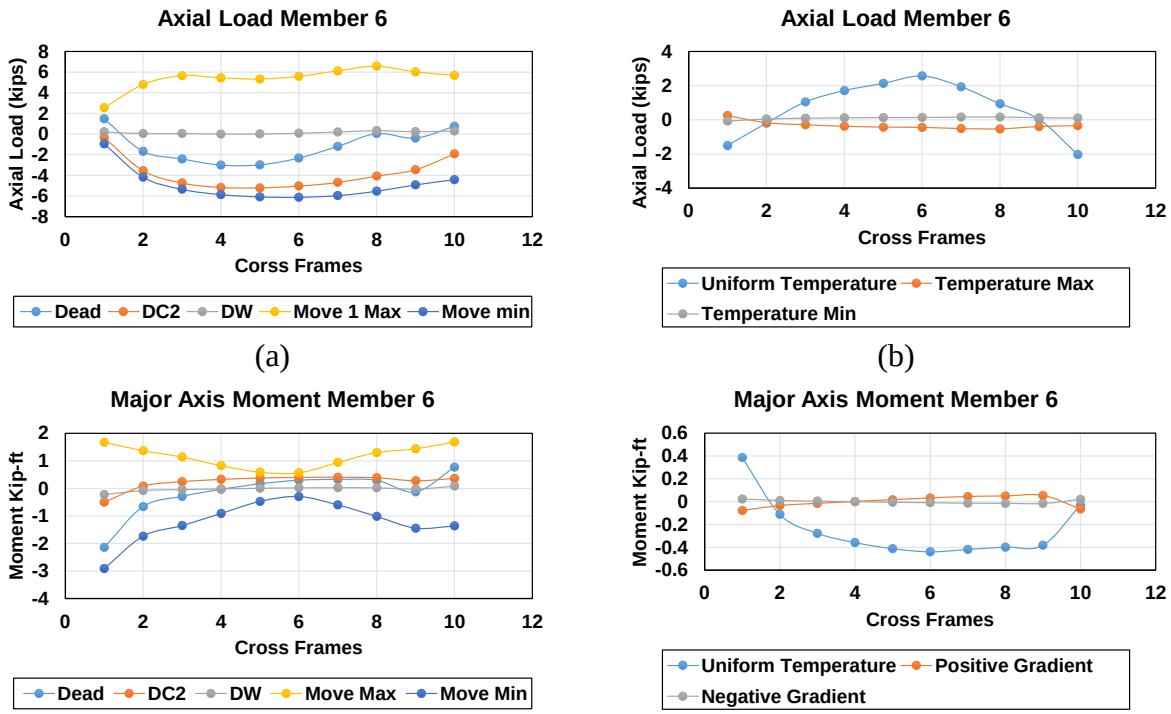

Figure 34. Forces in Member 6 within Span 1, right brace

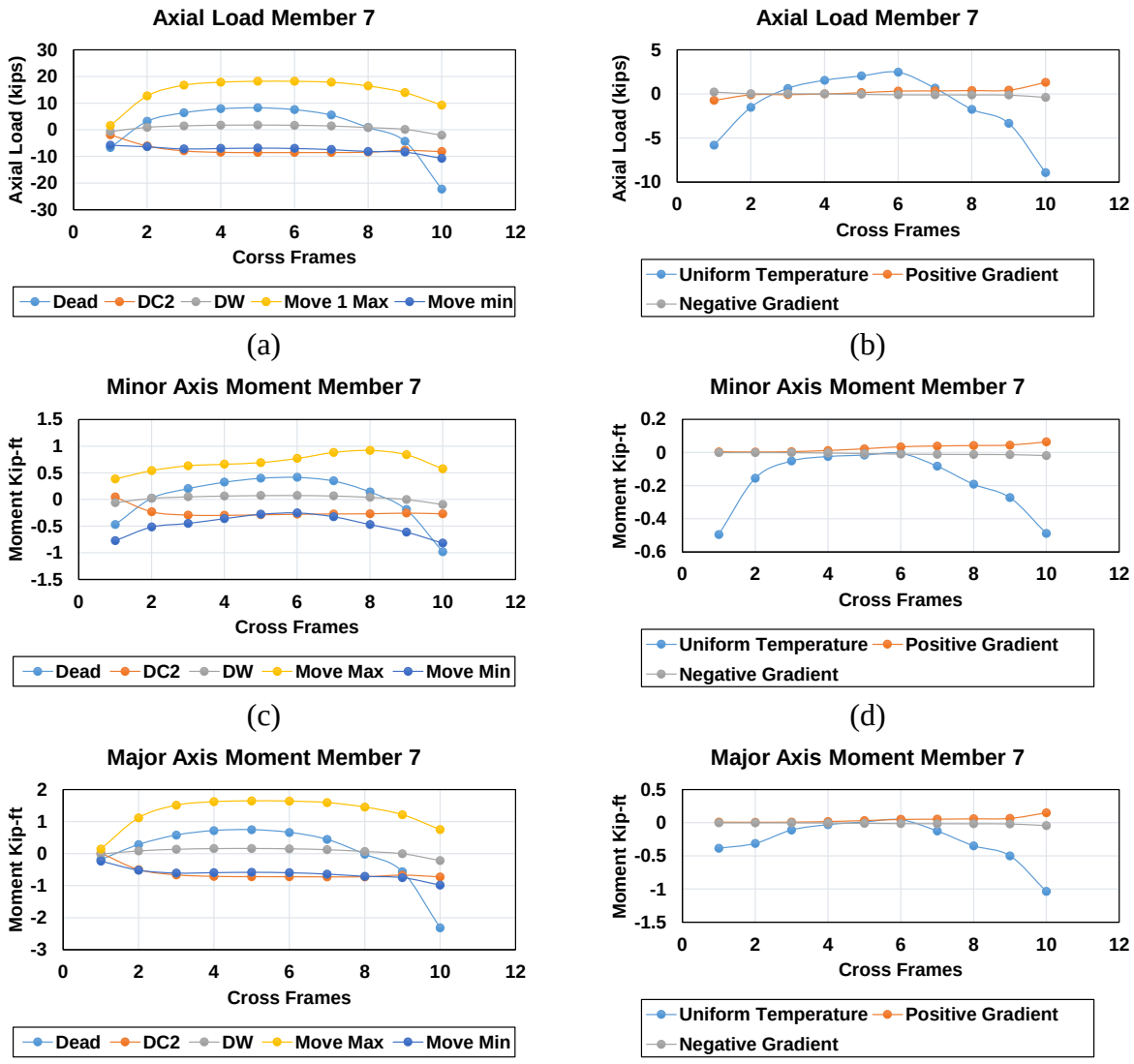

Figure 35. Forces in Member 7 within Span 1, right brace

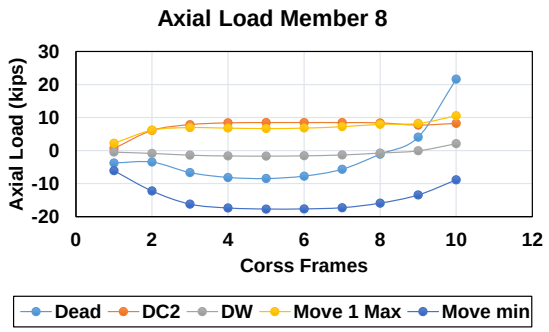

(a)

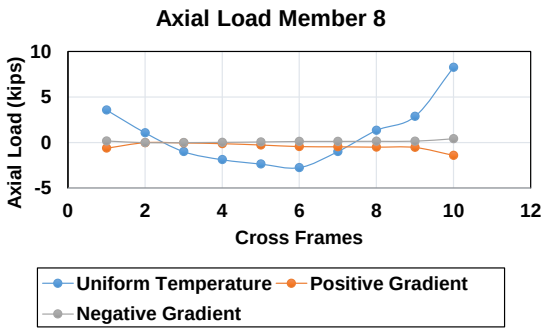

(b)

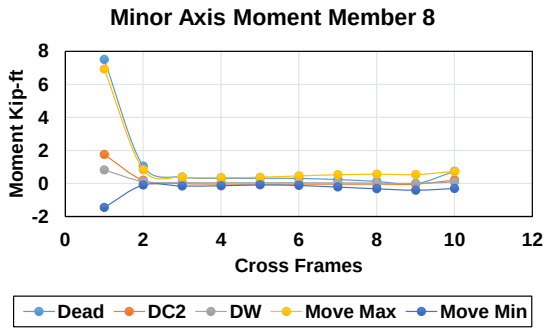

(c)

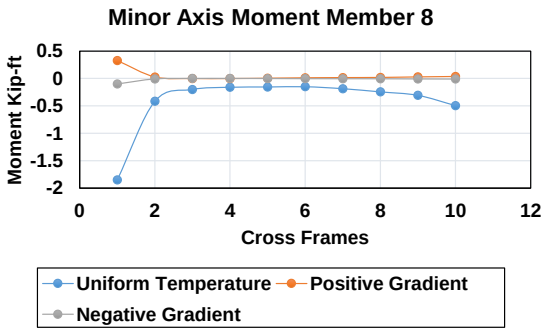

(d)

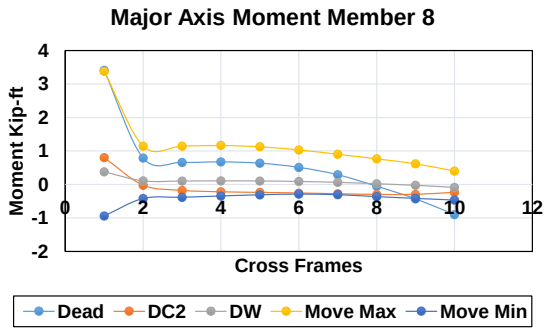

(e)

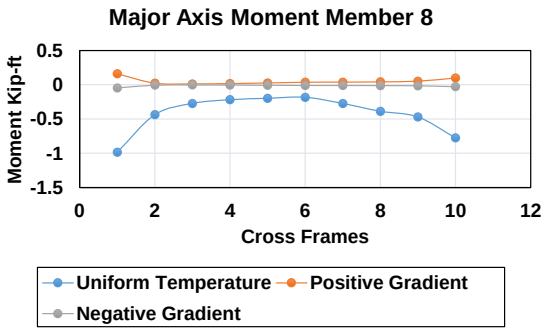

(f)

Figure 36. Forces in Member 8 within Span 1, right brace

Span 2

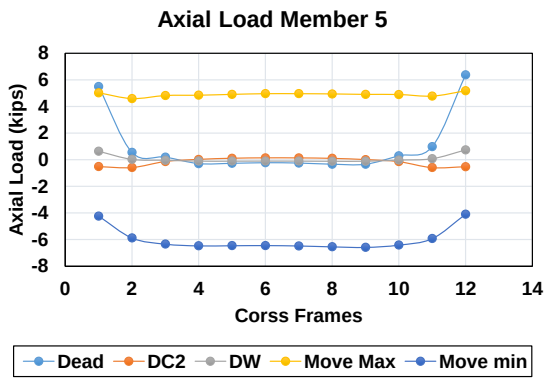

(a)

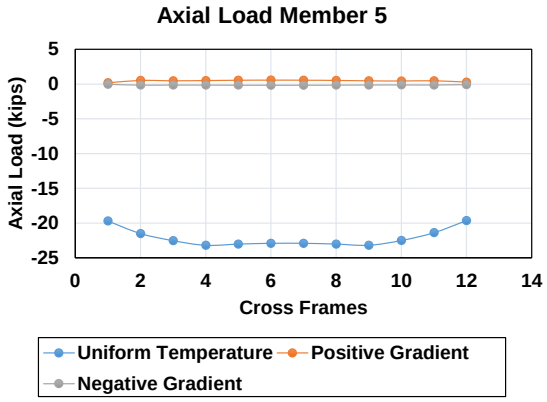

(b)

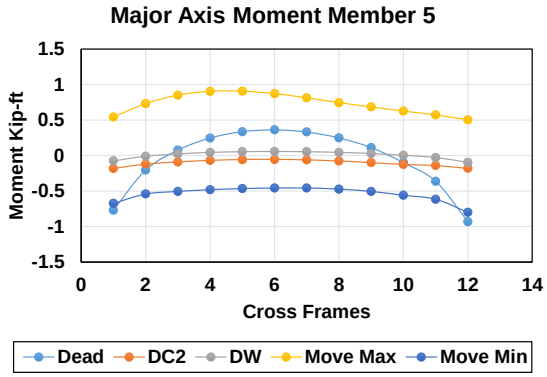

(c)

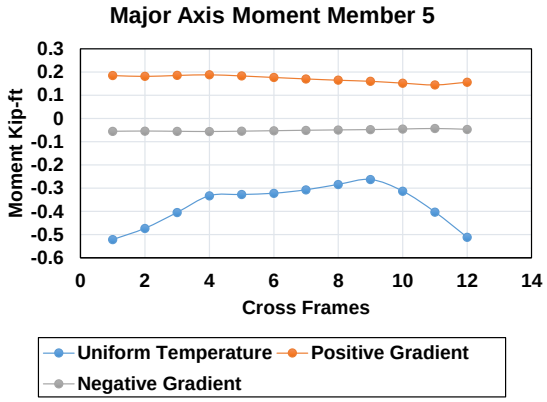

(d)

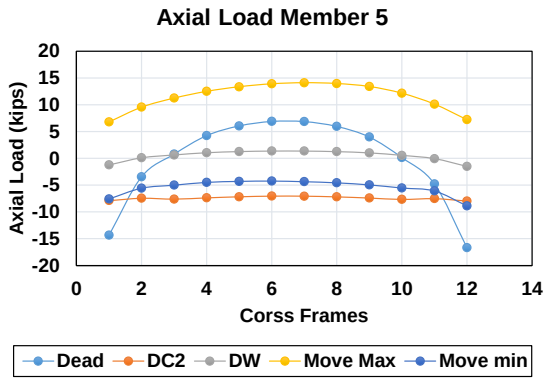

(e)

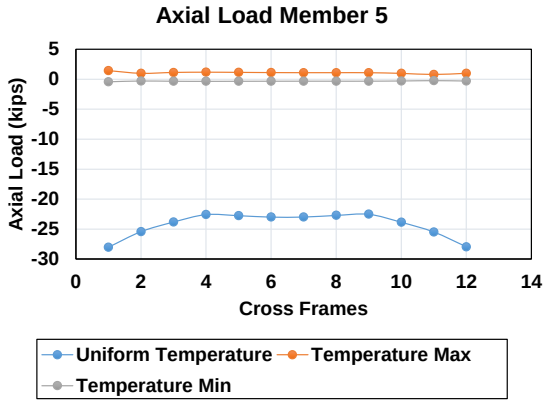

(f)

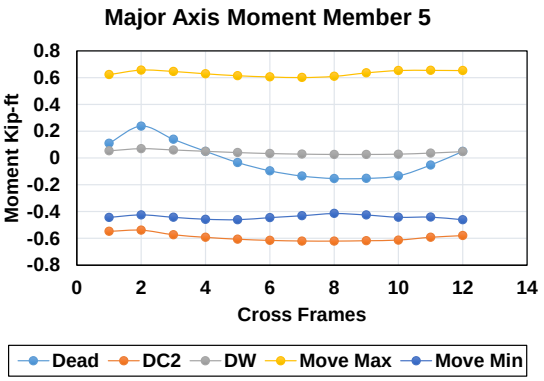

(g)

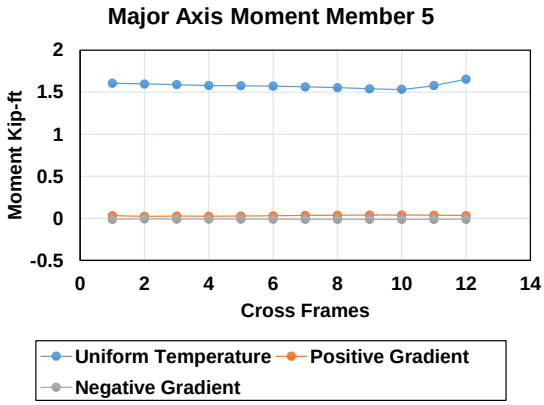

(h)

Figure 37. Forces in Member 5 within Span 2, right brace

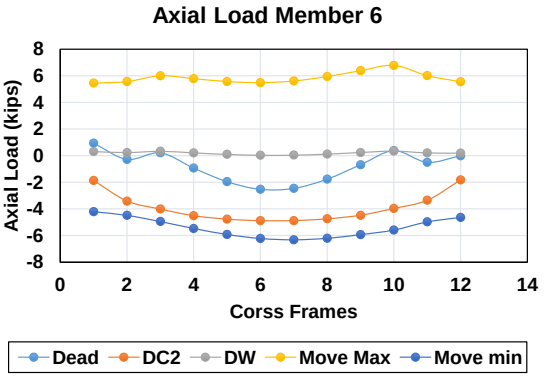

(a)

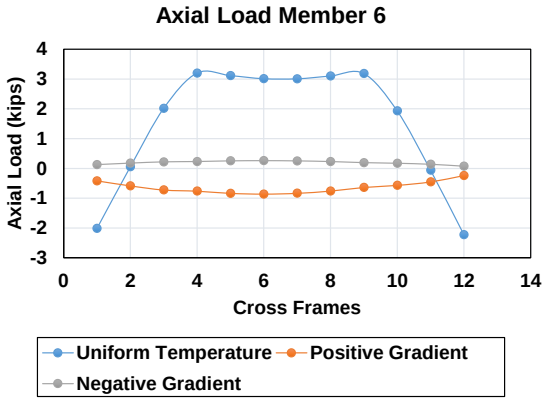

(b)

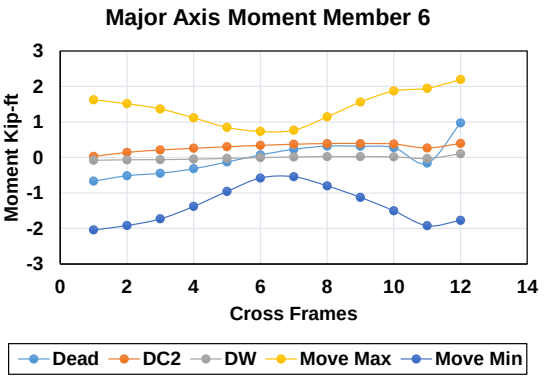

(c)

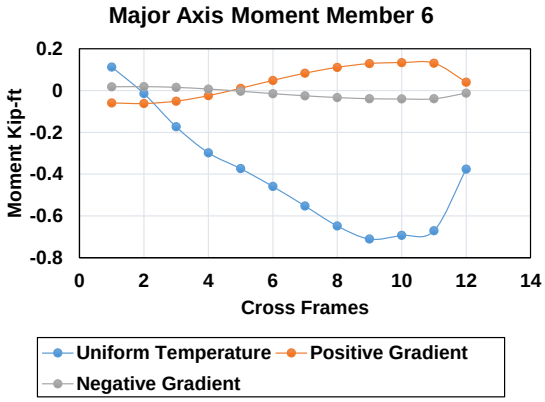

(d)

Figure 38. Forces in Member 6 within Span 2, right brace

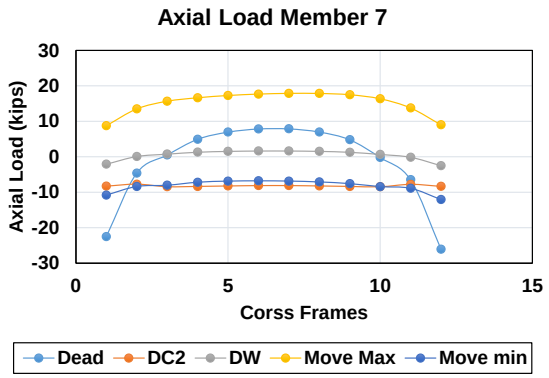

(a)

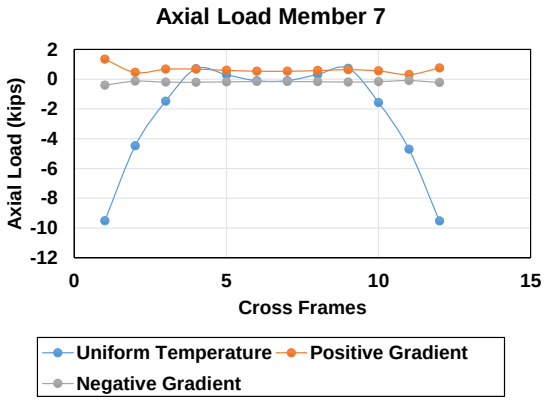

(b)

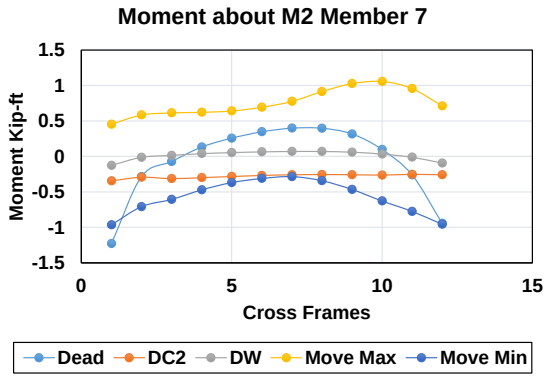

(c)

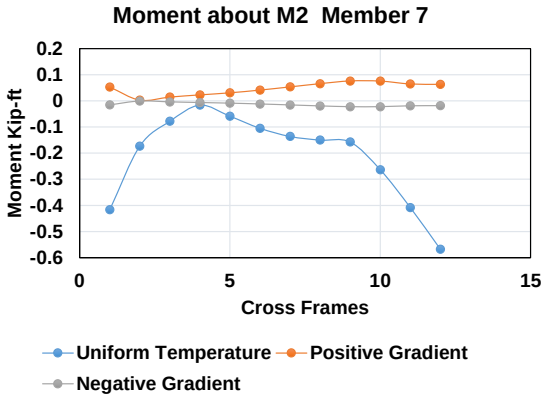

(d)

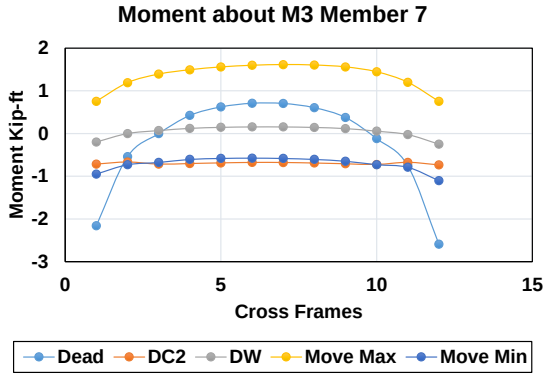

(e)

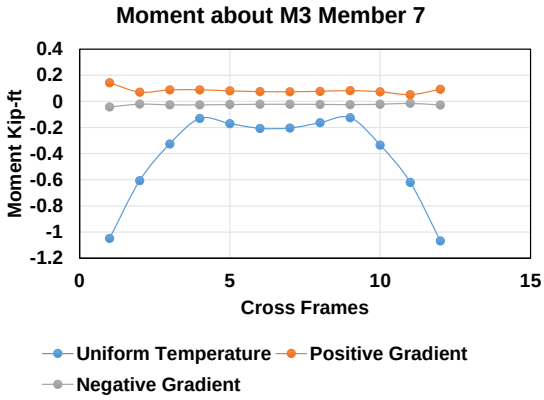

(f)

Figure 39. Forces in Member 7 within Span 2, right brace

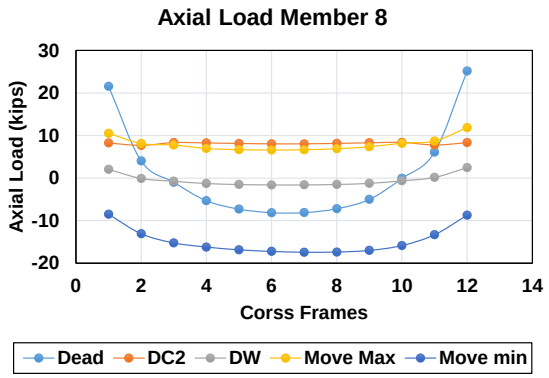

(a)

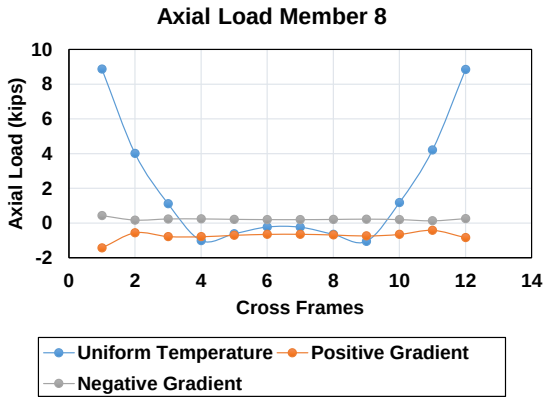

(b)

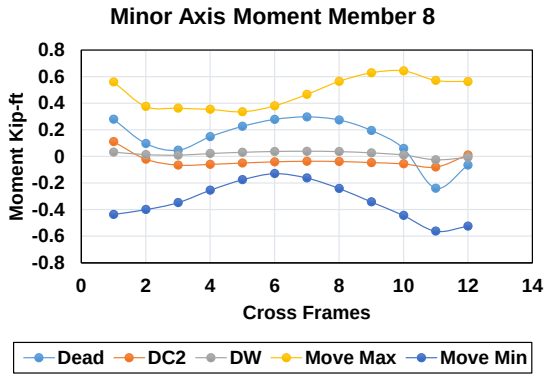

(c)

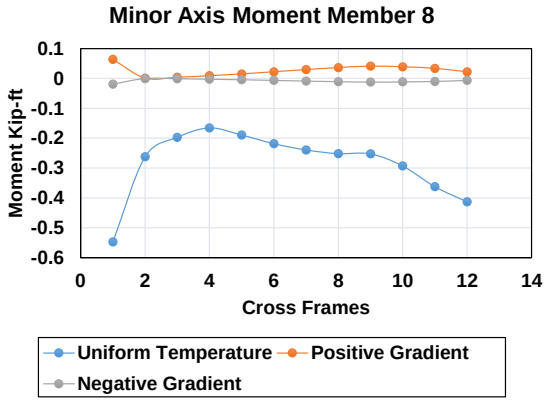

(d)

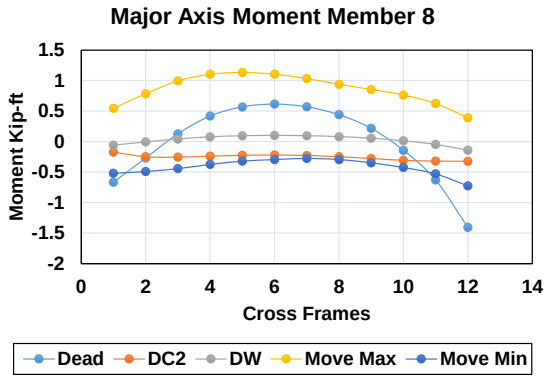

(e)

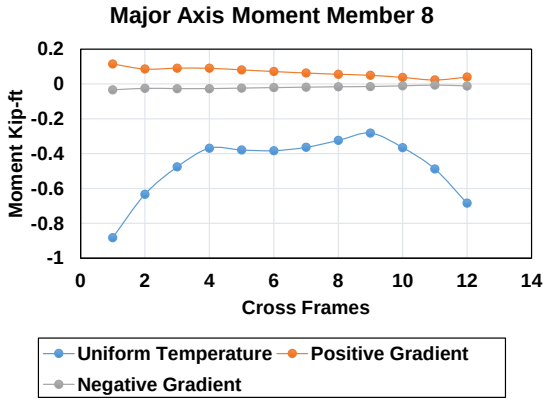

(f)

Figure 40. Forces in Member 8 within Span 2, right brace

Span 3

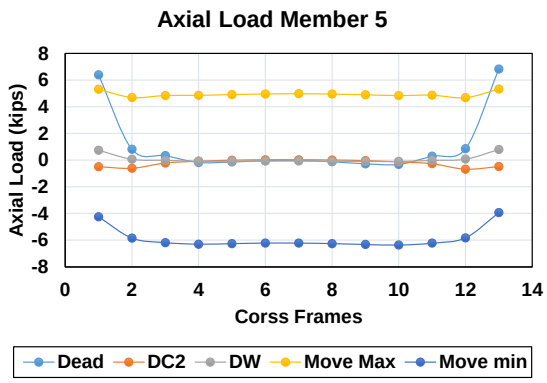

(a)

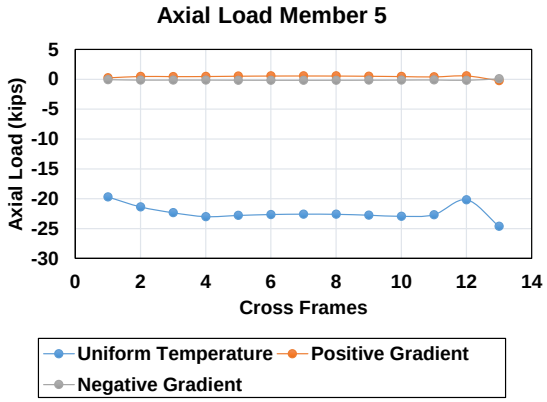

(b)

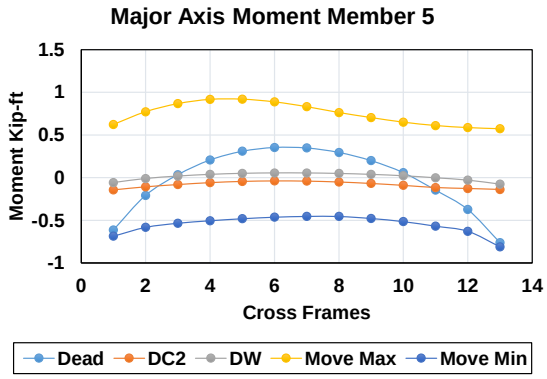

(c)

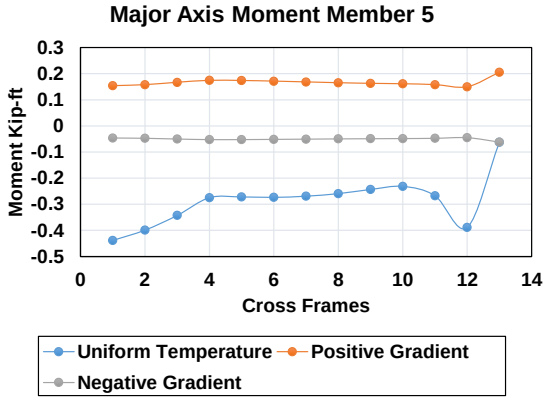

(d)

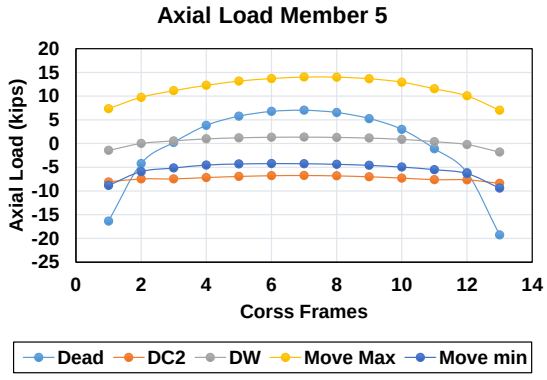

(e)

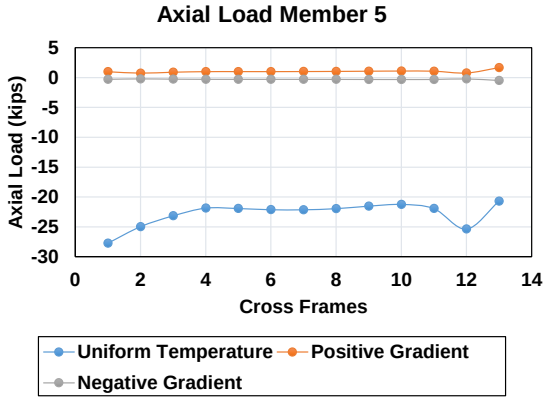

(f)

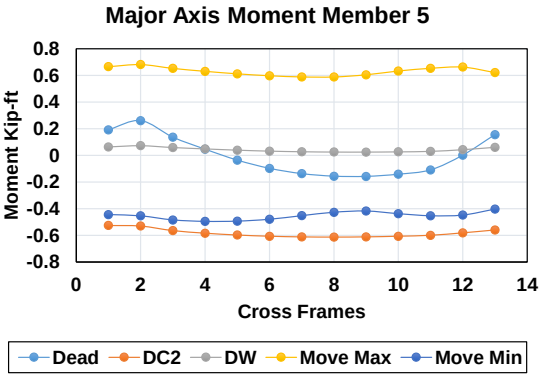

(g)

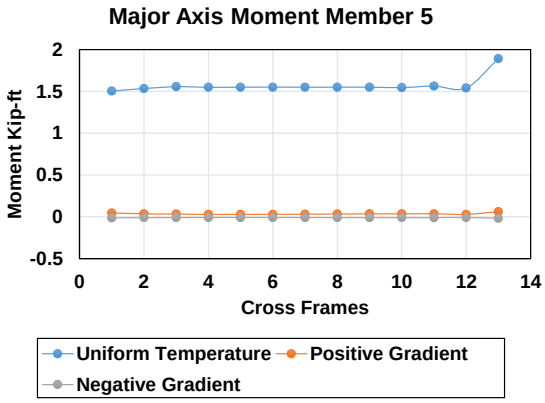

(h)

Figure 41. Forces in Member 5 within Span 3, right brace

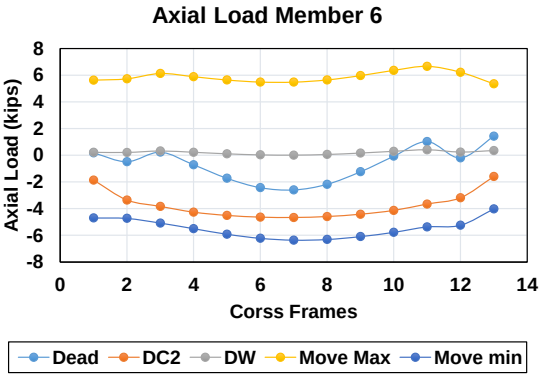

(a)

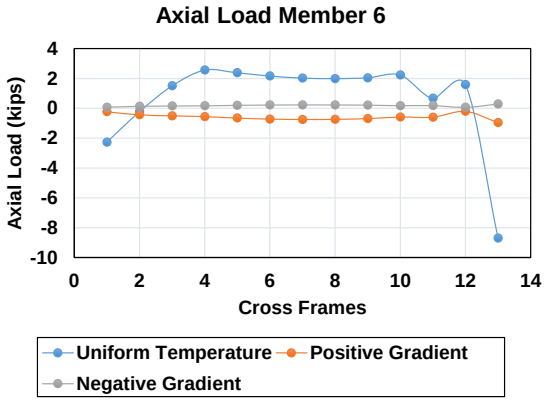

(b)

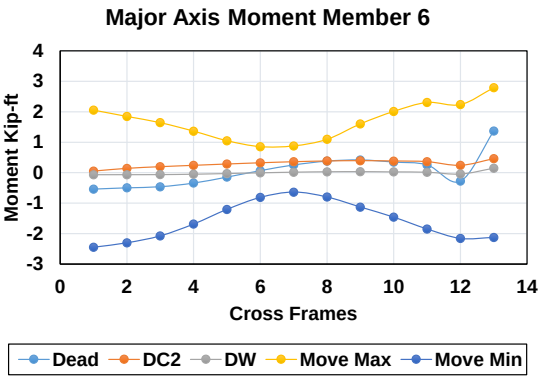

(c)

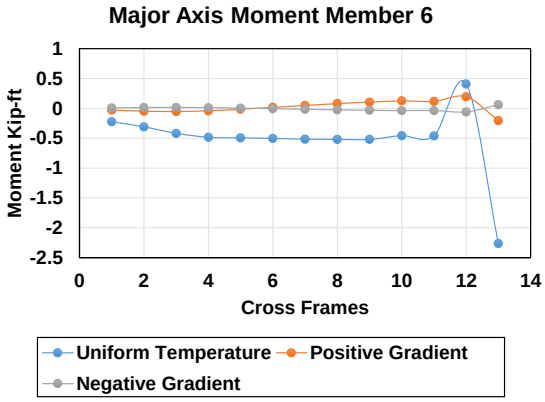

(d)

Figure 42. Forces in Member 6 within Span 3, right brace

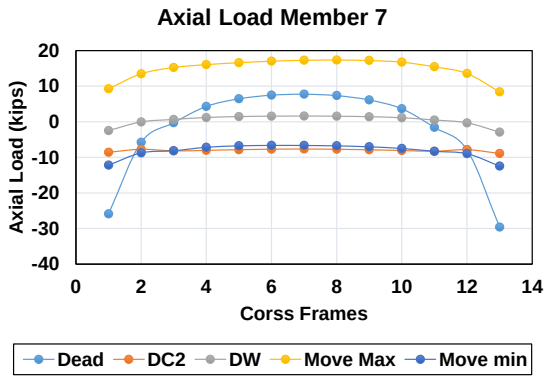

(a)

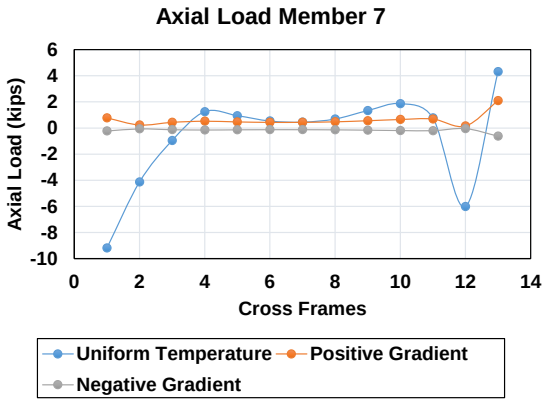

(b)

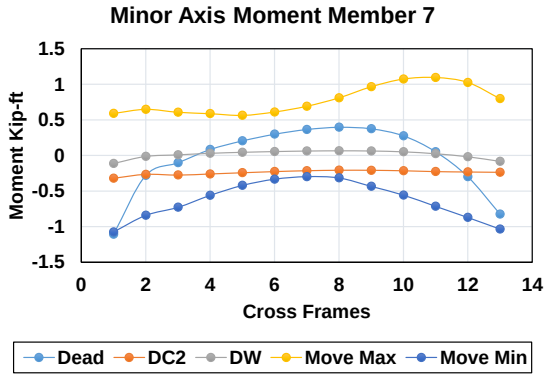

(c)

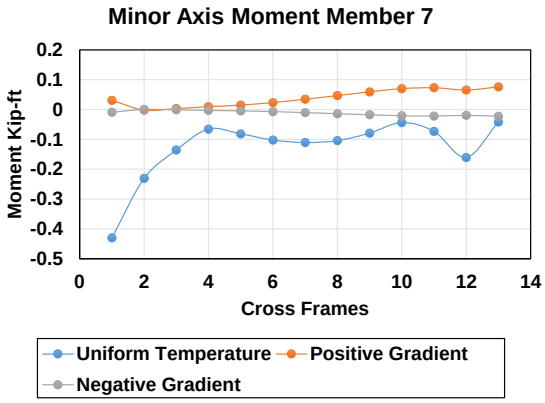

(d)

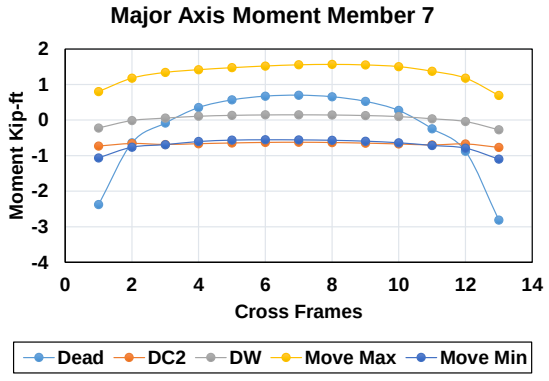

(e)

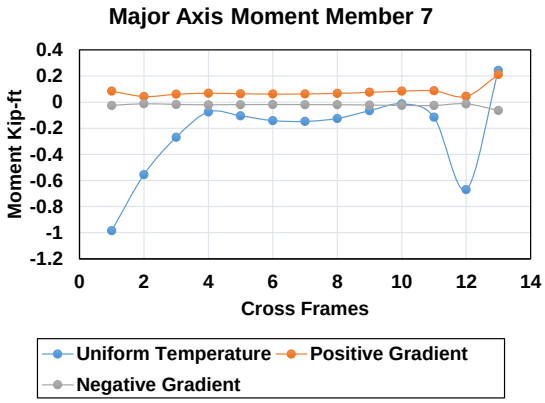

(f)

Figure 43. Forces in Member 7 within Span 3, right brace

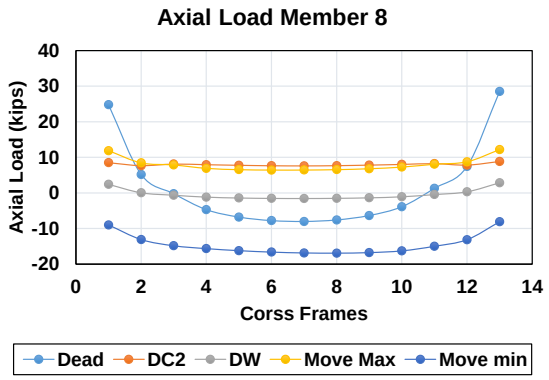

(a)

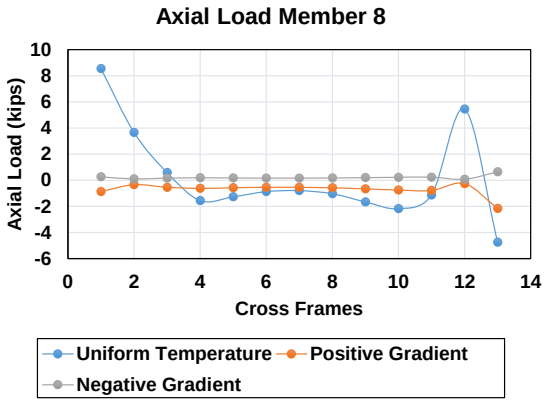

(b)

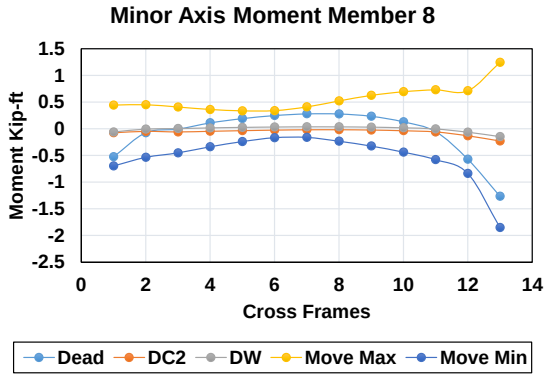

(c)

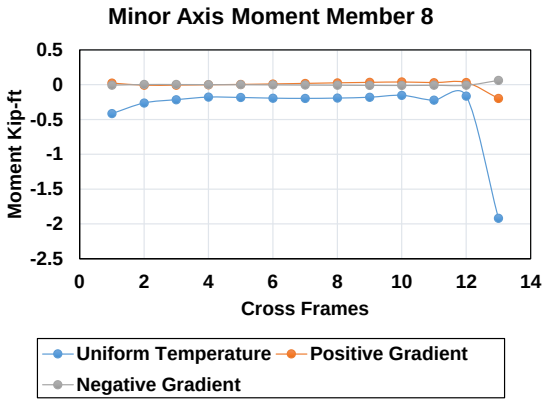

(d)

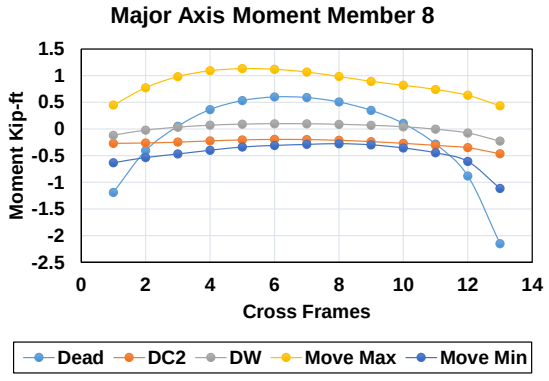

(e)

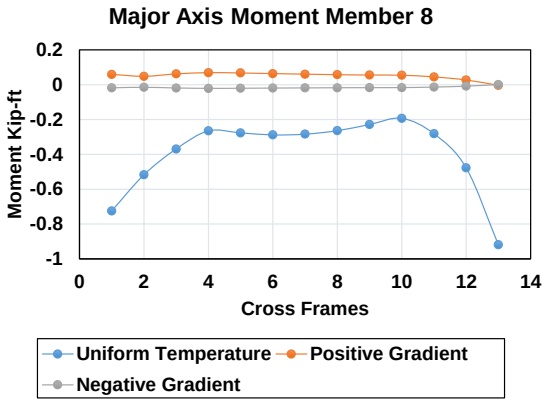

(f)

Figure 44. Forces in Member 8 within Span 3, right brace

Span 4

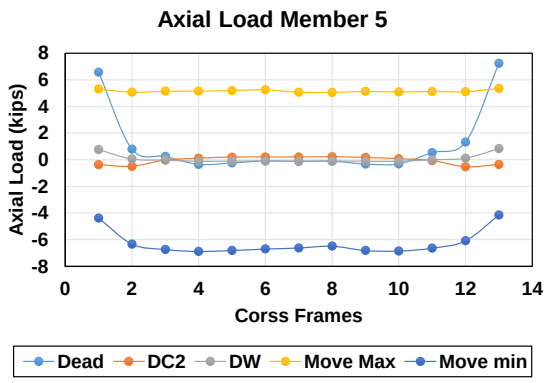

(a)

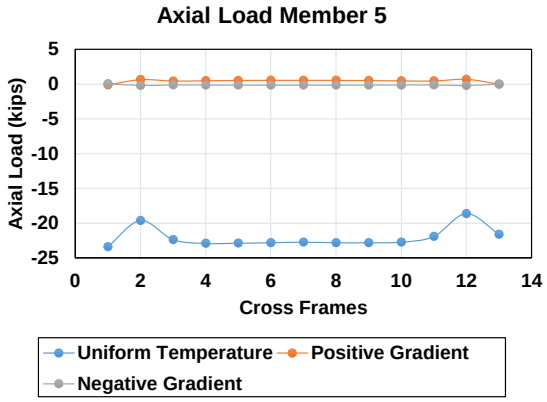

(b)

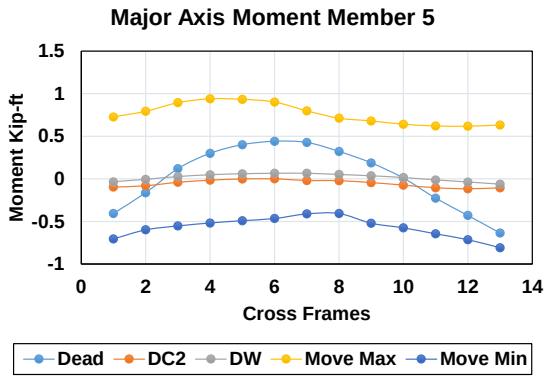

(c)

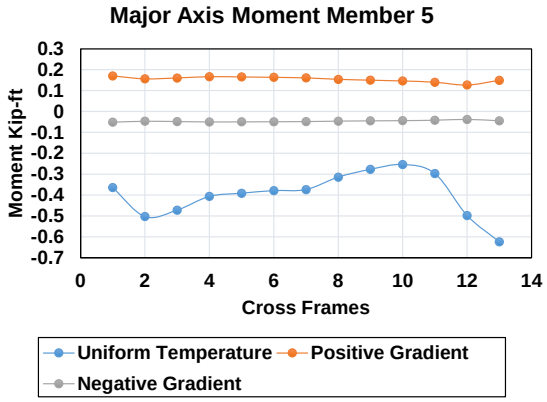

(d)

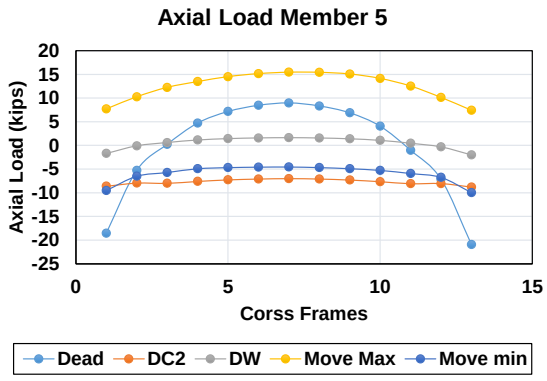

(e)

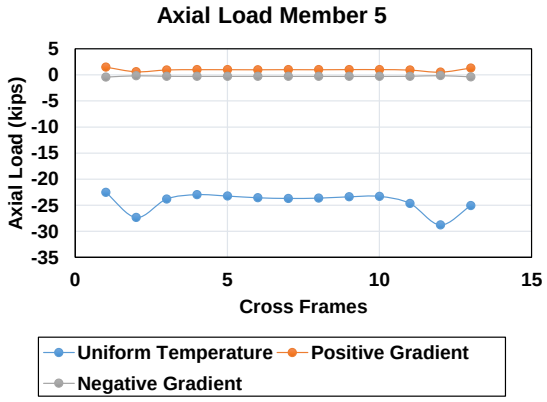

(f)

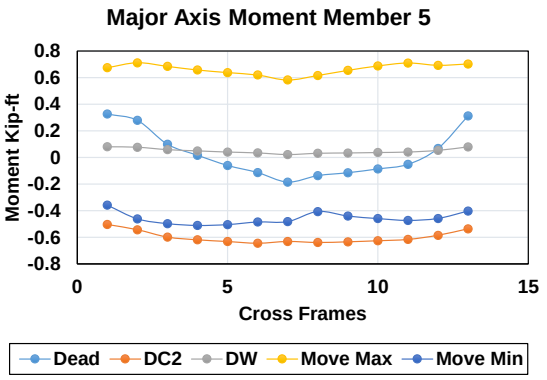

(g)

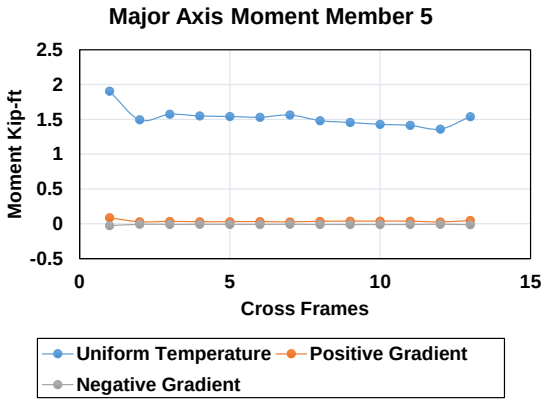

(h)

Figure 45. Forces in Member 5 within Span 4, right brace

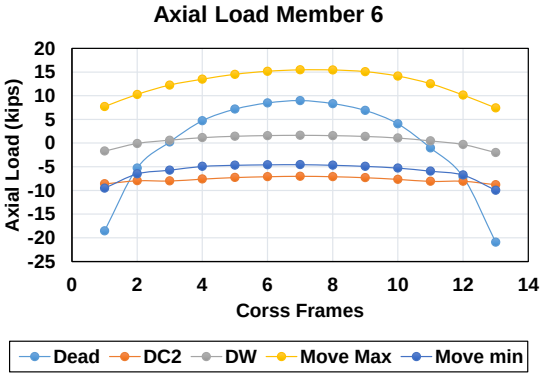

(a)

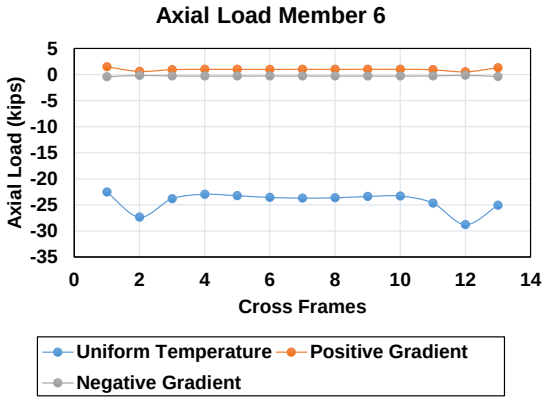

(b)

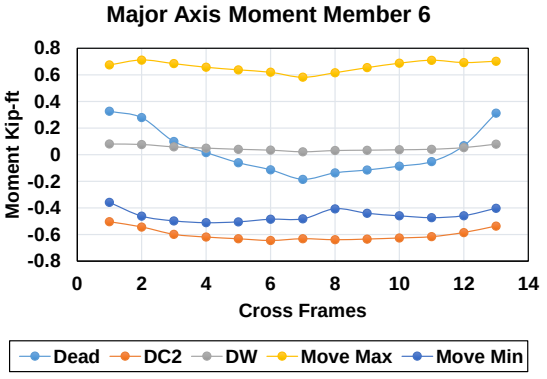

(c)

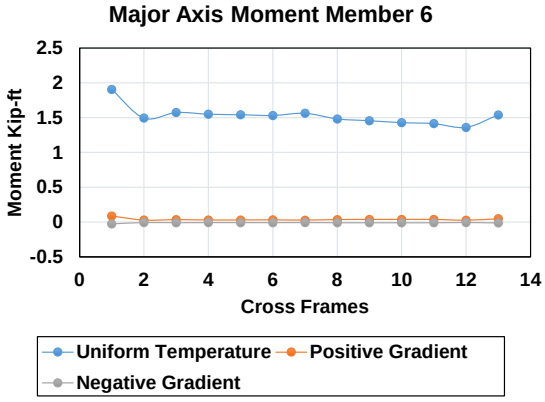

(d)

Figure 46. Forces in Member 6 within Span 4, right brace

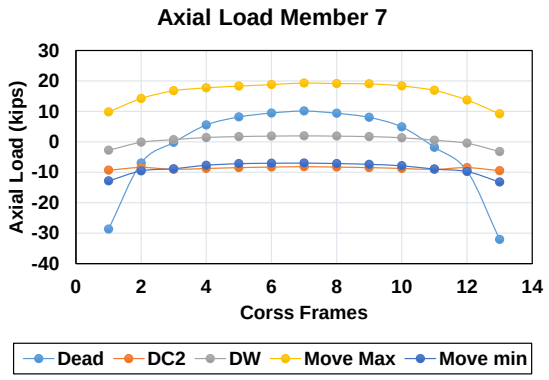

(a)

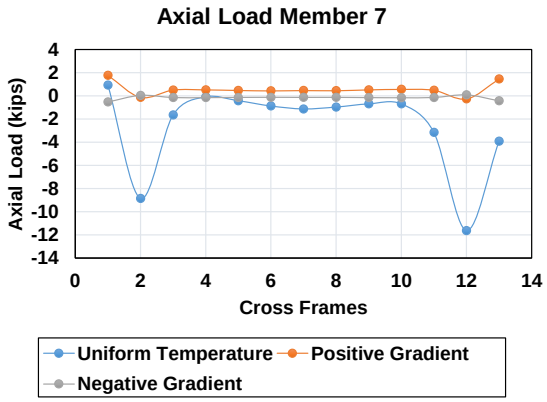

(b)

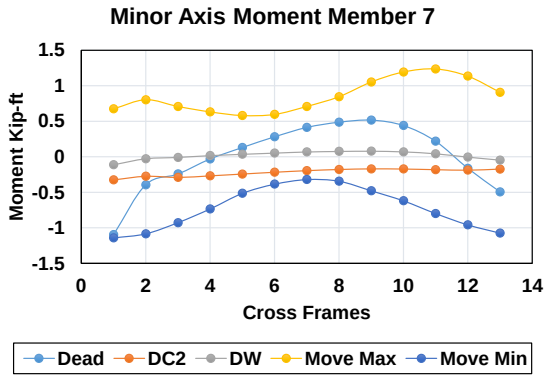

(c)

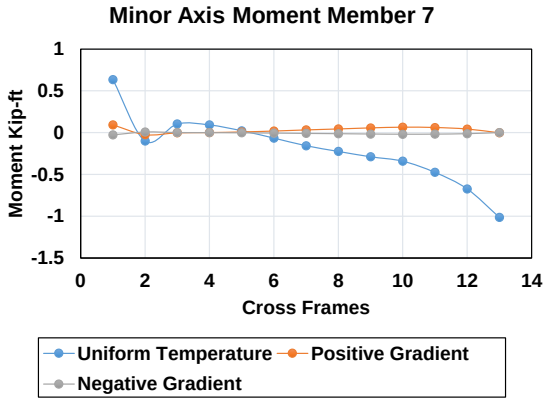

(d)

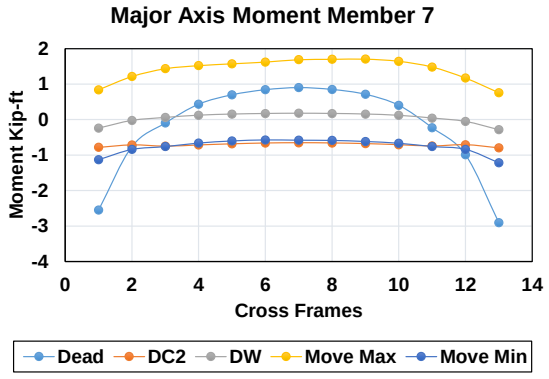

(e)

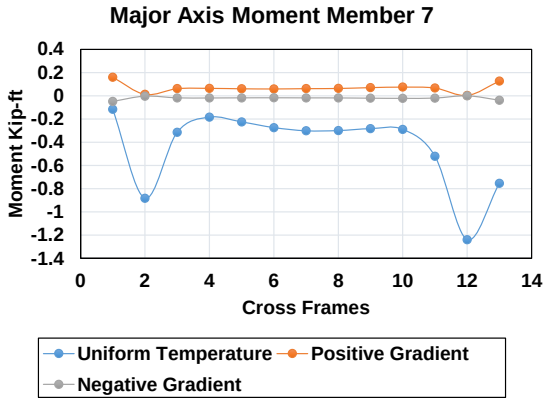

(f)

Figure 47. Forces in Member 7 within Span 4, right brace

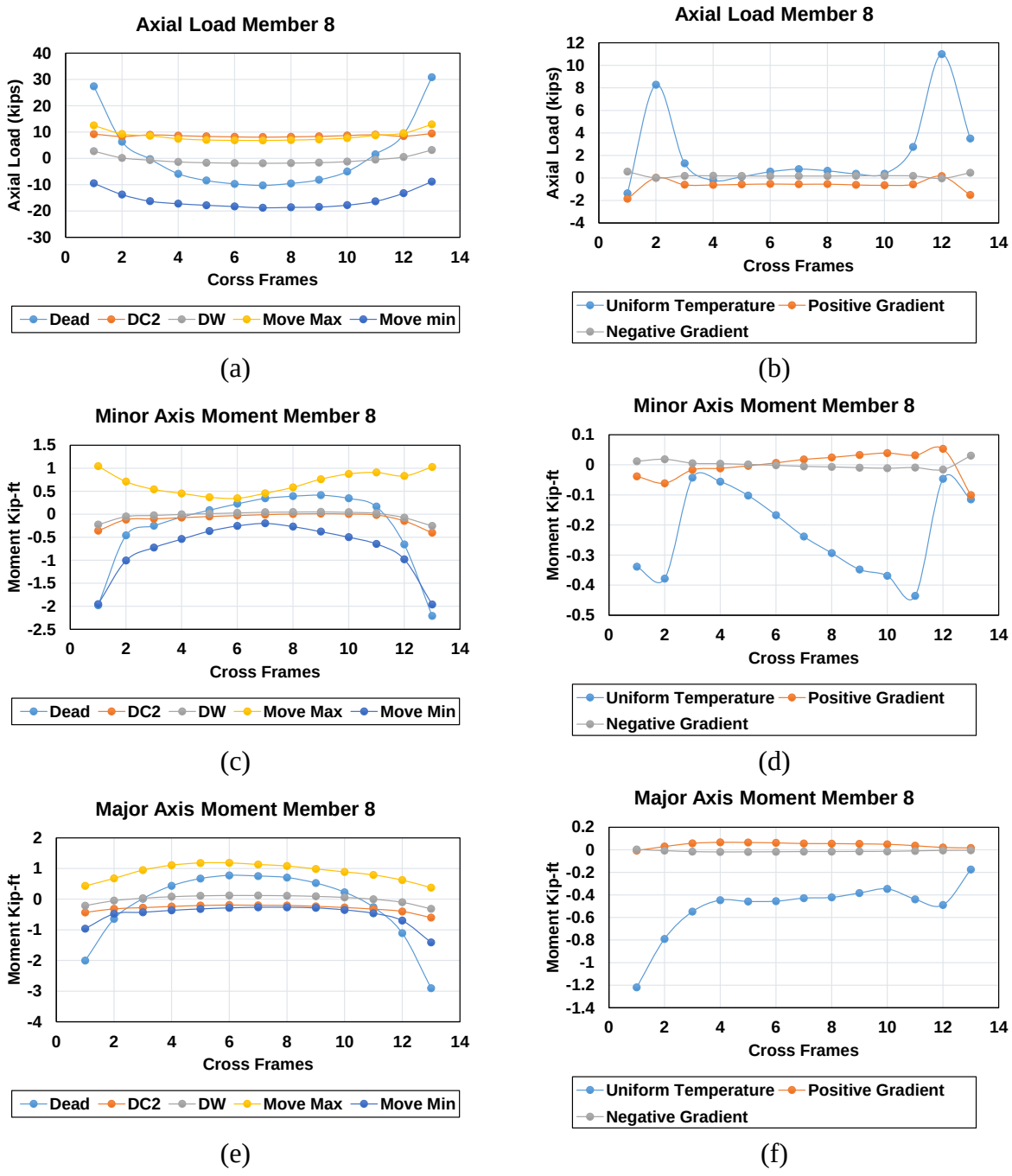

Figure 48. Forces in Member 8 within Span 4, right brace

Observations from the Numerical Analysis

The following observations resulted from the numerical analysis:

- During the upward movement due to temperature loading, the girders were forced to translate vertically and radially.

- At the fixed support, the bottom part of the web experienced excessive warping.
- Similar to the torsional response due to gravity loads, the girder cross-sections twisted within the unbraced length of the girders, creating a zigzag pattern of torsion forces. At the supports, the forces from this type of load distribution were substantial. (For the gradient load cases, no significant behavior was seen.)
- For the positive temperature gradient, the first and seventh spans experienced negative vertical translation (upward deflection), whereas the entire bridge cross-section twisted in the other spans. The direction of twisting was clockwise. For the negative temperature gradient, the opposite behavior was seen.
- As result of the upward deflection within the fourth span, there is a good chance of significant lateral forces acting on the bridge piers.
- The significant load pattern varied for the top chords of individual braces. For example, the top chord of the left brace was under heavy compression near the supports compared to the top chord of the right brace.
- Because of high torsion, large shear forces can form in the cross-frames, with high axial forces developing in individual members
- Removing the moment releases did not affect the bending moment, torsion, and shear of the girders. The results were found to be in accordance with the data provided by the Iowa DOT. The observed difference was about 5% to 10%.
- As a result of removing the moment release, the W-shaped members that formed the top chords at the abutments saw an increase in the axial forces and moments carried by those members.
- No significant increase in the axial forces of the individual members within the spans was observed as a result of removing the moment release. However noticeable differences were observed in the forces in the cross-frames near the supports.
- The forces in the top chords varied at the start and end locations. These are potentially important locations for strain gauges.
- The moment effects were minimal for the dead, DC2, DW, live, and temperature effects in the L 6 X 6 X 5/8 beams in the cross-frame sections. However, the W 16 X 67 beams had a higher moment demand when used as a top chord than when used in the angle sections. This may be because of the latter beam's higher stiffness compared to that of the L 6 X 6 X 5/8 used in the cross-frame sections.
- The axial load effects are most important because of the internal demand on individual members.
- The inclined struts (Members 3, 4, 7, and 8) had moments about their local two and three axes. The moment about the local two axis was greater than that about the local three axis. However, the magnitude was in the range of 0.5 to 0.9 kip/ft in some cases. The moments in the cross-frames near the supports are important for the combined axial load and flexure capacity of the members.
- The axial loads, too, are higher near the supports in the struts as well as in the top and bottom chords.
- Compared with the cross-frames within the spans, the moments and axial forces are larger at the cross-frames that are near the occurrence of the maximum positive moment.
- The axial forces in the interior cross-frames were observed to be minimal except in the high positive moment region.

- Member 1 (the top chord of the left brace) was observed to carry higher forces compared to Member 5 (the top chord of right brace). This pattern was observed in all intermediate cross-frames in all spans.
- The top chord of the left brace (Member 1) carried the maximum temperature loads, particularly when the member was closer to the supports. This was observed in all four spans.
- The magnitude of forces varied by as much as 50% between the start and end points of Member 1.
- The compressive forces caused by uniform temperature loads were at maximum for the top chord of the left brace for first and last three cross-frame locations in Spans 2, 3, and 4.
- For the inclined struts, the moments about the minor and major axes made a significant contribution.
- The temperature gradient magnitudes were observed to be small when compared to the uniform temperature range (about 2% to 5%).
- The results of the analysis suggest that the left brace was greatly affected by temperature loading.
- Within the positive bending moment region, the magnitude of loads was similar to the magnitude for the adjacent members.

As a general overview, following the labels provided in Figure 16, the set of plots presented in Figures 17 through 48 report the magnitude of force/moment (i.e., axial load as well as major-axis and minor-axis moment) expected in each cross-frame member of Span 1 through 4. This helped identify the most critical cross-frames from the numerical simulation results. In particular, Figure 49 below shows the demand/capacity ratios (DCRs) of the cross-frames located at the midspan and near the support of all four spans. Furthermore, Figures 56 through 59 below present the strain gauge readings, which have been paired with their corresponding maximum and minimum stress values, as presented in Figures 60 through 63 below. The DCRs suggest that the top chord (i.e., Member 1) of the left brace (between Girders A and B) near the supports can experience a high DCR in the case of the service load combination. A comparison of the service load combination to the strength load combination was also made to evaluate the governing load combination. This led to the conclusion that the top chords are fine when evaluated using the strength load combination.

In the following section of this chapter, a summary of the DCRs is provided for the cross-frames, where bullet points 4 and 5 highlight the higher forces observed in the top chord of the cross-frames. A subsequent chapter in this report also presents the strains and stresses due to temperature that were recorded in the field from September through November 2019 (Figures 56 through 59). During this period, the maximum equivalent stress observed in the top chord located near the support of Span 4 was 5 ksi. Considering that the angles are made of A36 steel, which has a yield strength of 36 ksi, it was evident that the top chord is not overly stressed. However, when the DCR of the top chord was evaluated, the service load combination was found to be critical. The following Strength I and Service I combinations were used to derive the maximum DCRs, as per AASHTO:

- Strength Combination: 1.25×DL+1.25×DC2+1.5×DW+1.75×LL+0.5×TU
- Service Combination: 1.0×DL+1.0×DC2+1.0×DW+1.0×LL+1.0×TU

The service limit state is generally considered to limit the stress, deformation, and crack widths under regular service conditions, whereas the strength limit state is intended to ensure that strength and stability, both local and global, are provided to resist the specified load combination (AASHTO 2014). Thus, the variation in DCRs stems from the difference in the load factors used in the Strength I and Service I load combinations.

For the numerical simulations, a uniform temperature loading of 150°F was considered, following AASHTO 3.12.2.1-1 (plus DL, DC2, and LL). This led to the finding that the DCR of the top chord installed between Girder A and B can exceed 1.0 in service, which suggests a need for further evaluation during the design phase. In reality, however, the temperature range recorded by the research team in the field did not exceed 90°F during the period from September through November 2019. The equivalent maximum forces recorded in the cross-frames during the field tests were in the range of 6.5 kips. This loading demand is not significant, especially with the angles stressed to only 4% (under compression) and 3% (under tension) of their capacity. This led to the conclusion that the live load effect is not as significant as the thermal load effect.

Demand/Capacity Ratios of Brace Members

To study the combined effect of all forces, the DCRs of the individual members of the cross-frames at midspan and near the supports were plotted (Figure 49).

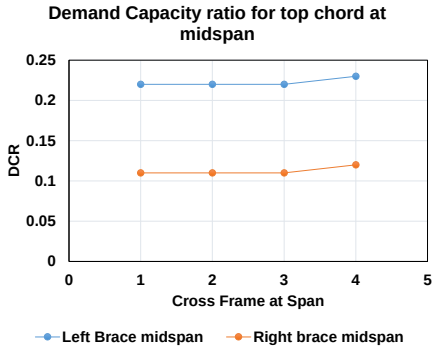

(a)

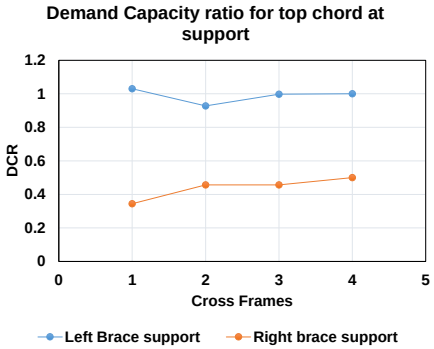

(b)

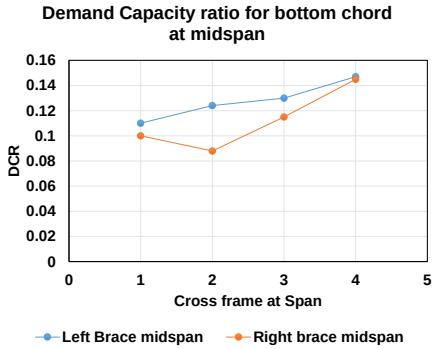

(c)

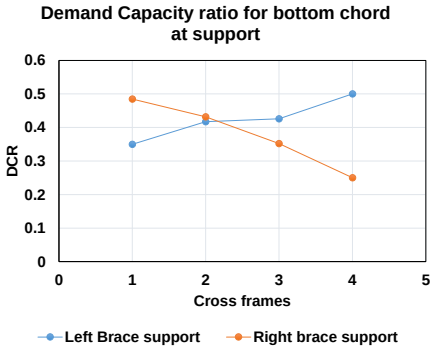

(d)

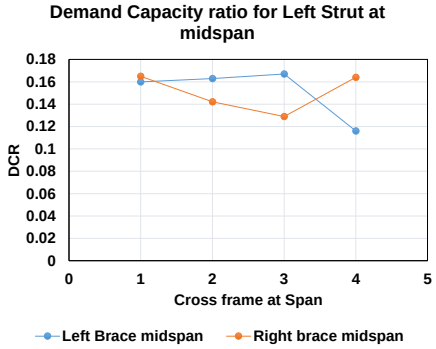

(e)

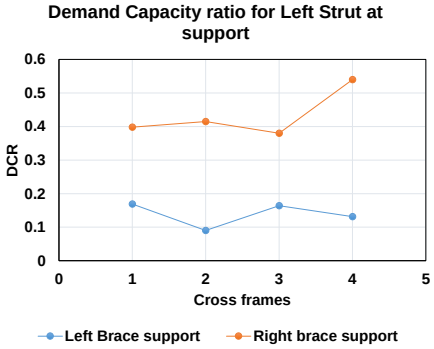

(f)

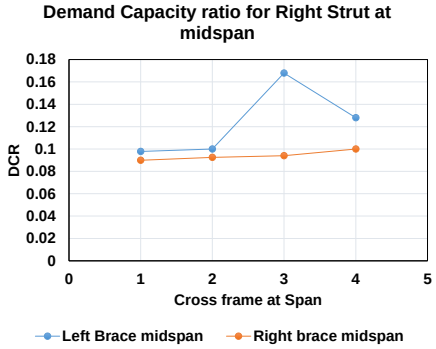

(g)

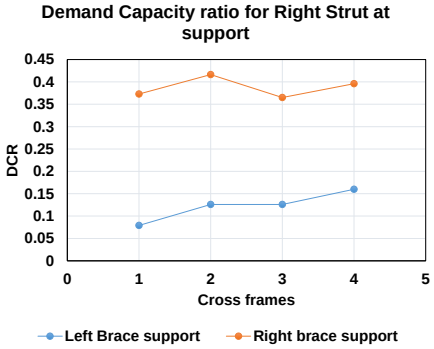

(h)

Figure 49. Demand/capacity ratios of the members of the cross-frames at midspan and near the supports

Plotting the DCRs provided an opportunity to understand the capacity of the cross-frames. The capacity of the members under combined axial tension, axial compression, and flexure was calculated according to AASHTO 6.8.2.3 and 6.9.2.2:

If $\frac{P_u}{P_r} < 0.2$, then

$$\frac{P_u}{2.0P_r} + \left(\frac{M_{ux}}{M_{rx}} + \frac{M_{uy}}{M_{ry}}\right) \leq 1.0$$

If $\frac{P_u}{P_r} \geq 0.2$, then

$$\frac{P_u}{P_r} + \frac{8}{9}\left(\frac{M_{ux}}{M_{rx}} + \frac{M_{uy}}{M_{ry}}\right) \leq 1.0$$

The following observations were made in the study of the DCRs:

- The results of the analysis suggest that the left brace was greatly affected by temperature loading.
- Within the positive bending moment region, the magnitude of loads was in a similar range to the magnitude for the adjacent members.
- When uniform temperature loading was present, the top chord of the left brace loaded to its capacity. Thus, it was found that the cross-frames near the interior bridge supports would require special design consideration compared to the intermediate cross-frames.
- The DCRs of the top chords show that even within the positive bending moment region, the left brace carried as much as twice the load carried by the top chord in the right brace.
- The cross-frames near the supports were found to have higher DCRs than the other cross-frames, and the loads predicted by the numerical analysis for the cross-frames near the supports are three times higher than the loads predicted for the cross-frames at midspan.

LONG-TERM INSTRUMENTATION LAYOUT

Instrumentaion Plan

The long-term instrumentation layout for the Story County bridge was designed to study the effects of environmental conditions such as temperature on the cross-frames by measuring changes in strains, displacements, and temperatures during the bridge monitoring period for the project. During the analysis phase, it was noticed that there is a significant difference between the left and right braces in terms of the start and end locations of the top chords. Regarding the behavior of bridges under thermal loading, Moorty and Roeder (1992), Beckett (2013), and Reynolds (1972) noted that significant movements and forces have been detected near the fixed bearings of bridges. Therefore, to measure the maximum recorded forces within the cross-frames, Span 4 was chosen for instrumentation. The exterior cross-frame at the midspan of Span 4 and the exterior cross-frame near the fixed bearing were instrumented. Figure 50 shows the instrumented locations.

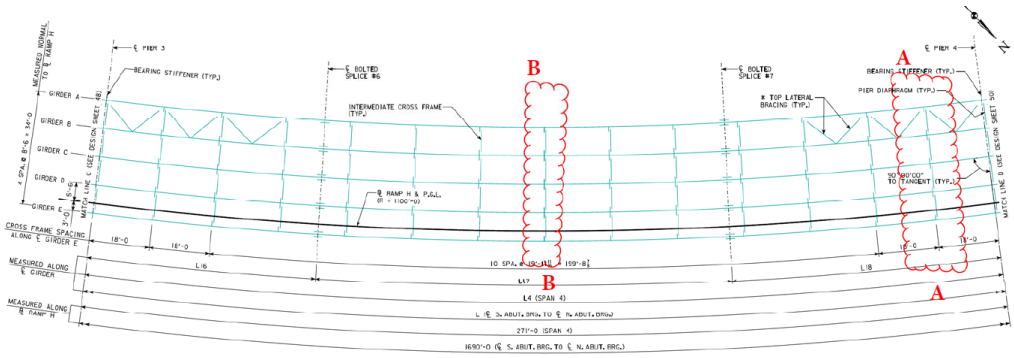

Figure 50. Layout of the instrumentation plan for the Story County bridge

Section A-A is the instrumented location near the support, while Section B-B is the instrumented location at the midspan of Span 4. The vertical legs of the angle section were instrumented with strain gauges, as shown in Figures 51 and 52.

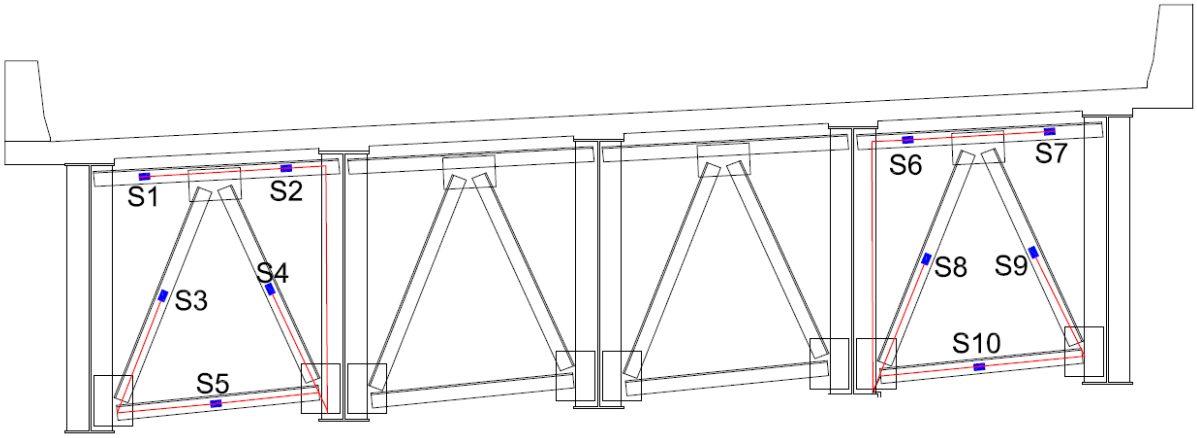

Figure 51. Location of strain gauges in Section A-A

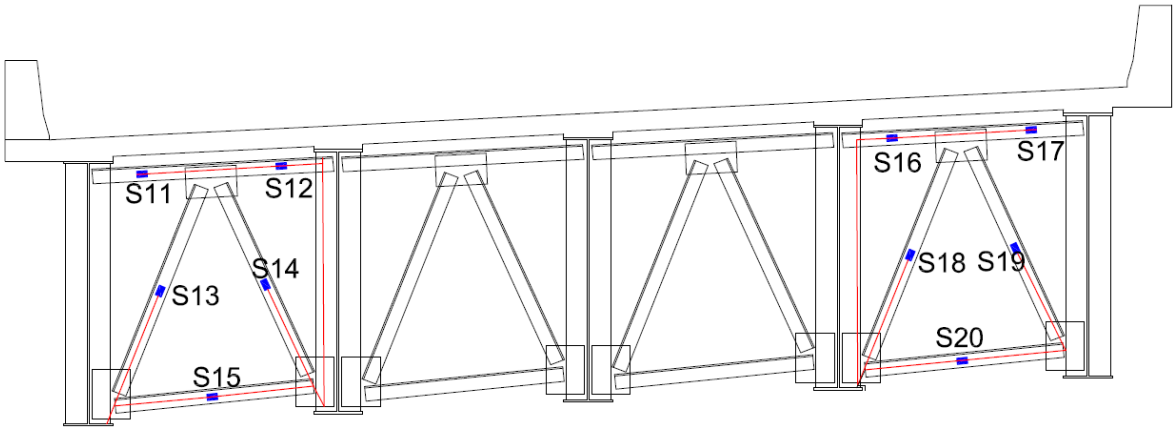

Figure 52. Figure 51 Location of strain gauges in Section B-B

Figure 53 shows the location of the strain gauges on the cross-frames.

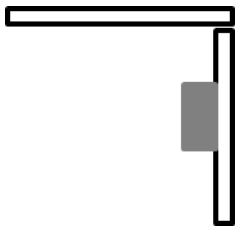

Figure 53. Strain gauge location on the cross-frames

Strain Gauge Installation

The gauges that were selected for the purpose of measuring strain and temperature were Geokon 4150 vibrating wire strain gauges (Geokon 2017). The Model 4100/4150 strain gauge has a 51 mm gauge length (3,000 με range, 1 με sensitivity) and is specifically designed to measure

strains on the surface of steel structures and, for Model 4150, on reinforcement bars where space may be limited. The gauge consists of a steel wire tensioned between two mounting blocks that are attached to stainless steel shim-stick tabs, which can be spot welded as shown in Figure 54.

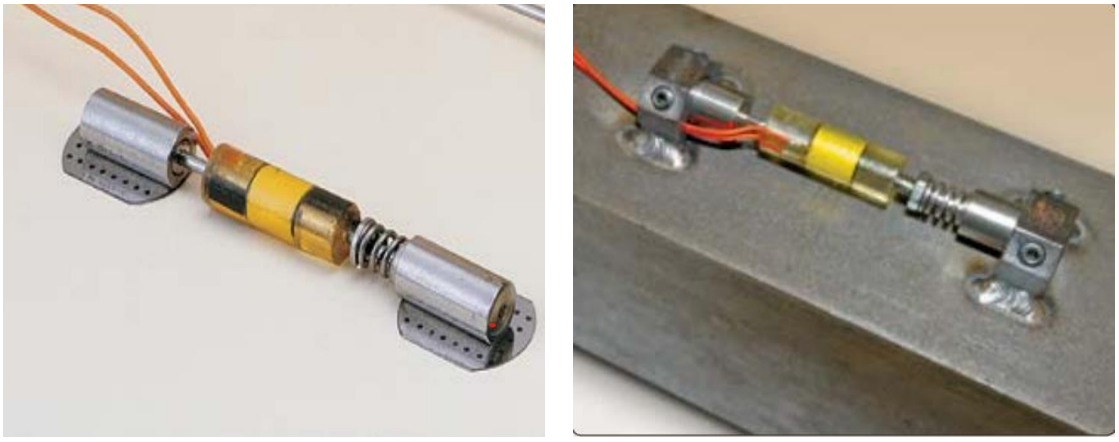

(a) (b)

Figure 54. Geokon Model 4150 strain gauge

The gauge is installed quickly and easily by means of a capacitive discharge spot welder or, for short-term use, with special epoxy adhesives; the latter method of attachment permits the use of this gauge on concrete. In the instrumentation phase for the present project, the gauges were installed using spot welds.

Deformation or movement in the structure due to load effects causes the welded ends of the mounting blocks to move relative to one another, which causes a change in tension within the wire and a corresponding change in the resonant frequency of the vibration of the wire. The wire is plucked by means of an electronic coil and a permanent magnet connected by a signal cable to a readout, which sends voltage pulses to the coil. The vibration produced in the wire by the voltage pulse induces an alternating current in the coil. The frequency of the alternating current is the same as the vibration frequency of the wire, which is measured using the readout. The frequency is squared and multiplied by a constant so that the values displayed by the readout are presented directly in microstrain. The Model 4150 strain gauges are small enough to be used in confined spaces and have excellent long-term stability, maximum resistance to the effects of water, and a frequency output suitable for transmission over very long cables. Each gauge is also equipped with a thermistor to record temperature (Geokon 2017).

The guages were installed on the cross-frames of the Story County bridge during construction while the girders were on the ground (Figure 55). Thus, the data analysis that was performed included the effects of girder lifting on the forces generated in the cross-frames.

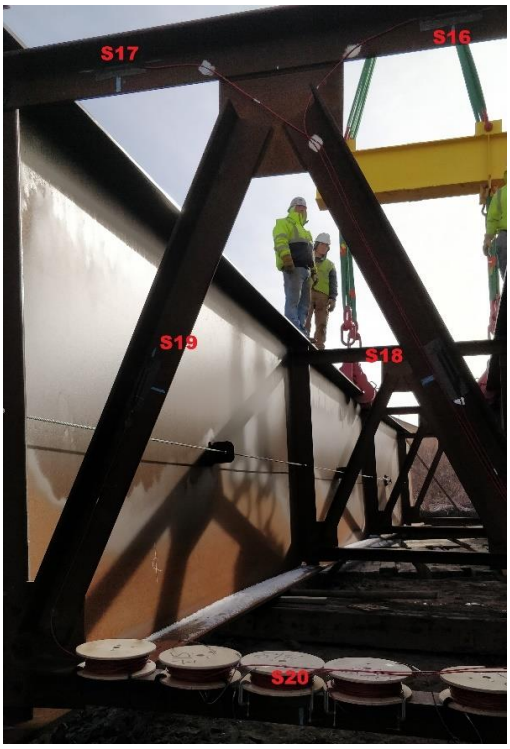

Layout of S16-S20

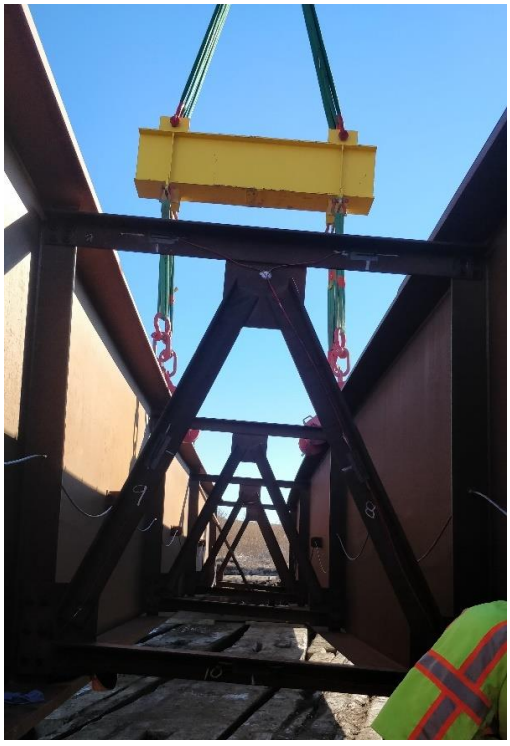

Layout of S11 – S15

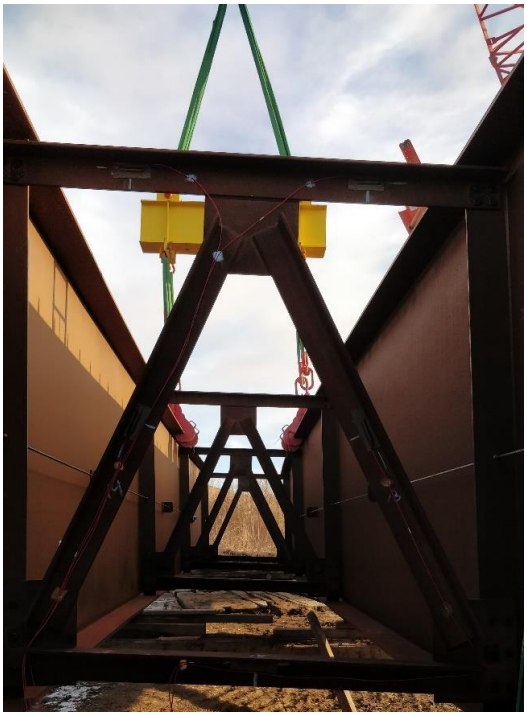

Layout of S6 – S10

Layout of S1 – S5

Figure 55. Strain gauge installation on cross-frames

Results

The initial readings taken while the girders were on the ground are presented in Table 4.

Table 4. Initial readings from strain gauges on the Story County bridge

Gauge	11-Dec		12-Dec		13-Dec		17-Dec		20-Dec	
No.	µE	°C	µE	°C	µE	°C	µE	°C	µE	°C
S16	2425.6	8.5	2469.1	1.9	2489	2.9	-	-	-	-
S17	2483.6	5	2241.2	1.9	2248.2	2.9	-	-	-	-
S18	2438.7	1.7	2363.3	161	2338.1	1.9	-	-	-	-
S19	2385.4	4.5	2554.2	1.4	2576.8	1.9	-	-	-	-
S20	2447.4	3	2440.7	1.4	2445.5	1.9	-	-	-	-
S11	-	-	2201.7	4.8	2233.5	3	-	-	-	-
S12	-	-	2309	5.9	2357.5	2.9	-	-	-	-
S13	-	-	2363.3	2.8	2413.5	1.5	-	-	-	-
S14	-	-	1508.7	3.4	1479.7	2	-	-	-	-
S15	-	-	2456.6	2.9	2463.3	2	-	-	-	-
S6	-	-	-	-	-	-	2466.8	17	-	-
S7	-	-	-	-	-	-	2455.3	16.6	-	-
S8	-	-	-	-	-	-	2433.5	5.6	-	-
S9	-	-	-	-	-	-	2483	17.7	-	-
S10	-	-	-	-	-	-	2490.6	7	-	-
S5	-	-	-	-	-	-	-	-	2276.9	2.4
S4	-	-	-	-	-	-	-	-	2369.6	1.5
S3	-	-	-	-	-	-	-	-	2716.6	2.8
S2	-	-	-	-	-	-	-	-	2650	1.5
S1	-	-	-	-	-	-	-	-	2699.2	2.2

The time histories for strain and temperature over a two-month period between September 26 and November 25, 2019 were studied. These time histories are presented in Figures 56 through 59.

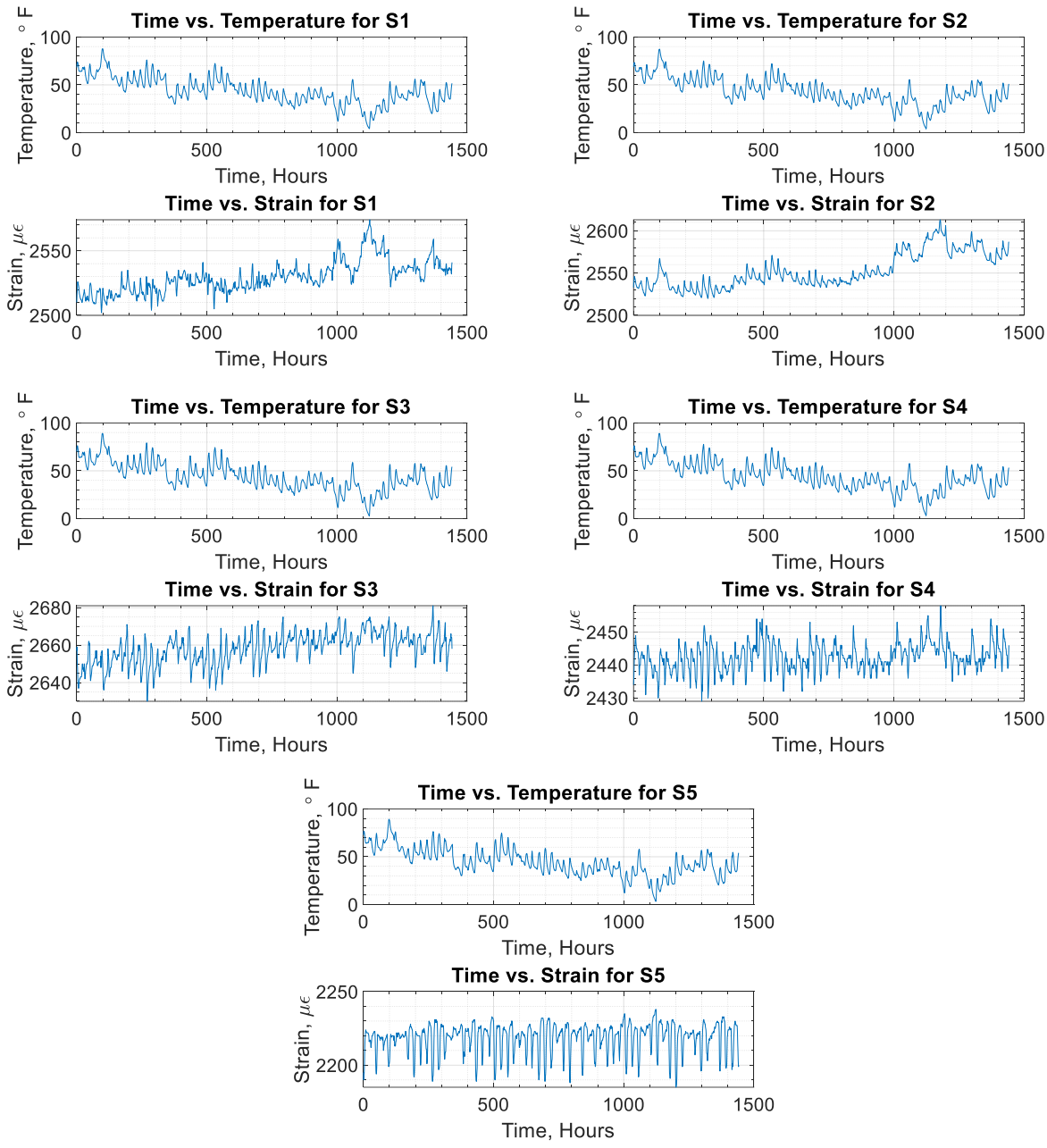

Figure 56. Observed strain gauge readings for cross-braces 1 through 5 from September through November 2019

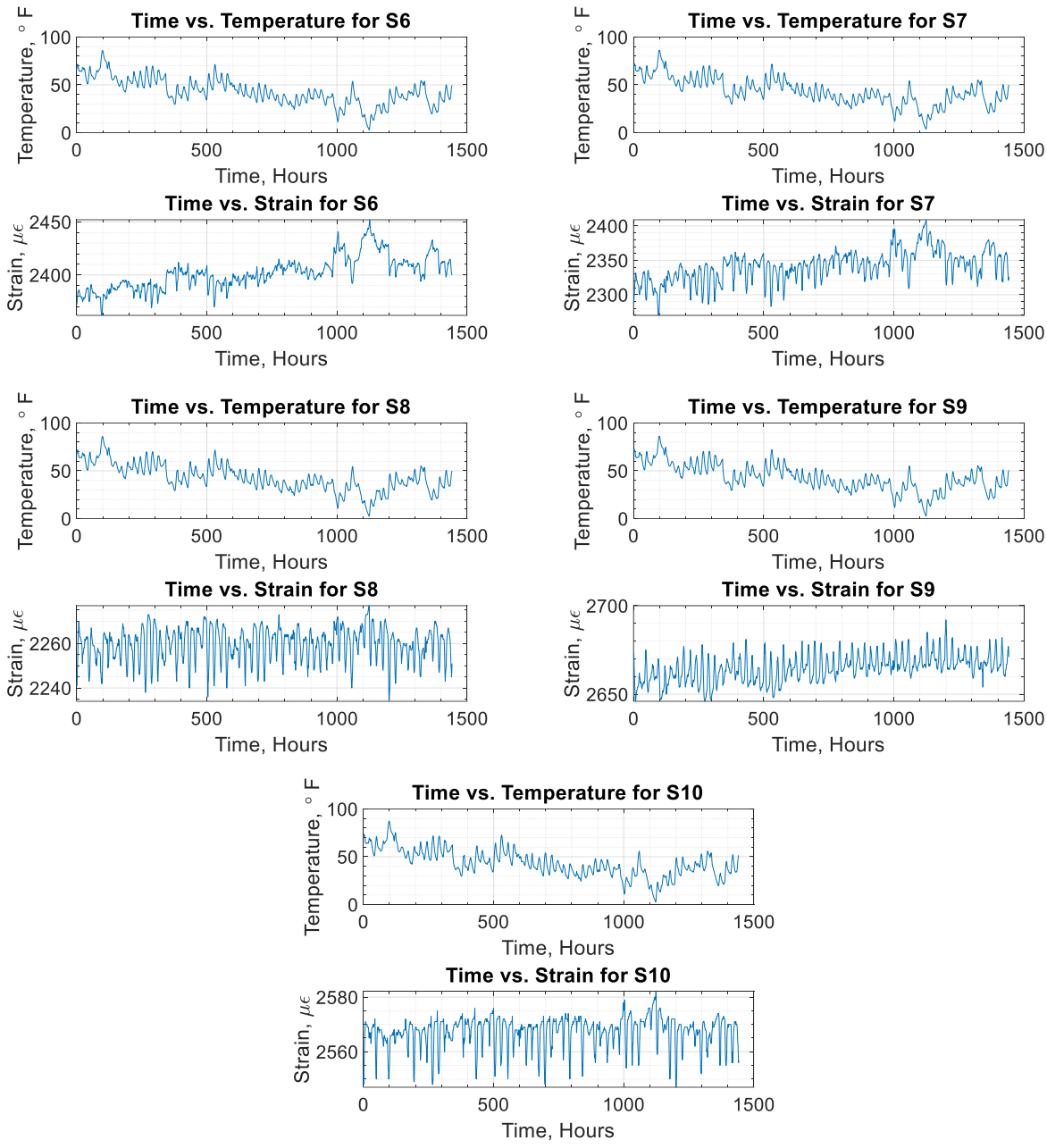

Figure 57. Observed strain gauge readings for cross-braces 6 through 10 from September through November 2019

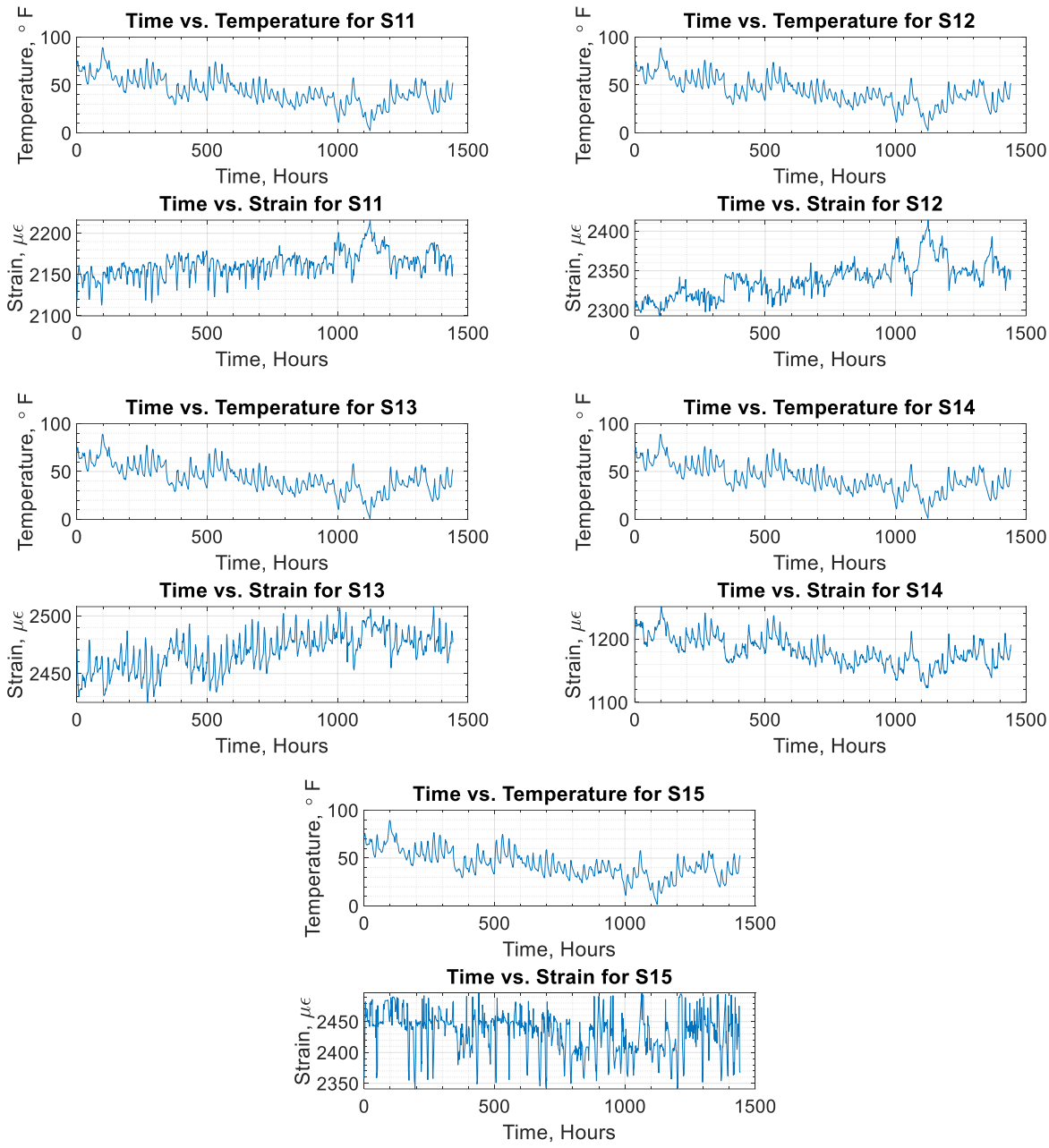

Figure 58. Observed strain gauge readings for cross-braces 11 through 15 from September through November 2019

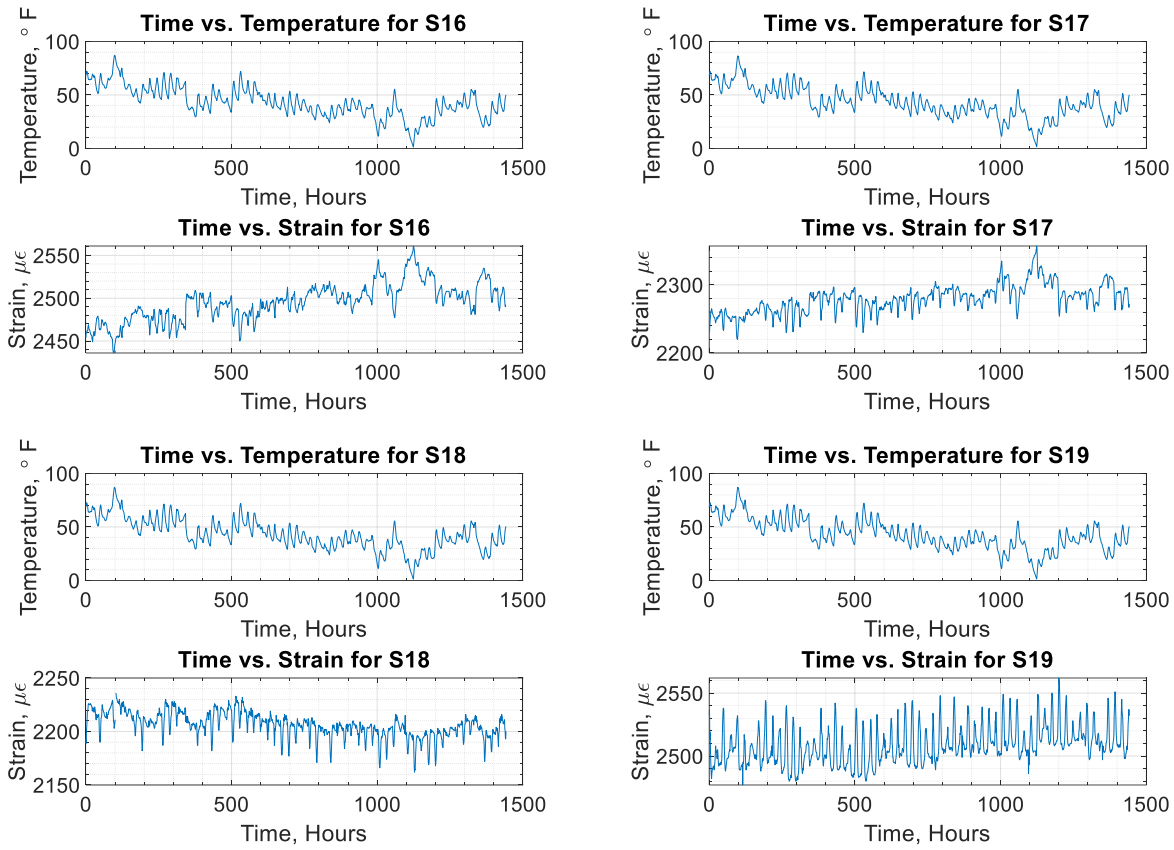

Figure 59. Observed strain gauge readings for cross-braces 16 through 19 from September through November 2019

During the two-month period between September and November 2019, the two occasions when the maximum and minimum temperatures were recorded were identified. A total window of 48 hours was studied for each occasion. The stress levels observed when these maximum and minimum temperatures were recorded are presented in Figures 60 through 63.

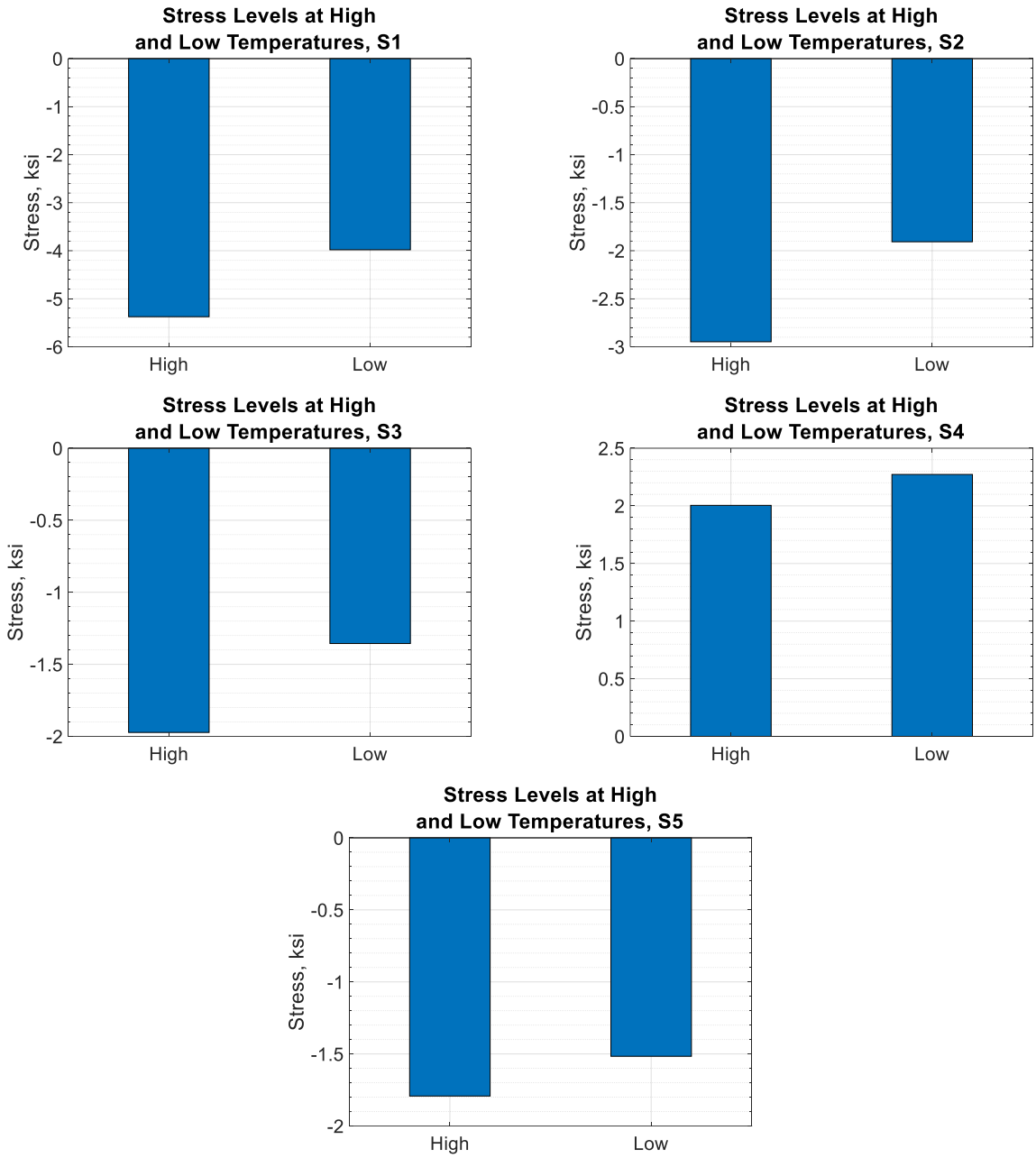

Figure 60. Observed stress levels at maximum and minimum temperatures for cross-braces 1 through 5 from September through November 2019

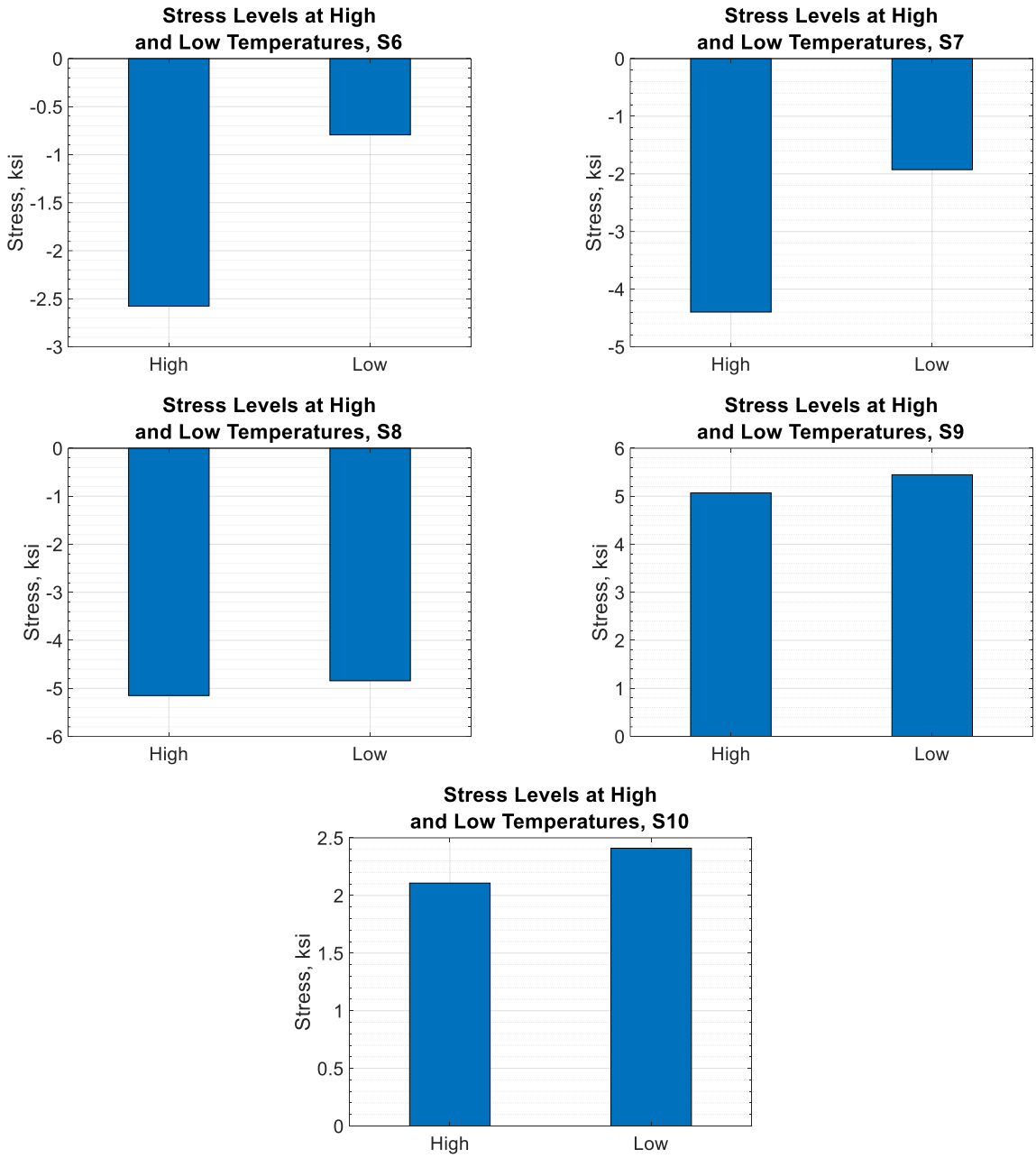

Figure 61. Observed stress levels at maximum and minimum temperatures for cross-braces 6 through 10 from September through November 2019

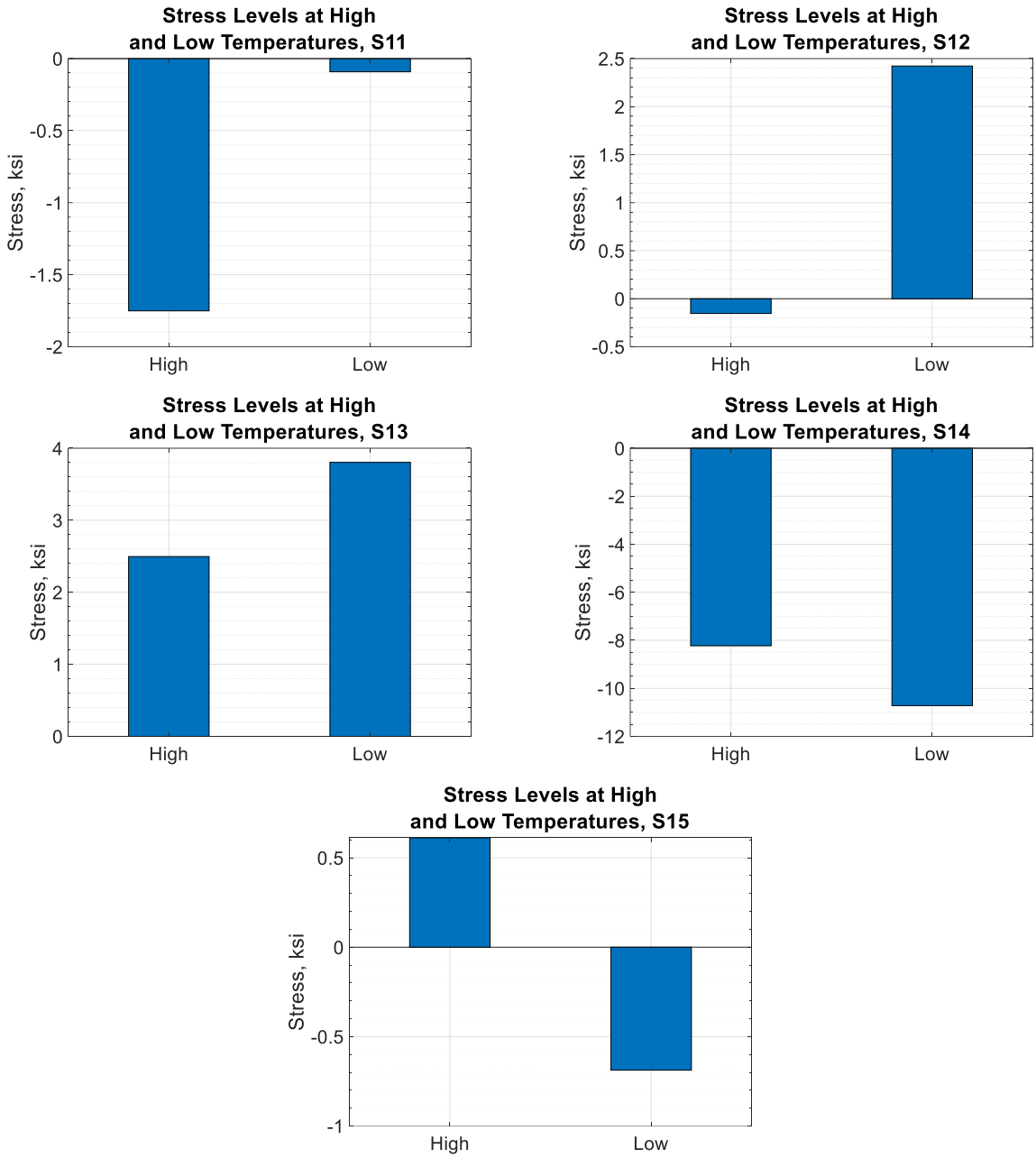

Figure 62. Observed stress levels at maximum and minimum temperatures for cross-braces 11 through 15 from September through November 2019

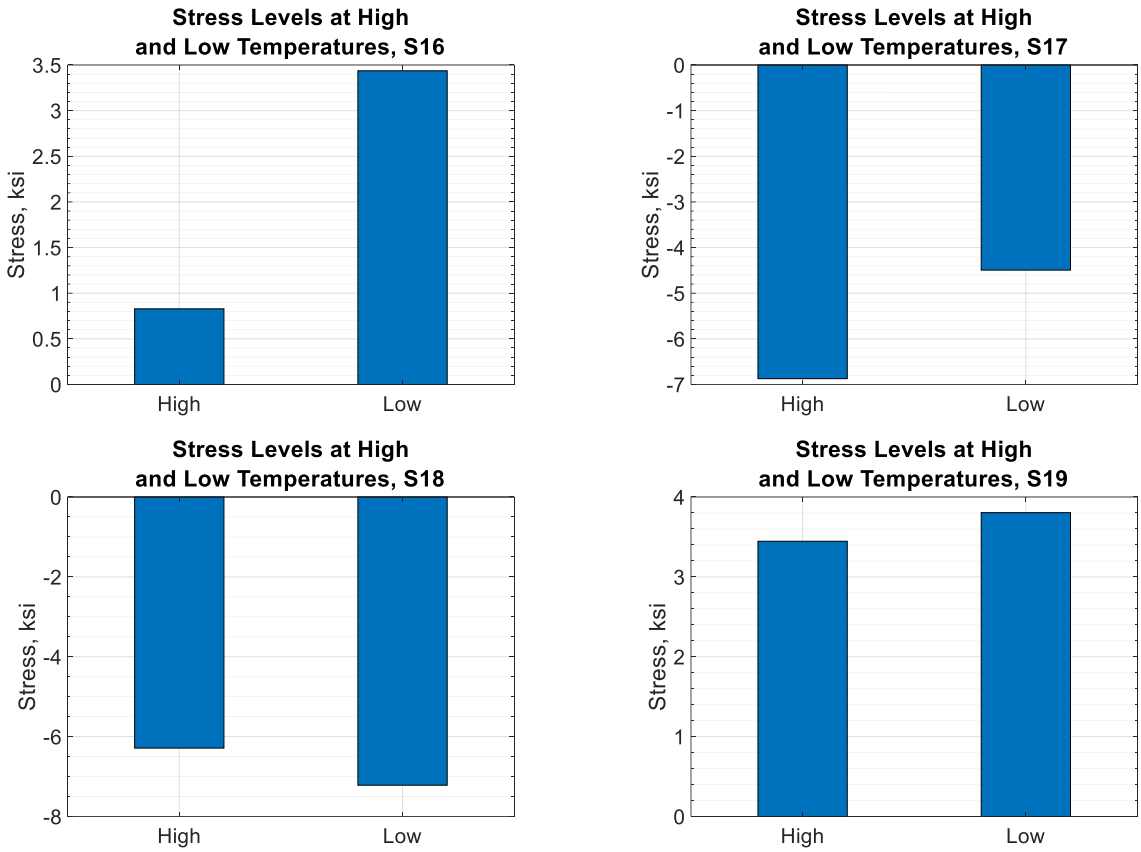

Figure 63. Observed stress levels at maximum and minimum temperatures for cross-braces 16 through 19 from September through November 2019

Temperature versus stress plots were generated for each strain gauge. The mean stresses during the maximum and minimum temperatures were plotted, and the maximum and minimum stresses recorded during the entire two-month period were plotted for comparison. A negative sign indicates compression, whereas a positive change in strain indicates tension. The difference in strain was calculated using the following equation:

$$\Delta\mu\varepsilon = (R_1 - R_0) \times B \times G \times E$$

where R_0 is the initial reading of the strain gauge taken when the girders were on the ground.

The temperature versus stress plots are presented in Figures 64 through 67.

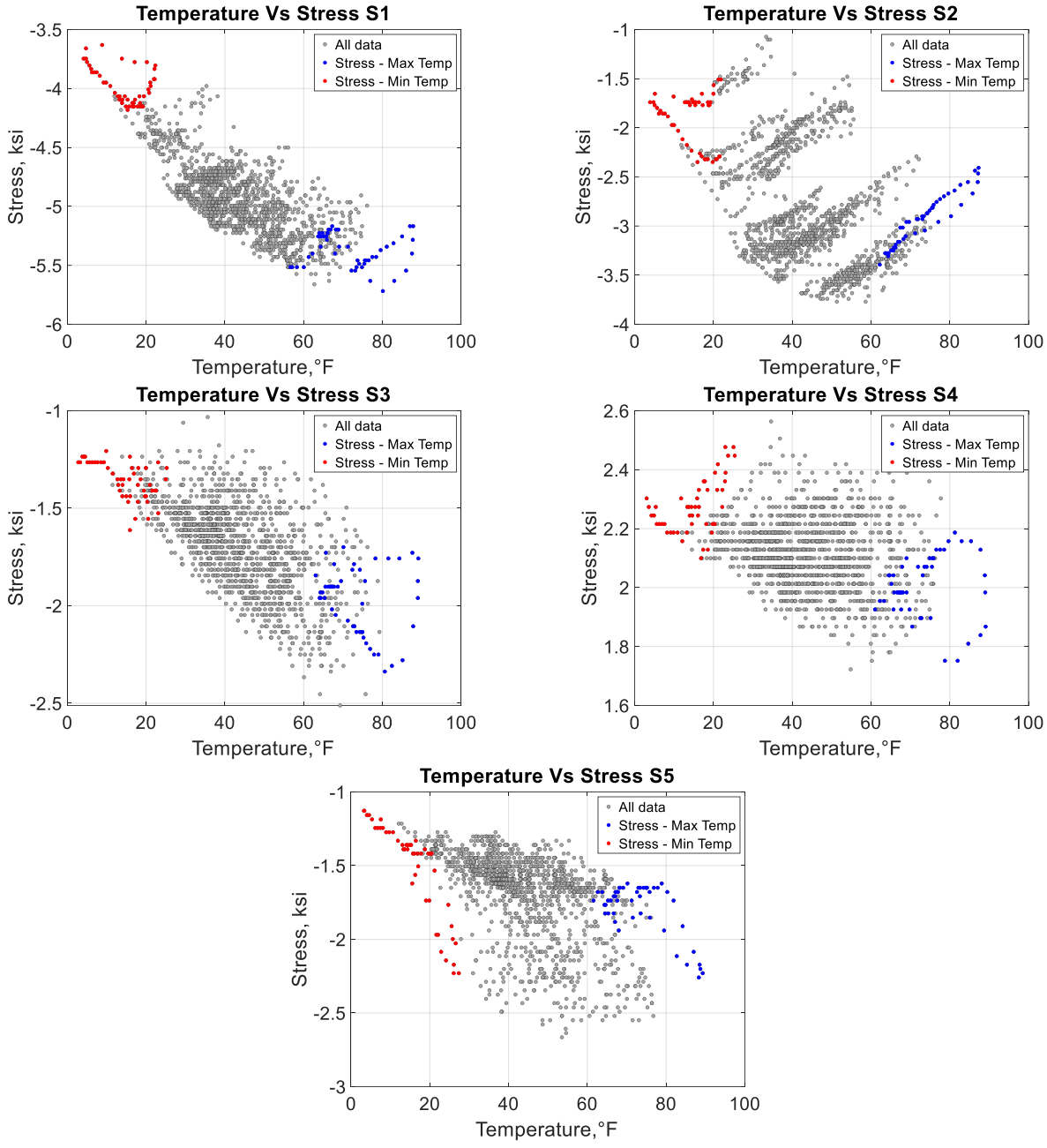

Figure 64. Temperature versus stress for cross-braces 1 through 5 from September through November 2019

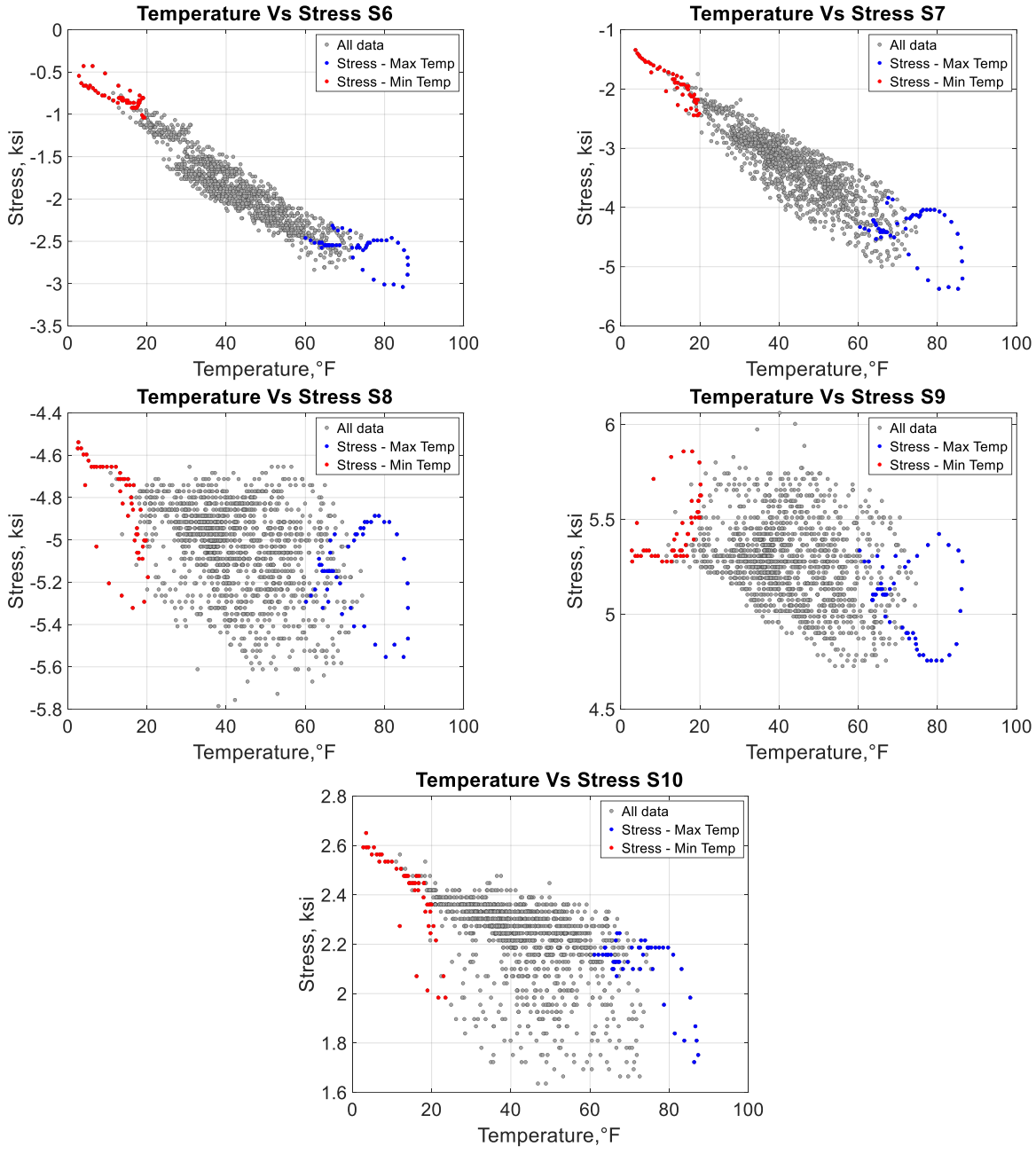

Figure 65. Temperature versus stress for cross-braces 6 through 10 from September through November 2019

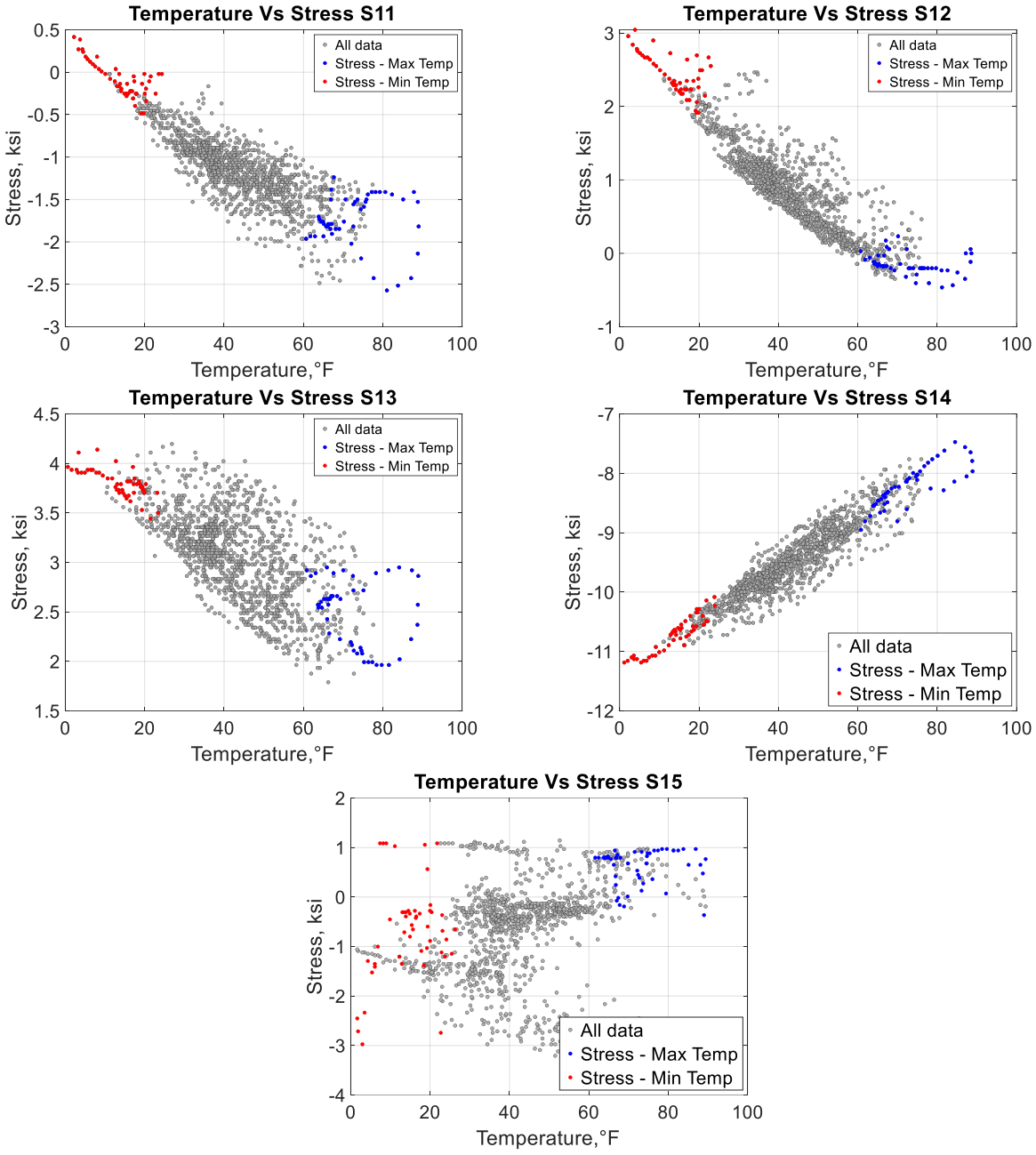

Figure 66. Temperature versus stress for cross-braces 11 through 15 from September through November 2019

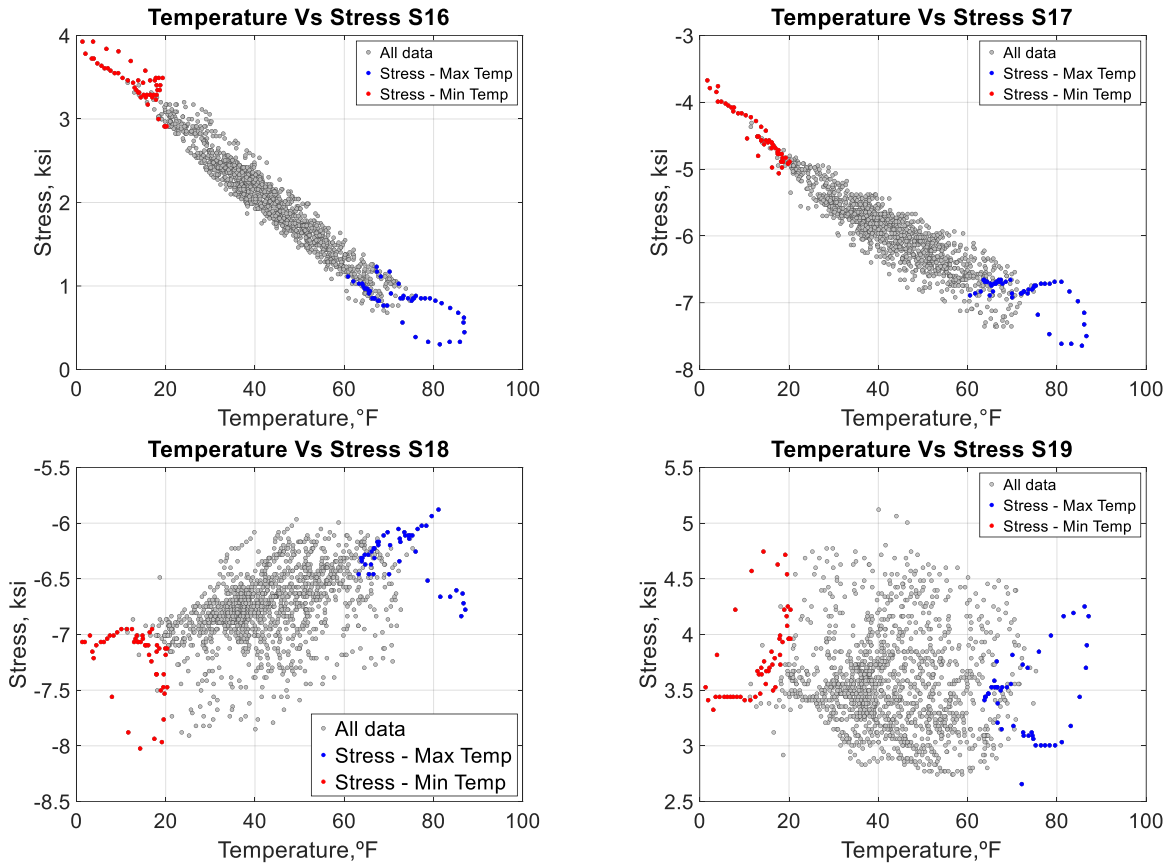

Figure 67. Temperature versus stress for cross-braces 16 through 19 from September through November 2019

The following conclusions were made regarding the temperature load effects on the cross-frames:

- The readings on Gauges S1, S4, S6, S7, S11, S12, S14, S16, and S17 illustrate that the forces in the members were highly dependent on temperature fluctuations.
- The overall trends in the range of stress values observed suggest that during the maximum and minimum temperatures, most members of the cross-frames experienced their maximum and minimum stresses, except for the members in the inclined cross-frames.
- A maximum compressive stress value of 11 ksi was found in Gauge S14 during the minimum temperature period.
- As anticipated from the FEM, a difference in stress of about 6 to 8 ksi was observed within the top chord member in the cross-frame located on Section B-B near the middle of the span. Top chords and their connections may become vulnerable to higher stress differences during extreme sustained and fluctuating temperatures.

LIVE LOAD TESTS

Introduction

To monitor changes in the cross-frames of the Story County bridge due to live loads, the cross-frames were instrumented with strain gauges. It was decided that Span 4 would be instrumented for live load testing because the maximum moments in the girders were observed in this span during the numerical analysis. Additionally, fixed bearings had been installed at the ends of Span 4, and previous studies have suggested that forces are especially pronounced near fixed bearings, where movement of the girders is restricted. Eighty strain transducers were installed at two of the cross-frames and on the flanges of the girders based on the numerical analysis results. The instrumented locations are shown in Figure 68.

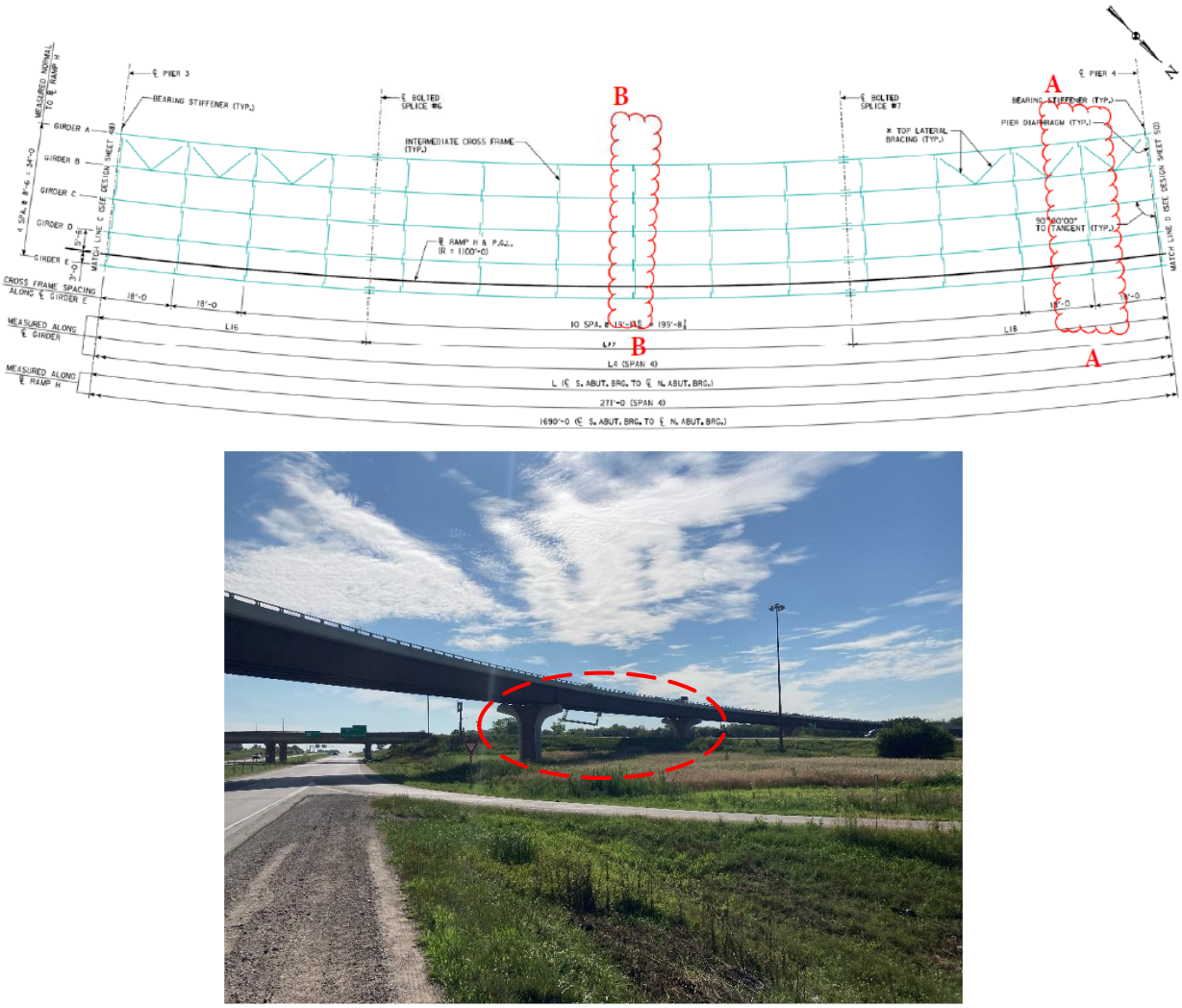

Figure 68. Structural steel framing plan for a section of Span 4 with the instrumented cross-frames highlighted (top) and a photograph of the instrumented span (bottom)

Instrumentation Plan

The proposed layout of the instrumentation for live load testing is shown in Figures 69 and 70.

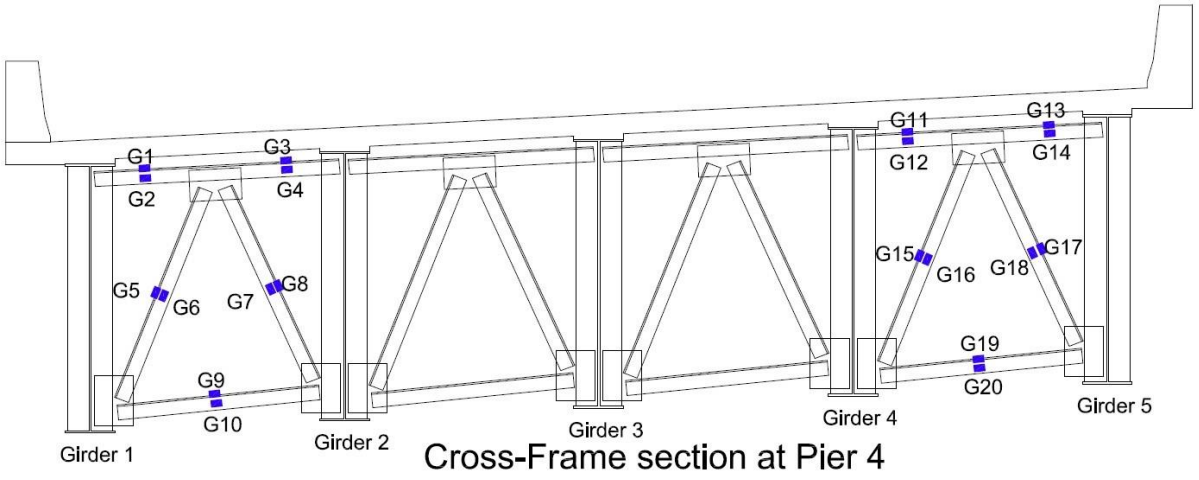

Figure 69. Strain gauge locations for live load tests (A-A)

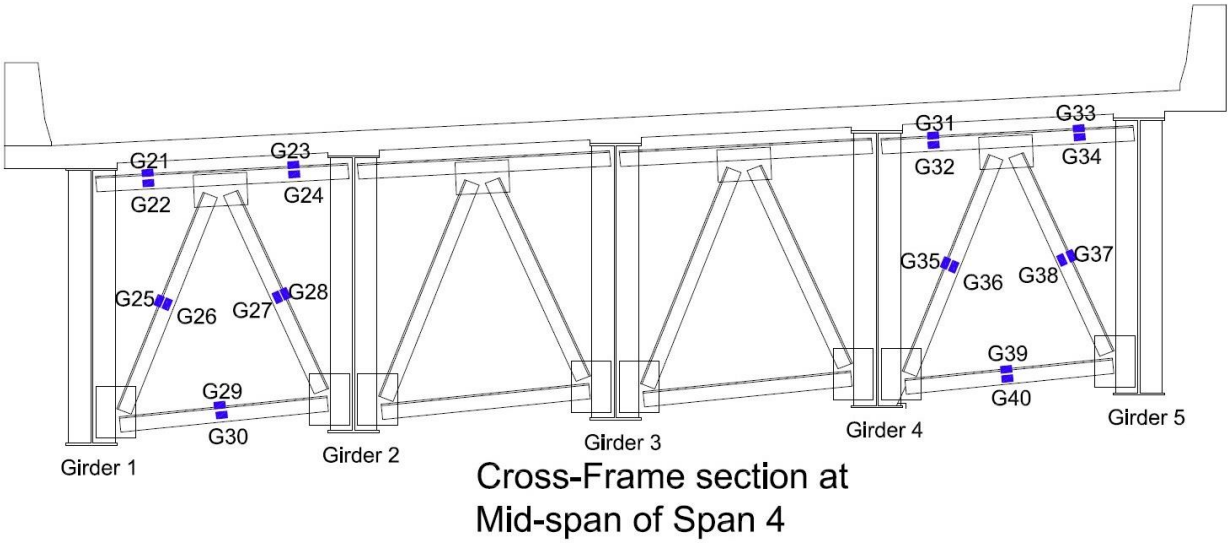

Figure 70. Strain gauge locations for live load tests (B-B)

Forty strain transducers were installed on both legs of the cross-frames at the midspan and end span of Span 4 in the exterior bays only (twenty sensors per cross-frame). Twenty-four sensors were installed on Girders 1, 3, and 5 at the midspan of Span 4 and at the location of the first cross-frame near Pier 4. Eight strain transducers were installed in the transverse direction on the top and bottom flanges of two exterior girders at the two cross-sections (sixteen sensors in total for both girders). The locations where sensors were connected to the girders and cross-frames are shown in Figure 71.

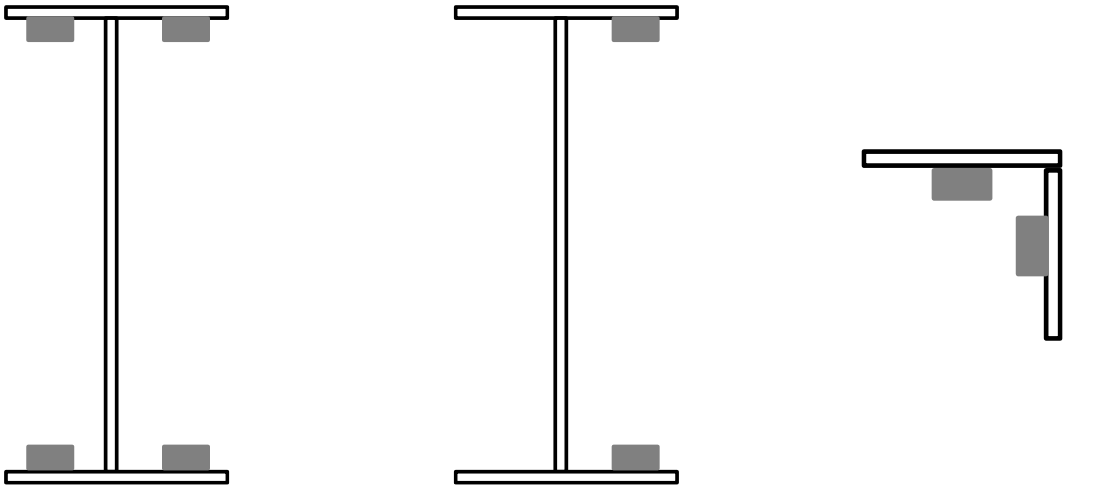

(a) Strain Gauge location for Girders 1,3 and 5

(b) Strain Gauge location for Girders 1 and 5

(c) Strain Gauge location for cross-frames

Figure 71. Strain gauge locations for live load test instrumentation

Figure 72 shows the installation of the strain gauges and an installed strain gauge on a steel girder.

(a)

(b)

Figure 72. (a) Instrumentation installation and (b) strain gauge installed on a steel girder

Loading Plan

The bridge was tested using ambient traffic with the aim of understanding the structural response of the girders and the cross-frames under different truck loadings. The data were collected as the traffic passed over the full length of the bridge, during which the type of each vehicle was recorded. The load cases tested in this study are documented in Table 5 in chronological order.

Table 5. Load cases used for live load testing

Load case	Description
LC 1	8 cars
LC 2	6 cars
LC 3	A volume of large trucks
LC 4	**2 large trucks**
LC 5	2 trucks plus random traffic
LC 6	1 semi-truck
LC 7	1 truck hauling large equipment
LC 8	1 large truck with livestock
LC 9	1 smaller truck plus traffic
LC 10	1 small truck
LC 11	1 small truck
LC 12	**1 semi-truck**
LC 13	**1 semi-truck plus random traffic**
LC 14	1 unloaded truck
LC 15	1 UPS double trailer
LC 16	**1 semi-truck**
LC 17	1 semi-truck plus 1 dump truck
LC 18	**2 semi-trucks**
LC 19	**1 semi-truck**
LC 20	1 small truck

Among these load cases, six (LC 4, 12, 13, 16, 18, and 19) were chosen for further data processing and analysis due to the greater traffic loading observed during these cases and the response of the bridge. These six cases are highlighted in red in Table 5.

Load Test Results

The six data sets processed for this analysis were recorded by the strain transducers when larger trucks passed over the bridge as part of the ambient traffic. Since the strain data recorded from the two legs of the angle were similar, for data processing purposes the strain results were analyzed by taking the average of the corresponding strain gauges. The strains ultimately analyzed are shown in Figures 73 and 74. For instance, S1 is the average strain value taken from G1 and G2.

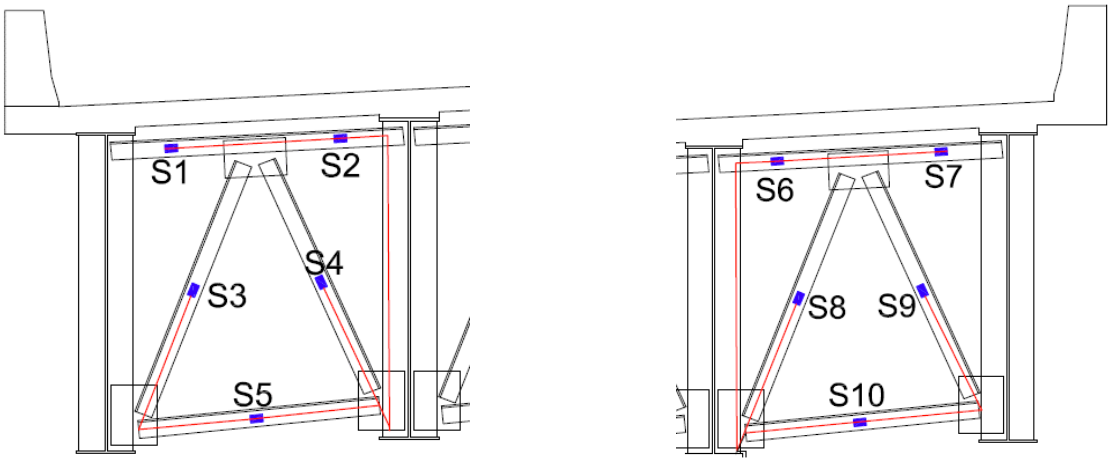

Figure 73. Strains measured during live load tests (A-A)

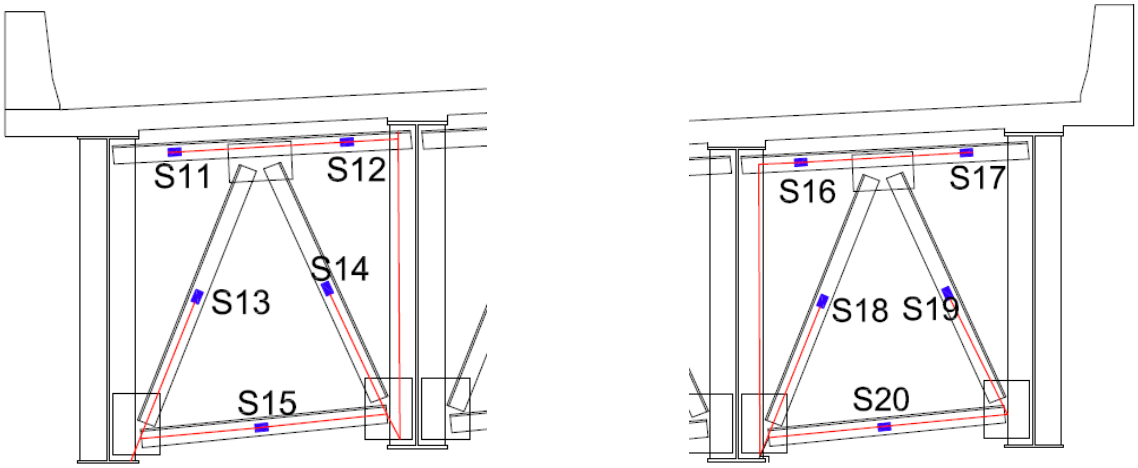

Figure 74. Strains measured during live load tests (B-B)

To facilitate the analysis of the live load data, the structural responses of both the girders and the cross-frames were determined as a function of the vehicles that passed over the full length of the bridge. Transverse lines were marked on the bridge to allow the time in seconds that it took for each truck to cross the bridge to be measured consistently. The data were then plotted to show the strain response versus time.

Figure 75 presents the longitudinal strain response versus truck passing time at midspan for each of the six ambient traffic loading scenarios.

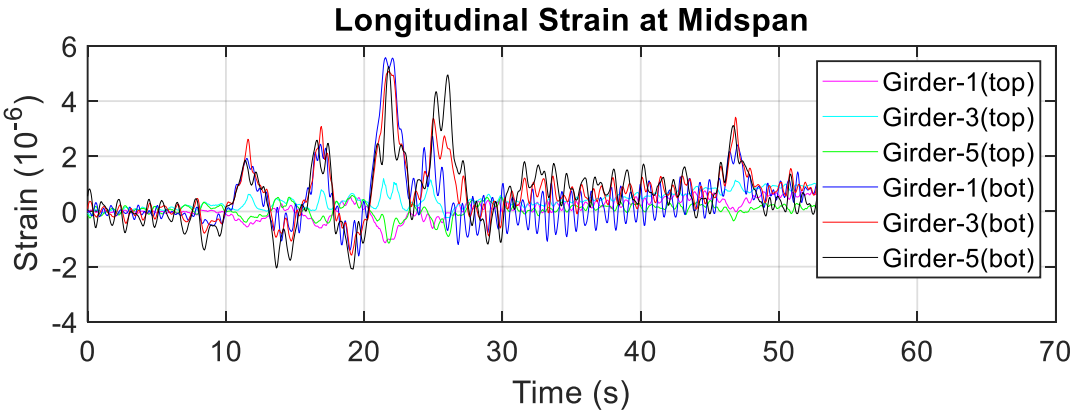

(a) LC4 – Heavy traffic plus large truck

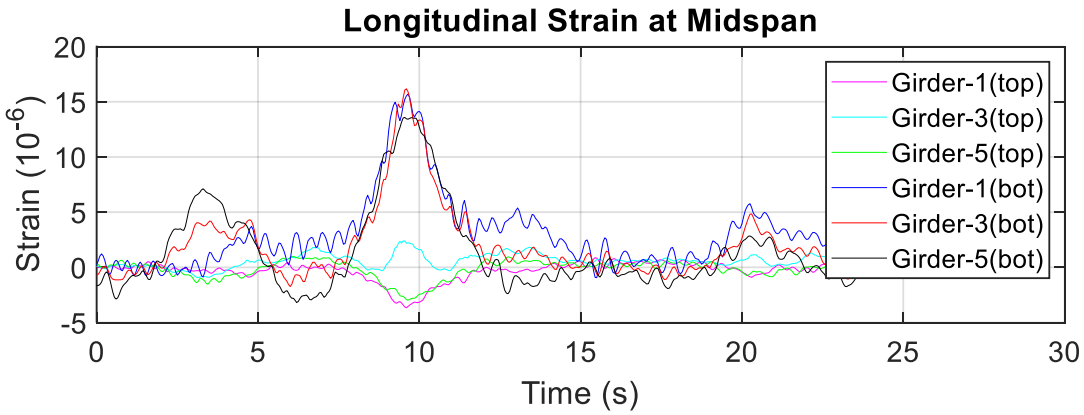

(b) LC12 – 1 Semi Truck

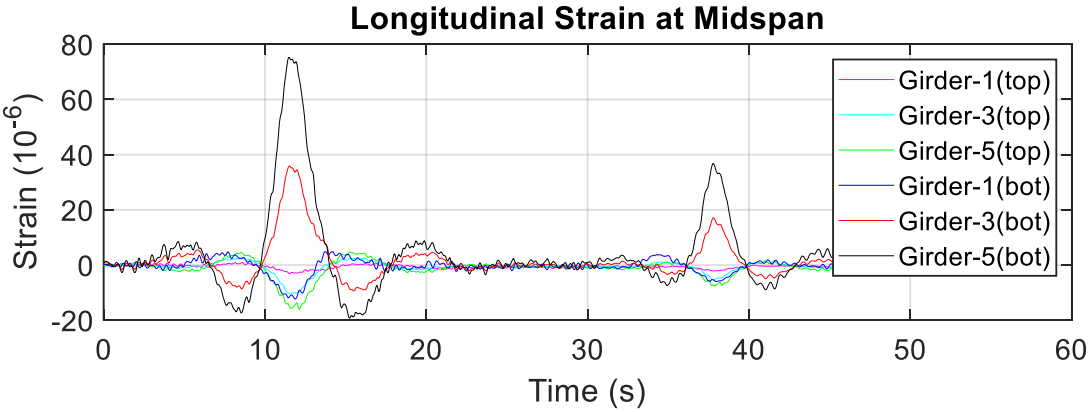

(c) LC13 – 1 Semi Truck

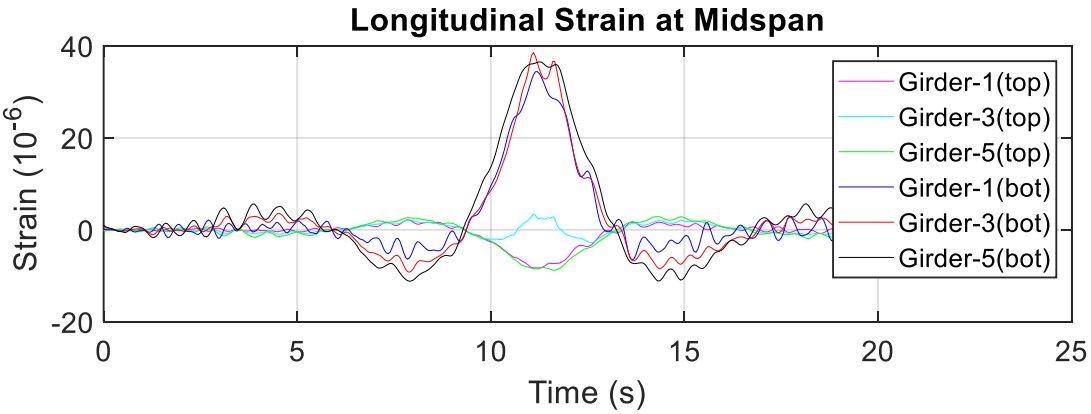

(d) LC16 – 1 Semi Truck

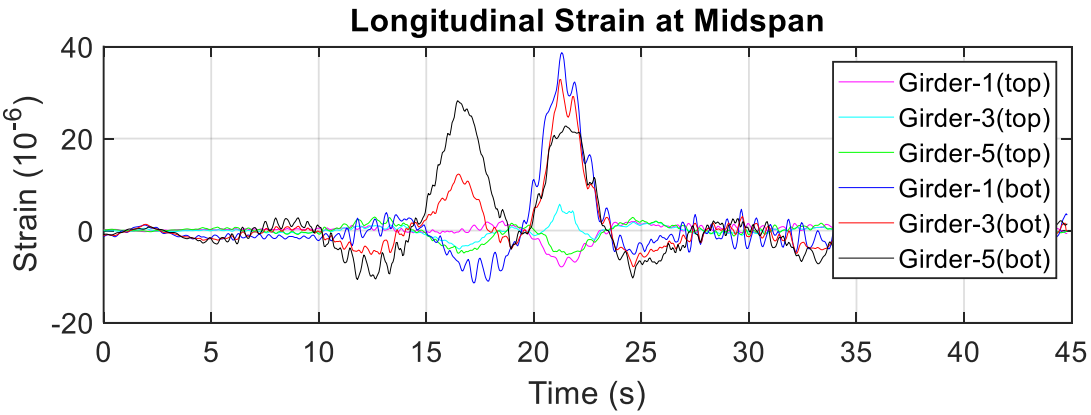

(e) LC18 – 2 Semi Trucks

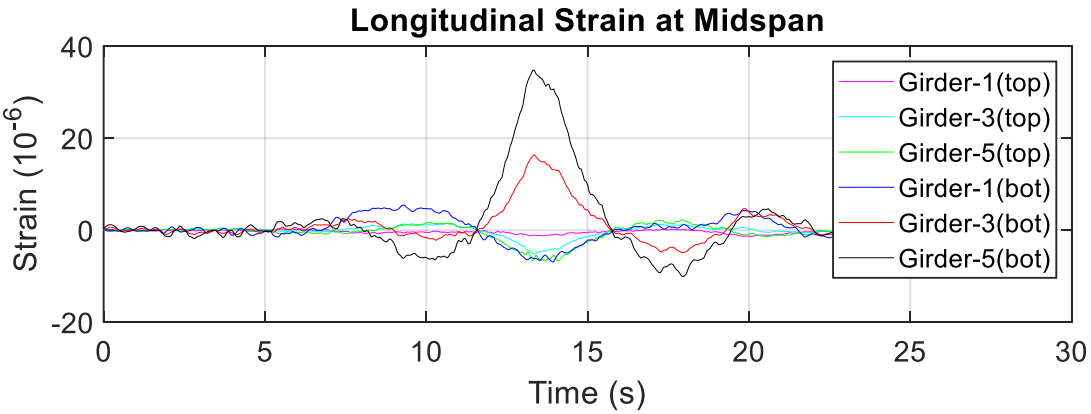

(f) LC19 – 1 Semi Truck

Figure 75. Longitudinal strain response of girders at midspan under six load cases

As the figure shows, the maximum strain (80 microstrain) was measured during LC 13 on the bottom flange of Girder 5. As for the other load cases, the maximum strains measured during LC 16, 18, and 19 were each about 40 microstrain; these strains were also measured on Girder 5. This may be because the passing truck in each of these four load cases was driving on the far side of the curve.

Figure 76 presents the transverse strain response versus truck passing time for each of the six ambient traffic loading scenarios.

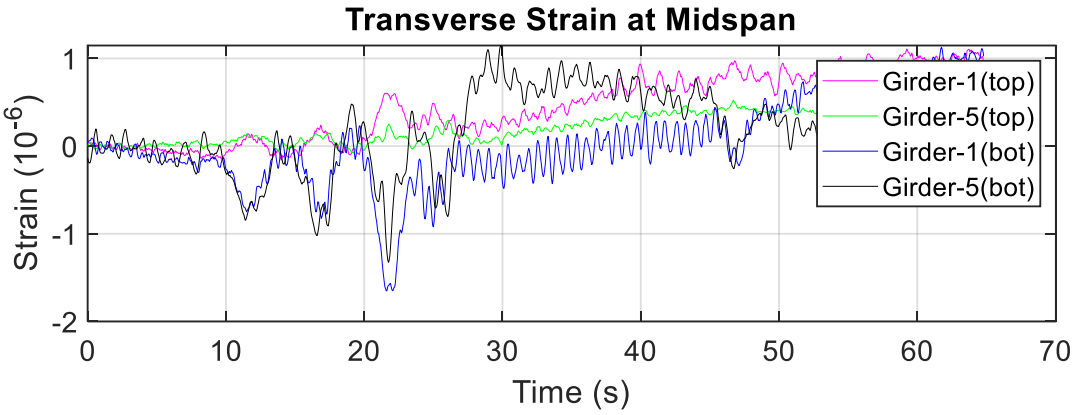

(a) LC4 – Heavy traffic plus large truck

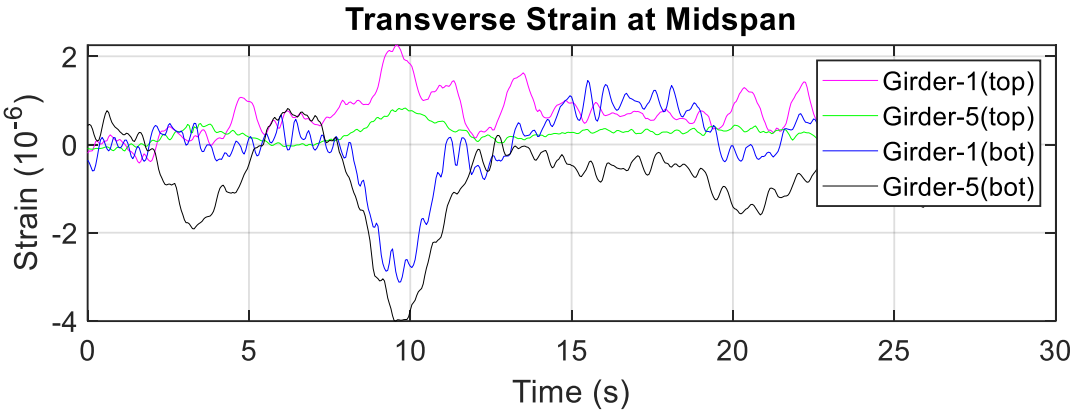

(b) LC12 – 1 Semi Truck

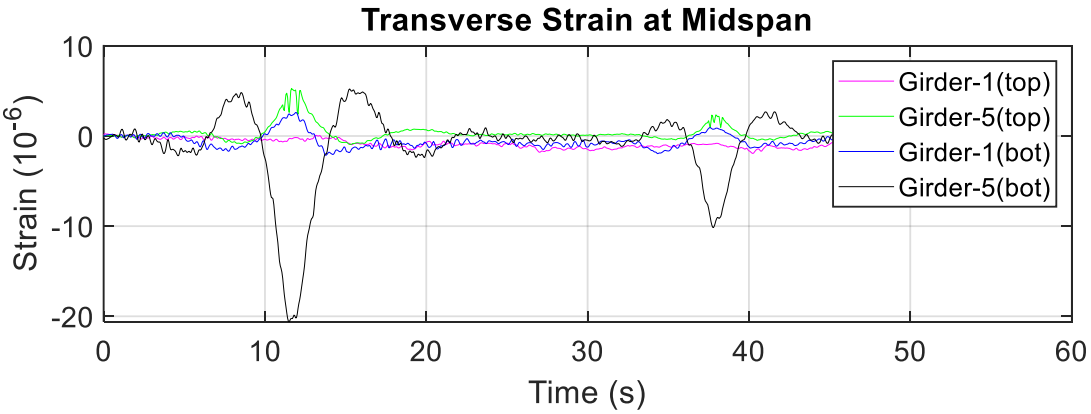

(c) LC13 – 1 Semi Truck

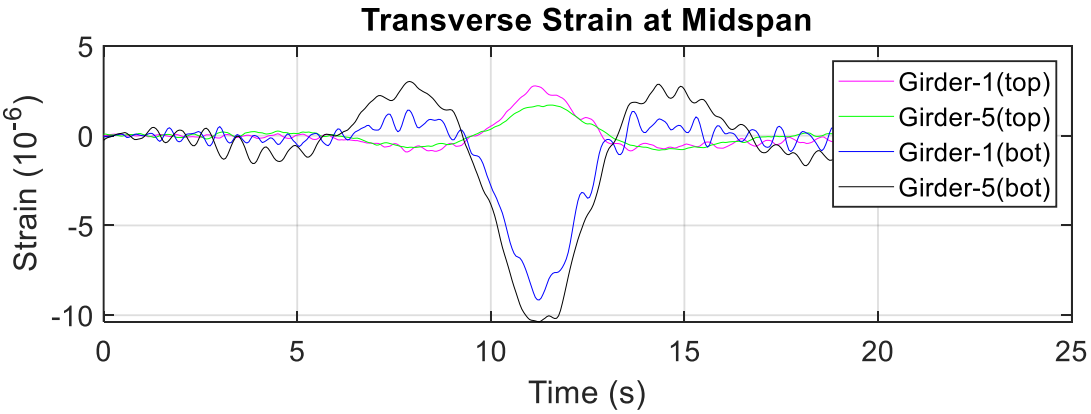

(d) LC16 – 1 Semi Truck

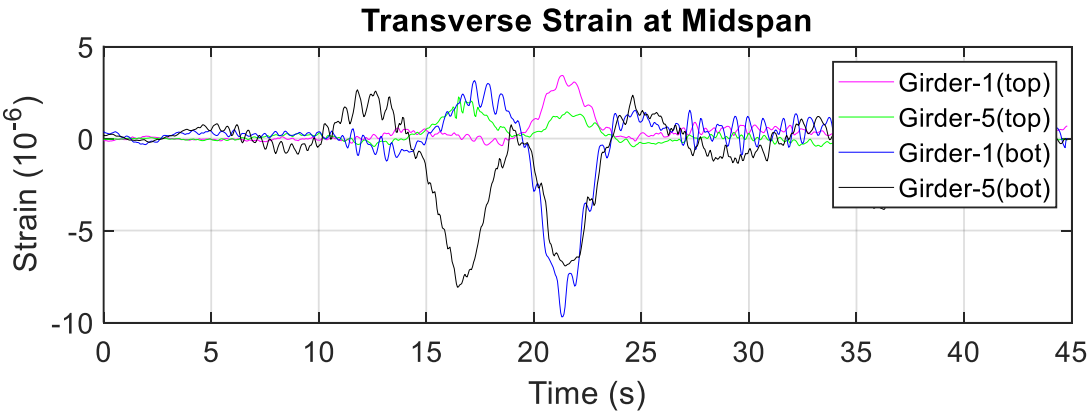

(e) LC18 – 2 Semi Trucks

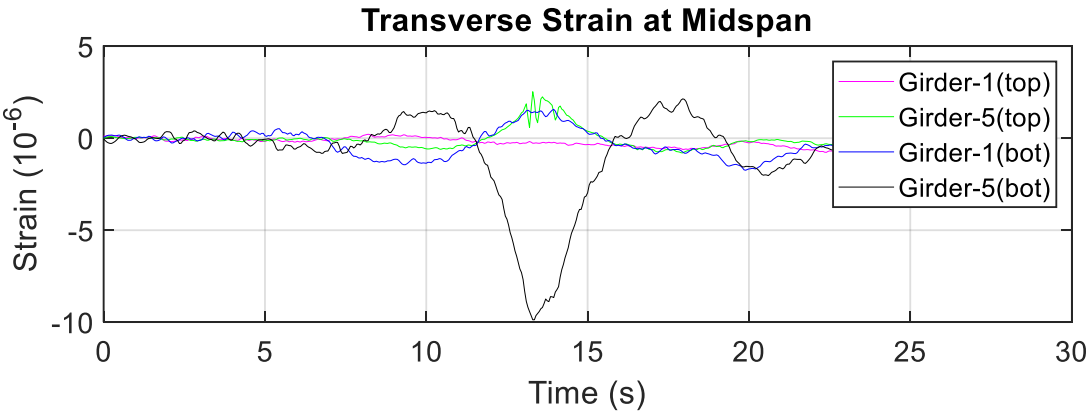

(f) LC19 – 1 Semi Truck

Figure 76. Transverse strain response of girders at midspan under six load cases

As this figure shows, the maximum strain was again recorded during LC13 on the bottom flange of Girder 5, but in this case the value was -20 microstrain, which indicates compression. The ratio between the transverse strain and the longitudinal strain is about 25%, though the two strains have opposite signs.

Figure 77 presents the strain response measured in the angles of the inside cross-frame.

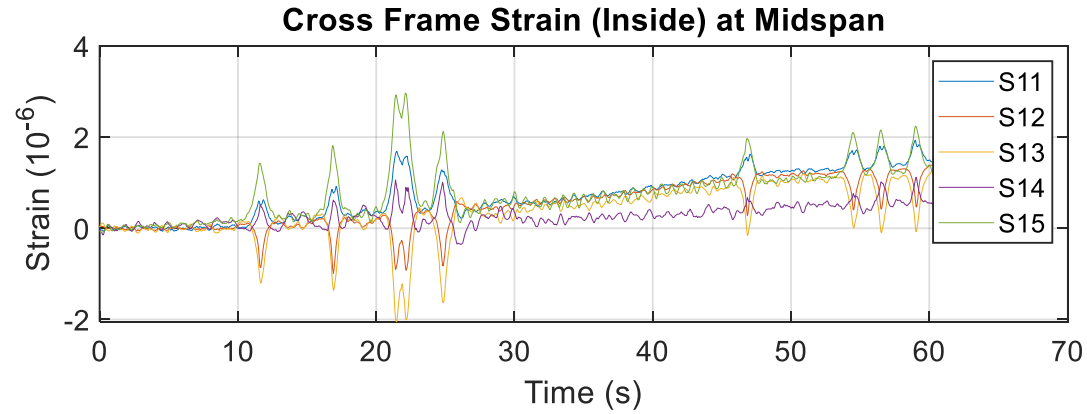

(a) LC4 – Heavy traffic plus large truck

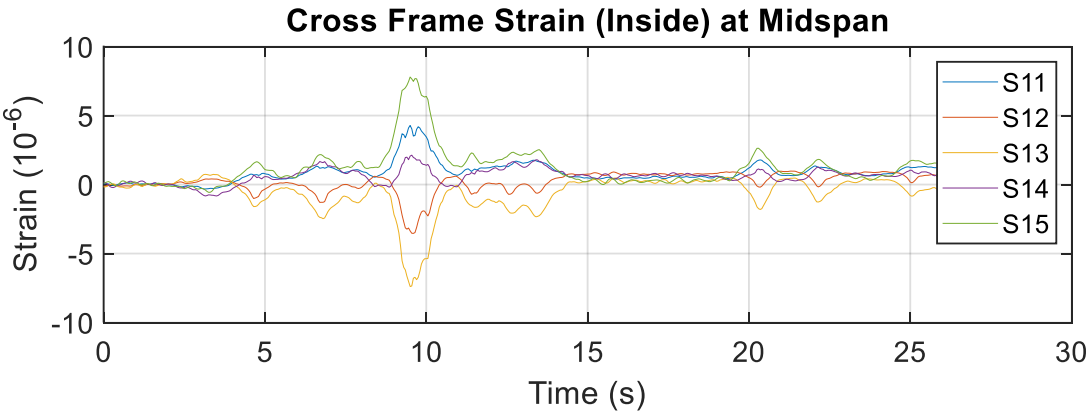

(b) LC12 – 1 Semi Truck

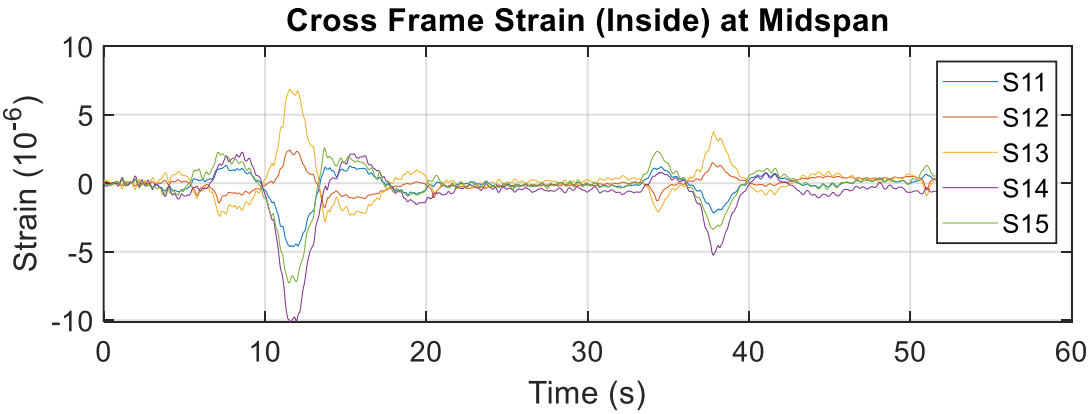

(c) LC13 – 1 Semi Truck

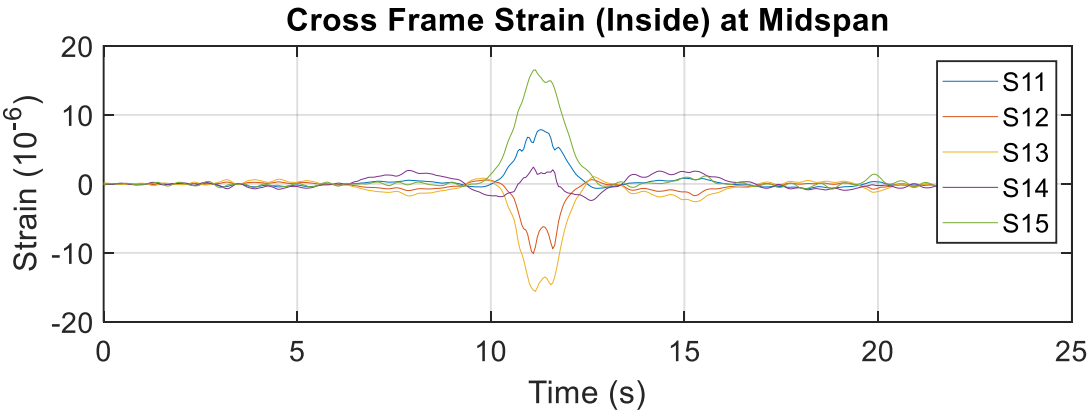

(d) LC16 – 1 Semi Truck

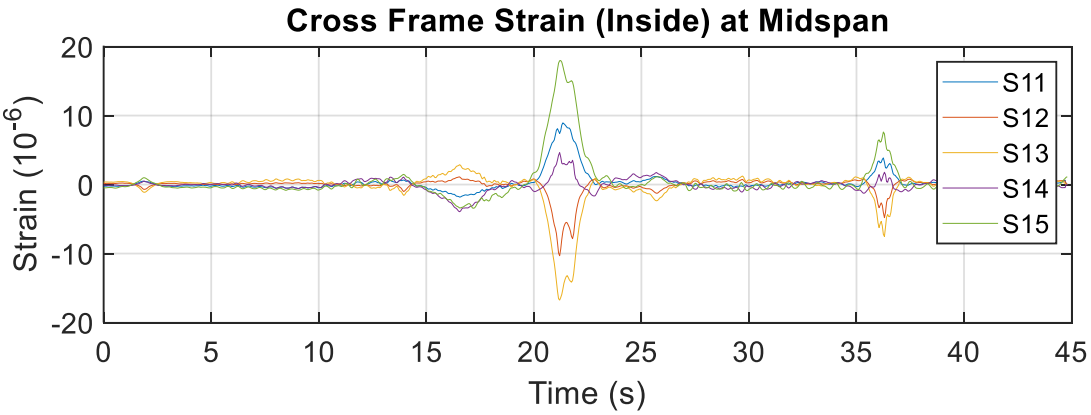

(e) LC18 – 2 Semi Trucks

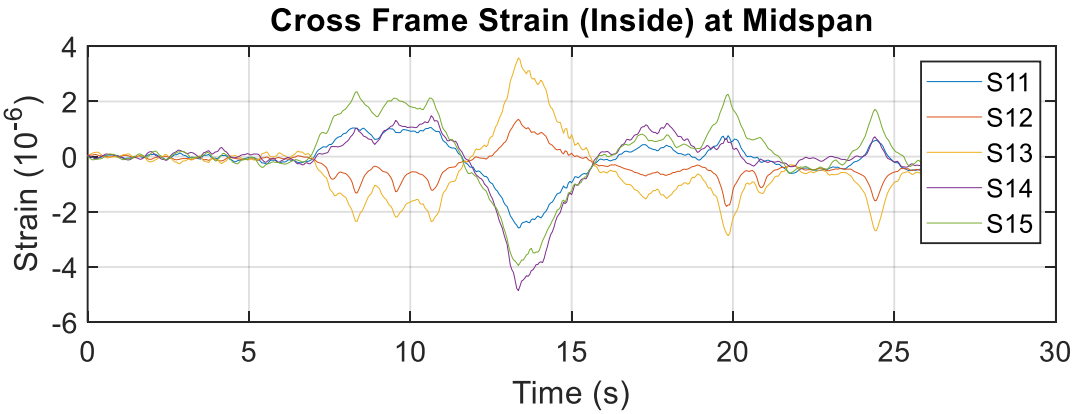

(f) LC19 – 1 Semi Truck

Figure 77. Cross-frame (inside) strain response of girders at midspan under six load cases

As this figure shows, the maximum strain was recorded during LC 16 and 18, each of which had the same maximum strain value of approximately 15 microstrain, which is approximately equivalent to 0.6 ksi. The maximum response was recorded for S13 (i.e., the left diagonal member) in compression and for S15 (i.e., the bottom chord member) in tension (refer to Figure 74 for the locations of these strains).

Figure 78 presents the strain response measured at the angles of the outside cross-frame.

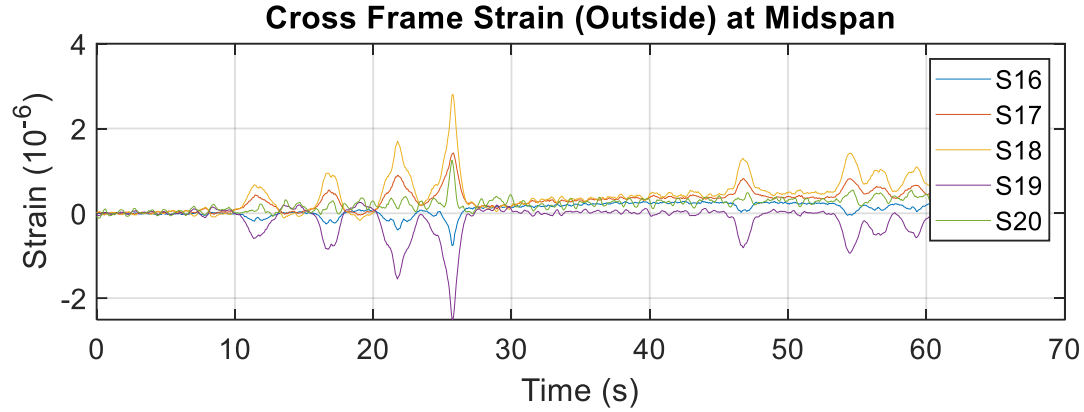

(a) LC4 – Heavy traffic plus large truck

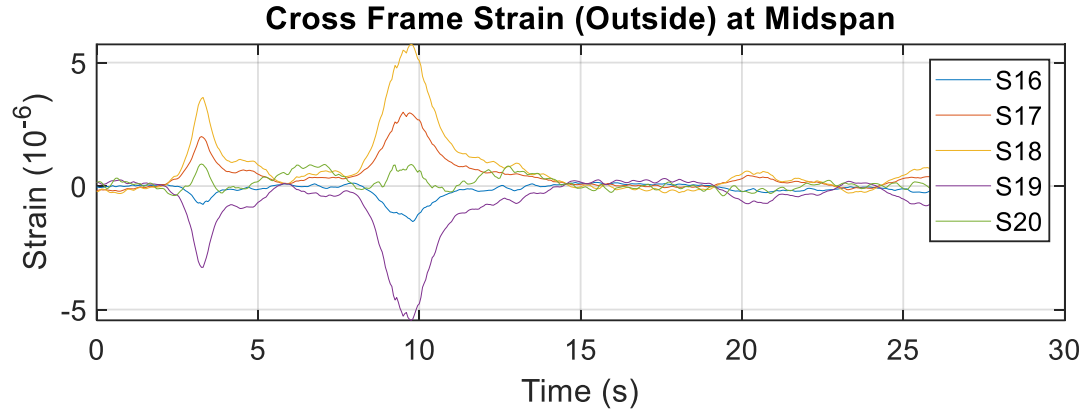

(b) LC12 – 1 Semi Truck

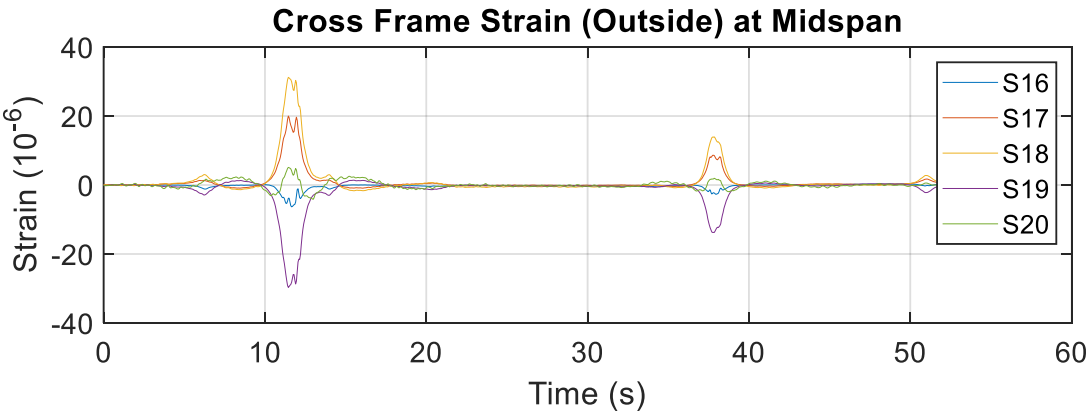

(c) LC13 – 1 Semi Truck

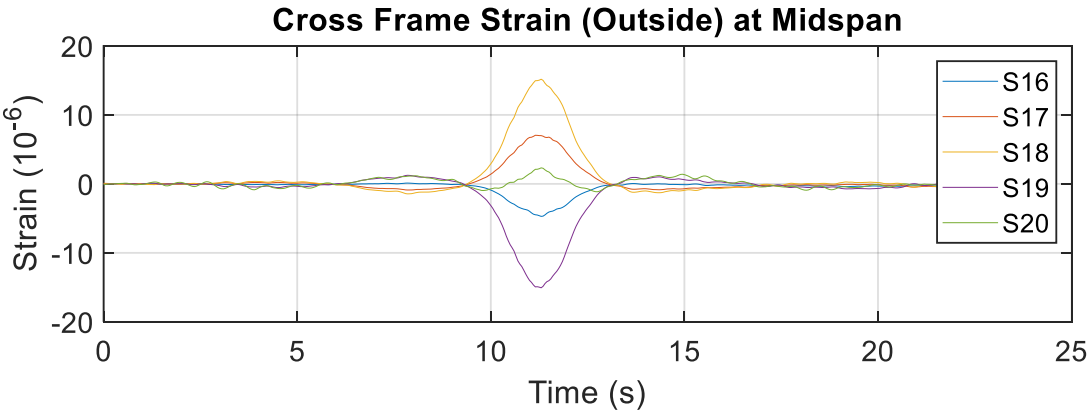

(d) LC16 – 1 Semi Truck

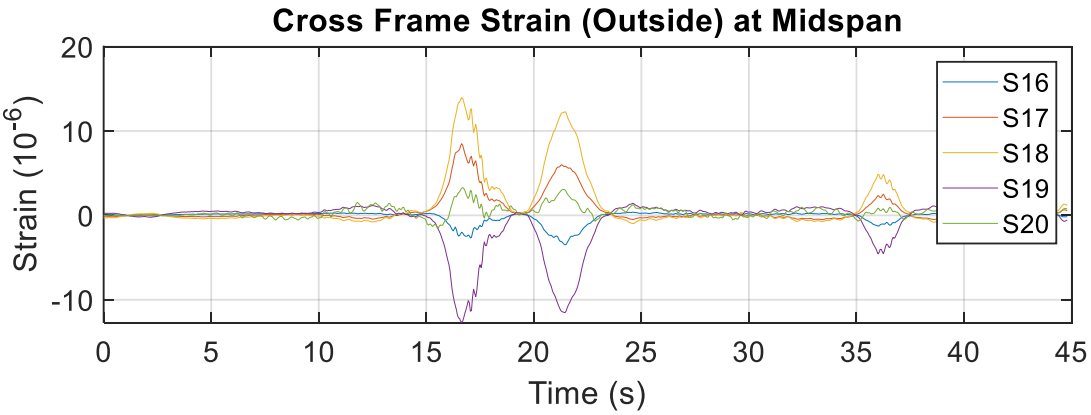

(e) LC18 – 2 Semi Trucks

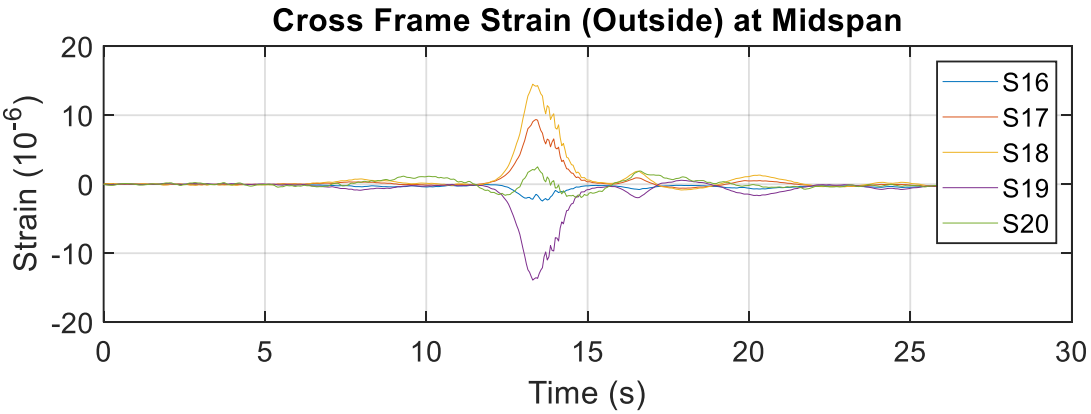

(f) LC19 – 1 Semi Truck

Figure 78. Cross-frame (outside) strain response of girders at midspan under six load cases

As the figure shows, the maximum strain was again measured during LC13, this time with a value of 30 microstrain, which is approximately equivalent to 0.9 ksi. The maximum response was recorded for S19 (i.e., the right diagonal member) in compression and for S18 (i.e., the left diagonal member) in tension (refer to Figure 74 for the locations of these strains).

Figure 79 presents the longitudinal strain response versus truck passing time at the end span for each of the six ambient traffic loading scenarios.

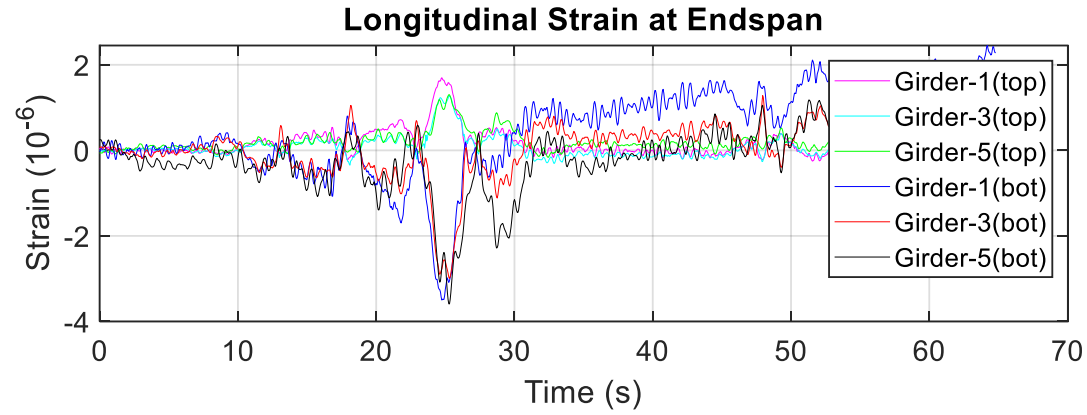

(a) LC4 – Heavy traffic plus large truck

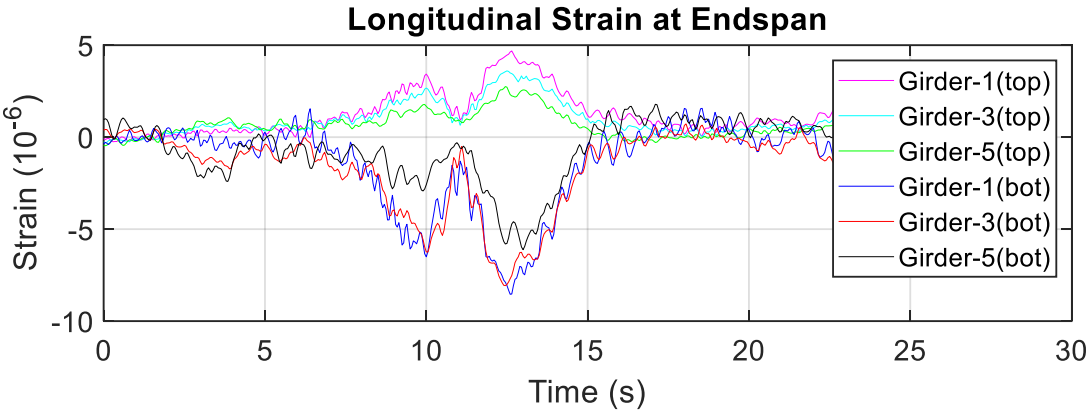

(b) LC12 – 1 Semi Truck

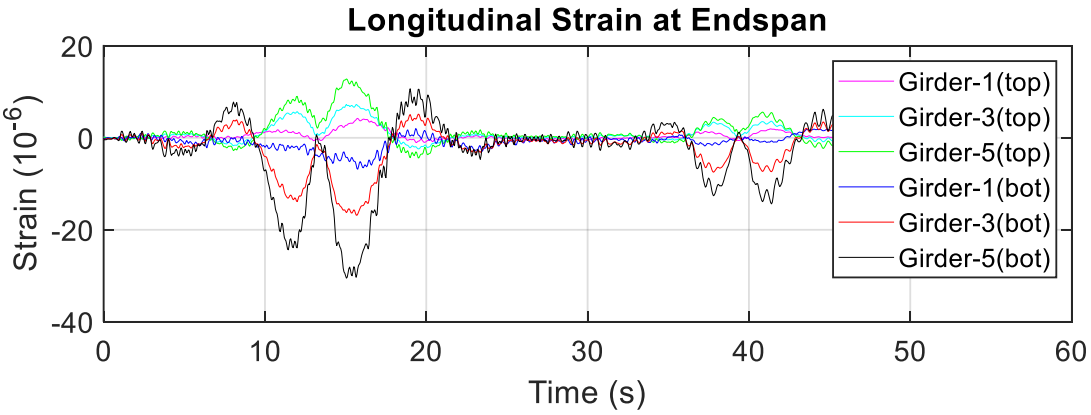

(c) LC13 – 1 Semi Truck

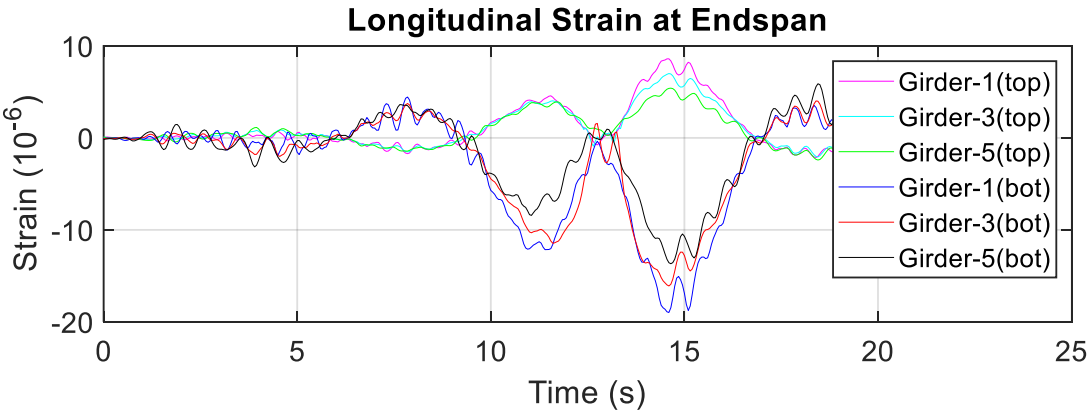

(d) LC16 – 1 Semi Truck

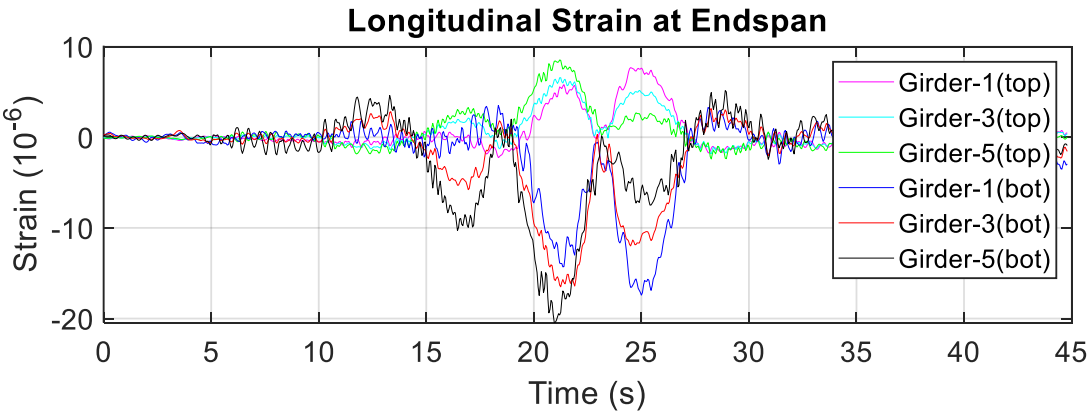

(e) LC18 – 2 Semi Trucks

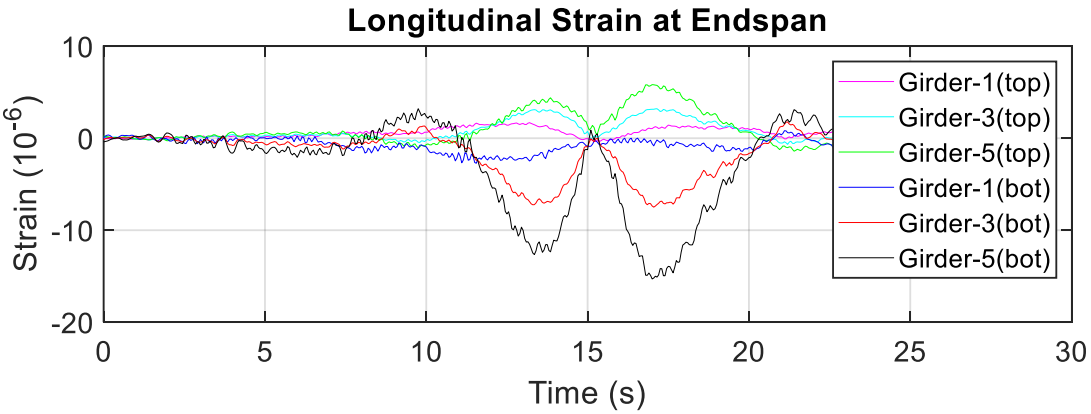

(f) LC19 – 1 Semi Truck

Figure 79. Longitudinal strain response of girders at the end span under six load cases

Similarly to the longitudinal strain response at midspan, the maximum response was recorded on the bottom of Girder 5 during LC 13, but in compression. This may be because the section is located in the negative bending region.

Figure 80 presents the transverse strain response versus truck passing time at the end span for each of the six ambient traffic loading scenarios.

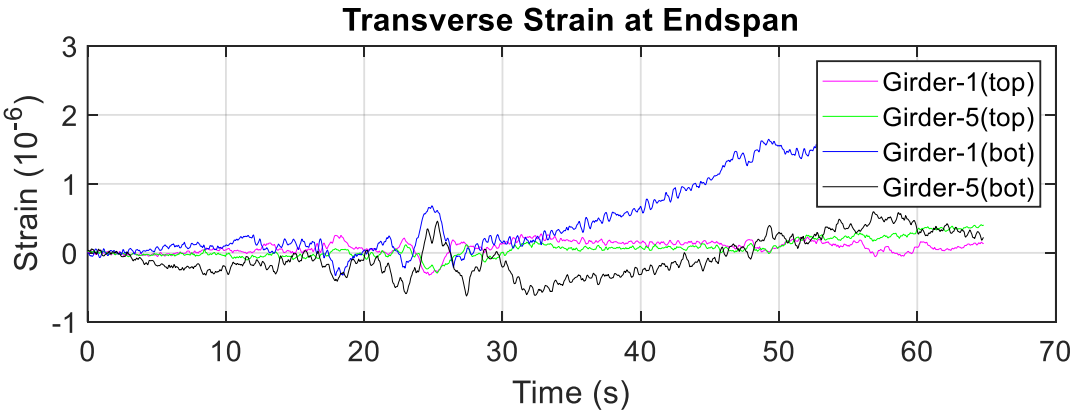

(a) LC4 – Heavy traffic plus large truck

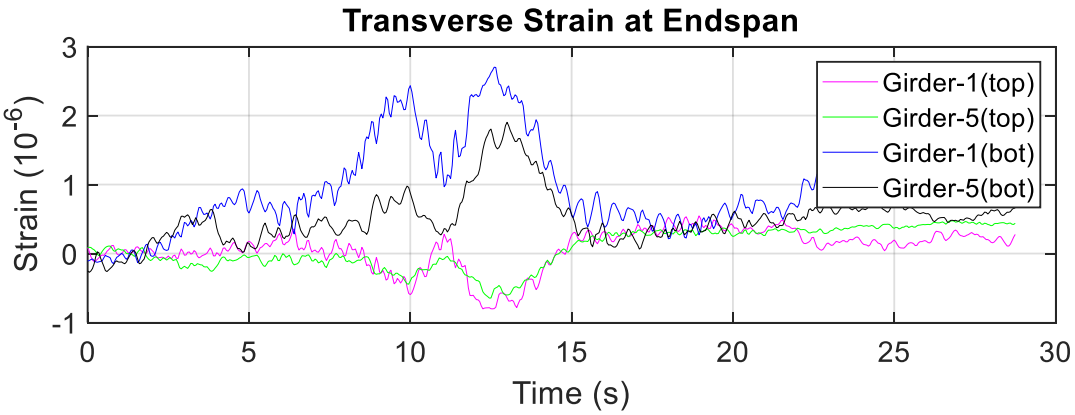

(b) LC12 – 1 Semi Truck

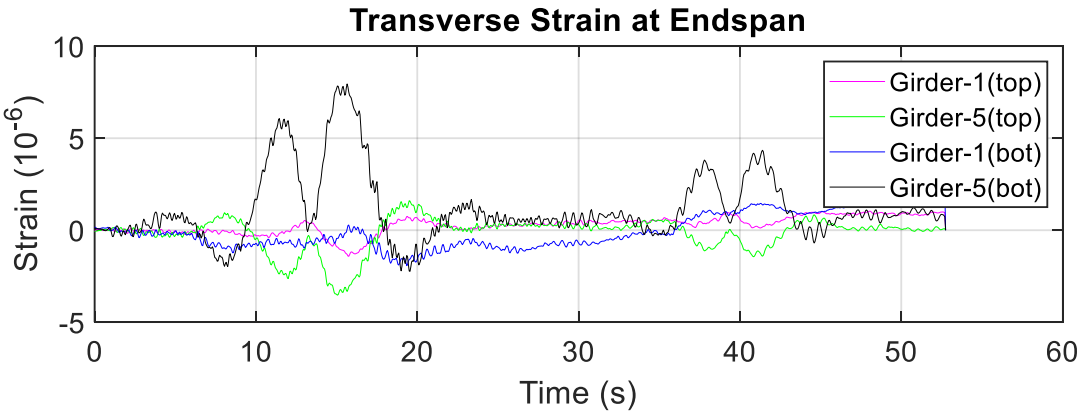

(c) LC13 – 1 Semi Truck

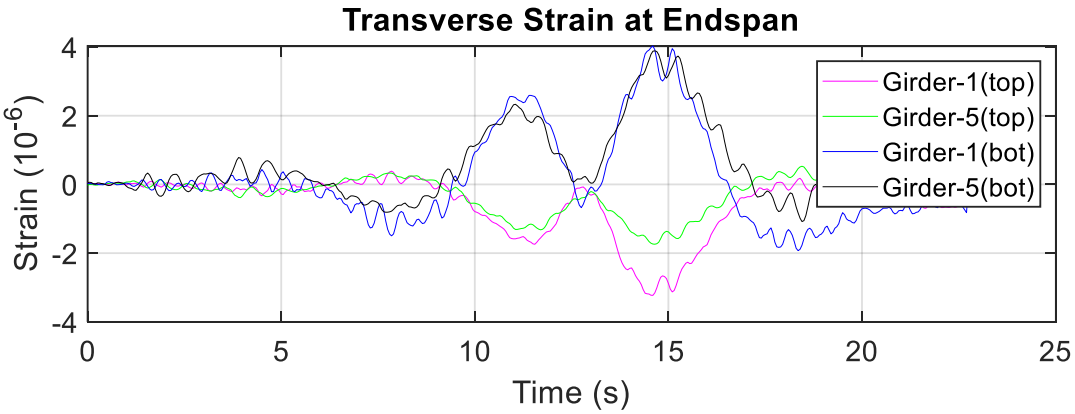

(d) LC16 – 1 Semi Truck

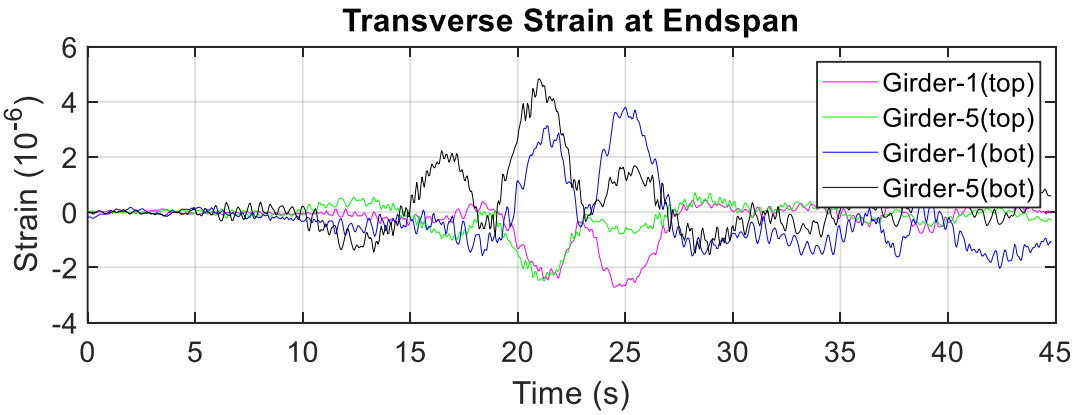

(e) LC18 – 2 Semi Trucks

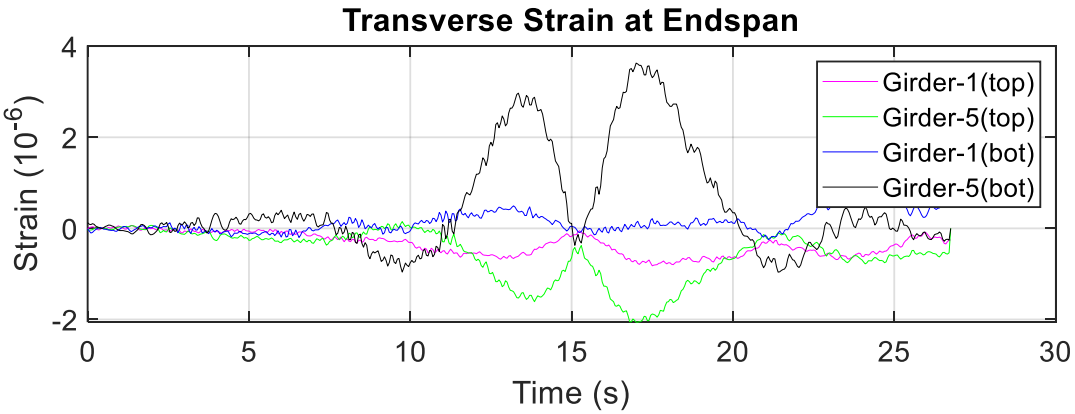

(f) LC19 – 1 Semi Truck

Figure 80. Transverse strain response of girders at the end span under six load cases

For the transverse strain recorded in the girders at the end span, the maximum response was again recorded on the bottom flange of Girder 5. The ratio between the transverse strain and the longitudinal strain is similar to that of the midspan, about 25%, but again the two strains have opposite signs.

Figure 81 presents the strain response measured in the angles of the inside cross-frame at the end span.

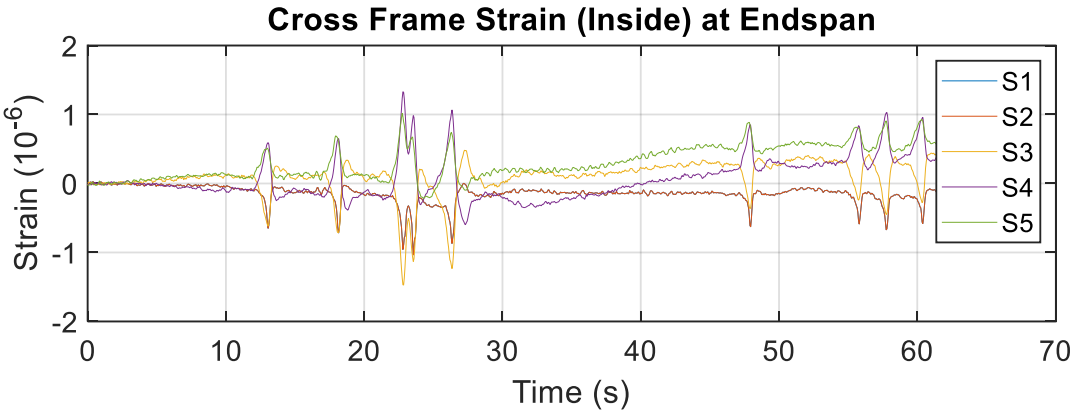

(a) LC4 – Heavy traffic plus large truck

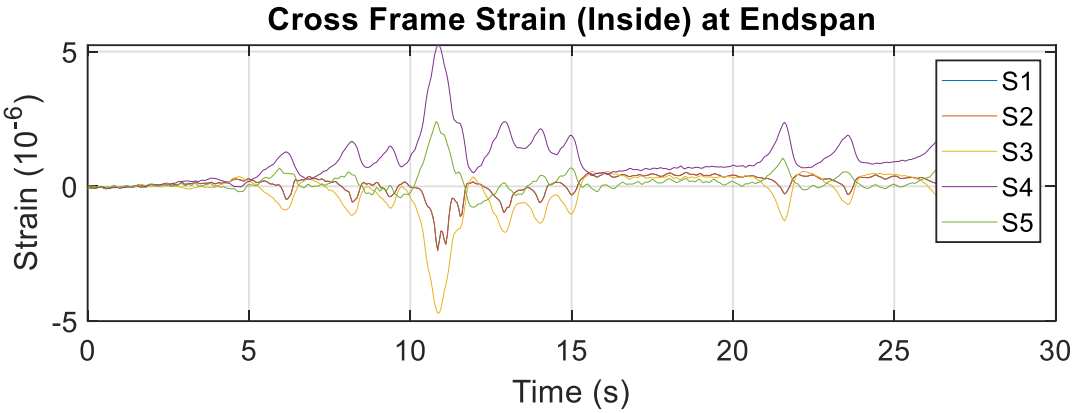

(b) LC12 – 1 Semi Truck

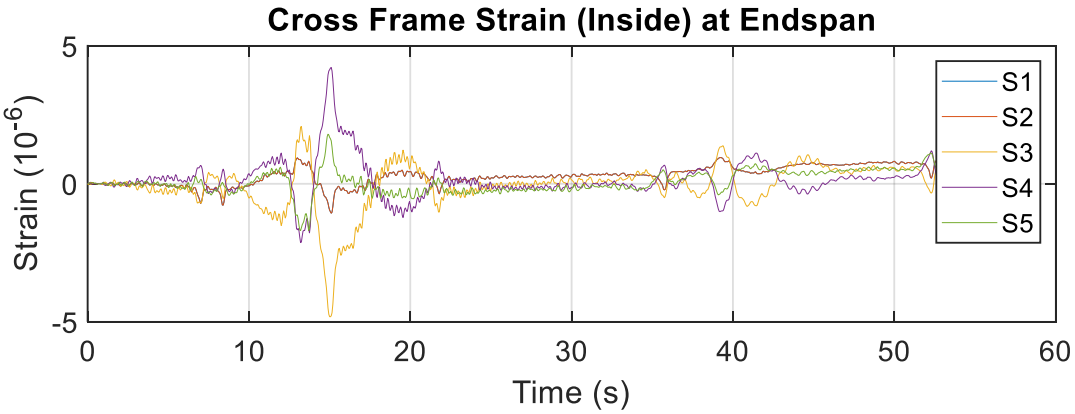

(c) LC13 – 1 Semi Truck

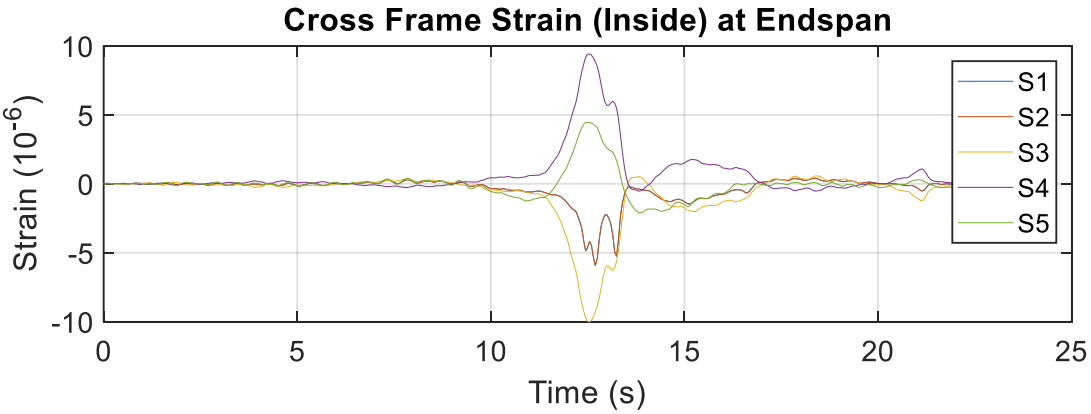

(d) LC16 – 1 Semi Truck

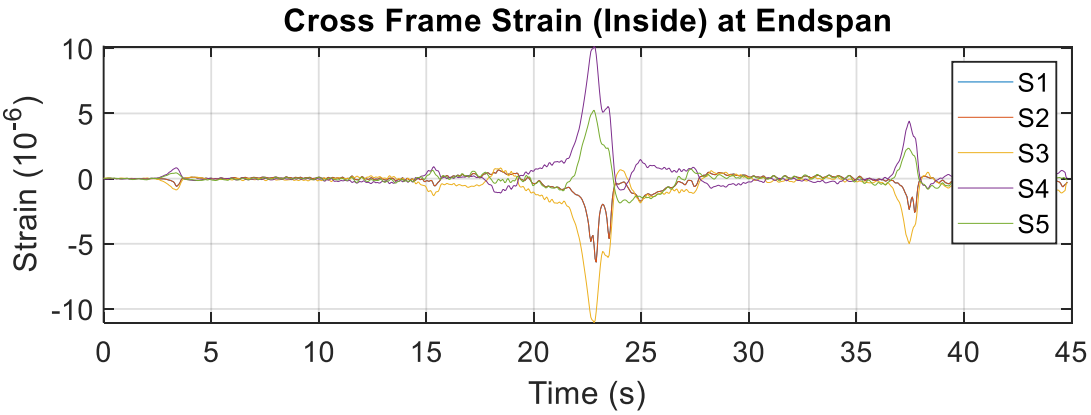

(e) LC18 – 2 Semi Trucks

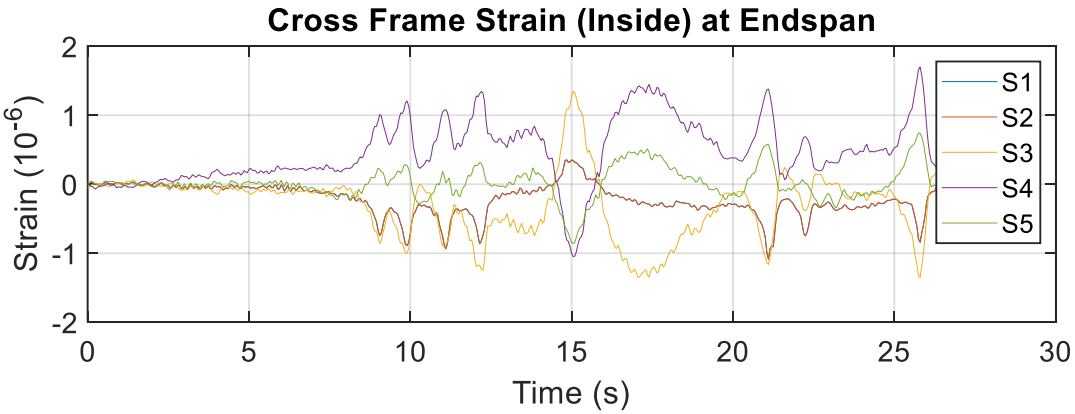

(f) LC19 – 1 Semi Truck

Figure 81. Cross-frame (inside) strain response of girders at the end span under six load cases

As this figure shows, the maximum strain was recorded during LC 16 and 18, each of which had the same maximum strain value of approximately 10 microstrain, which is approximately equivalent to 0.4 ksi. The maximum response was recorded for S3 (i.e., the left diagonal member) in compression and for S4 (i.e., the right diagonal member) in tension (refer to Figure 73 for the locations of these strains).

Figure 82 presents the strain response measured in the angles of the outside cross-frame at the end span.

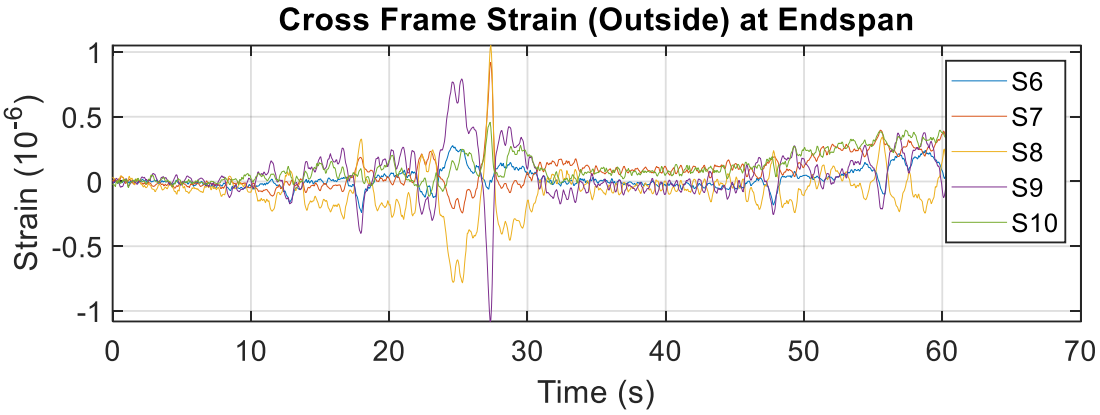

(a) LC4 – Heavy traffic plus large truck

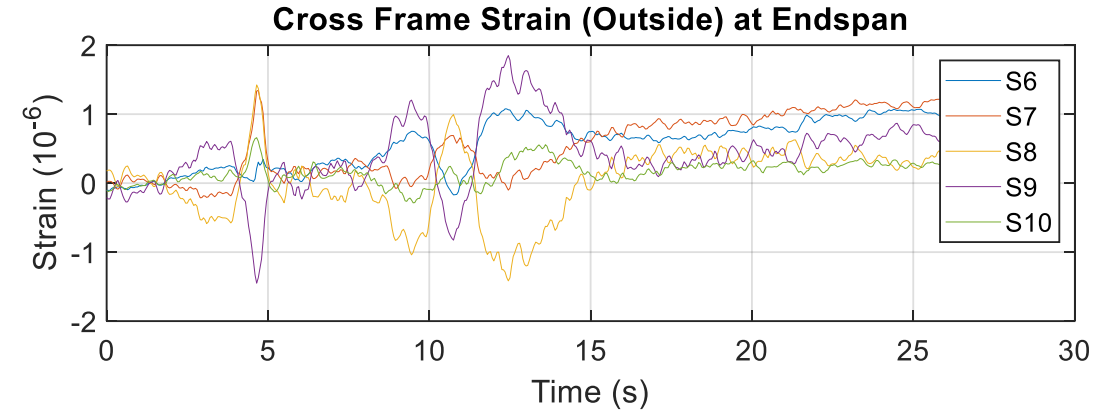

(b) LC12 – 1 Semi Truck

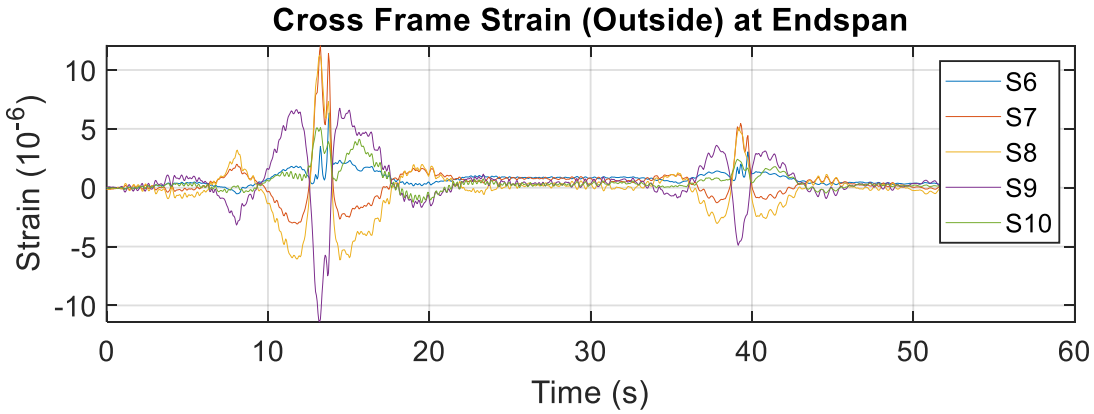

(c) LC13 – 1 Semi Truck

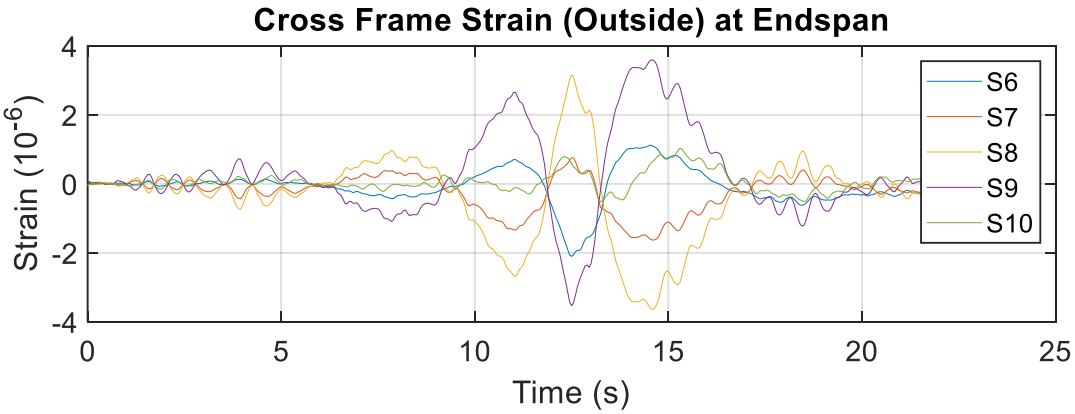

(d) LC16 – 1 Semi Truck

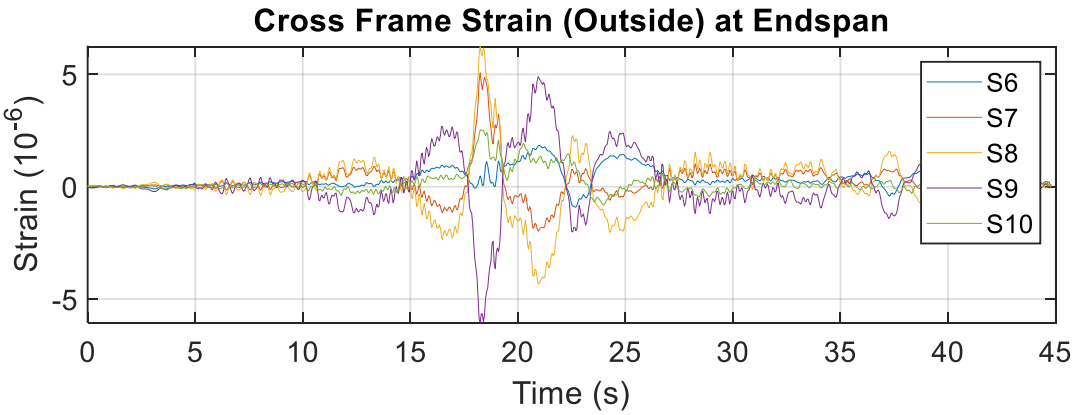

(e) LC18 – 2 Semi Trucks

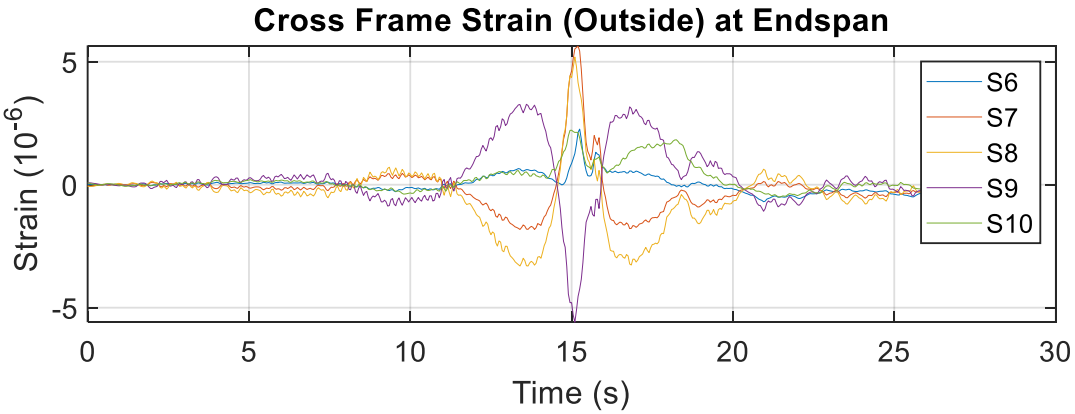

(f) LC19 – 1 Semi Truck

Figure 82. Cross-frame (outside) strain response of girders at the end span under six load cases

As the figure shows, the maximum strain was again measured during LC13, but with a value of 10 microstrain in compression. The maximum response was recorded for S9 (i.e., the right diagonal member) in compression and for S8 (i.e., the left diagonal member) in tension (refer to Figure 73 for the locations of these strains).

In the field tests carried out by the research team, live load was not found to have any significant effect on the cross-frames. The following observations were made based on the live load cases, i.e., LC1 through LC20:

- The maximum strain in the inside cross-frames was determined to occur in the diagonal members located at the midspan of Span 4. The magnitude of the strain was found to be in the range of 15 microstrain, which is approximately equal to 0.6 ksi (Figure 77 a–f).
- While the maximum strain in the outside cross-frames was also found to occur in the diagonal members located at the midspan of Span 4, the corresponding magnitude was in the range of 30 microstrain, which is approximately equivalent to 0.9 ksi.
- Likewise, the maximum strain in the inside cross-frame located at the end-span of Span 4 was recorded in the diagonal members. The corresponding magnitude was in the range of 10 microstrain, which is approximately equivalent to 0.4 ksi.
- The maximum strain the outside cross-frame located at the end-span of Span 4 was similar to that of the diagonal members, with a magnitude of 10 microstrain, which is approximately equivalent to 0.4 ksi.

Considering that the cross-sectional area of L6×6×5/8 is 7.13 in.^{2} and the maximum stress recorded during live load test was 0.9 ksi, the maximum force in the cross-frames was approximately 6.5 kips. The capacity of this angle, as per AASHTO, is 165.8 kips under compression and 243.8 kips under tension. Considering this capacity calculation, the cross-frames are stressed up to 4% (in compression) and 3% (in tension) under live loads. The live load employed in the numerical simulations, however, was different than that experienced during the field tests. The bridge is 36 ft wide inside of the curbs. This, ideally, allows the use of three design lanes. However, two design lanes were used in the initial analysis of the bridge. The forces/moments due to dead, live, and temperature loads are plotted in Figures 17 through 38 above. From the axial load in Members 3 and 4 (i.e., the diagonal members in the cross-frame located at the midspan of Span 4), the maximum compression and tension forces were found to be in the range of 10 to 12 kips.

Field Test Summary and Conclusions

In this analysis, load tests using ambient traffic were performed for the Story County bridge, with the goal of characterizing the structural response of the girders and the cross-frames. The data were analyzed to determine the longitudinal and transverse strains in the girders and the magnitudes and distributions of strains in the cross-frames at both the midspan and end span of Span 4.

From the field tests carried out for this analysis, the following conclusions can be drawn regarding the girder flange response:

- For the longitudinal direction, the maximum response was 80 microstrain (2.4 ksi), measured in the bottom flange of Girder 5 during LC 12 (i.e., 1 semi-truck).

- For the transverse direction, the maximum response was -20 microstrain (-0.6 ksi), measured in the bottom flange of Girder 5 during LC 12.

The following conclusions can be drawn regarding the cross-frame response:

- For the interior bay, both diagonal members and the bottom chord showed higher response values than the other members, with maximum stresses of 0.6 and -0.6 ksi.
- For the exterior bay, the two diagonal members showed higher response values than the top and bottom chords. The maximum stresses were recorded during LC 12, with values of 0.9 ksi (tension) and -0.9 ksi (compression).

SUMMARY AND CONCLUSIONS

Summary

While for decades horizontally curved steel girder bridges have been a solution for constructing interchanges between state and Interstate highways, concerns remain regarding their design and construction. The cross-frames in these bridges are especially critical because, unlike in straight bridges, they are major load carrying elements.

The design and analysis of cross-frames in curved bridges is complex due to complexities in how loads are transmitted throughout these types of bridges. The configuration of cross-frames has generally been based on standard designs that have depended principally on gross geometries, slenderness limits for tension and compression members, and other minimum requirements. As such, a unique opportunity exists to improve the design of these components using modern computer software and short- and long-term monitoring. The reconstruction of the Interstate system in western Iowa offers a unique opportunity to monitor the behavior of several yet-to-be-constructed horizontally curved steel girder bridges.

To estimate the forces in the cross-frames of horizontally curved bridges, this project investigated a horizontally curved bridge located in Story County near Ames, Iowa, on northbound I-35 and westbound US 30. The goal of this research project was to understand the behavior of cross-frames during various stages of construction and over the service life of the bridge. Special consideration was given to identifying critical locations for instrumentation on such components of the bridge superstructure as the main girders, cross-frames, and diaphragms as part of data collection efforts to evaluate the long-term performance of the cross-frames.

This project involved a numerical investigation using finite element modeling and short-term and long-term monitoring of the cross-frames in the field to achieve the following objectives:

- Identify the sections of the bridge to instrument under dead, live, and temperature loading
- Evaluate the performance of cross-frames through long-term monitoring
- Evaluate the performance of cross-frames using live load tests

Conclusions

The following general conclusions were made from the results of the study:

- From the finite element analysis carried out for this project, the following conclusions can be drawn: The maximum and minimum forces in the cross-frames were found within the third and fourth span of the bridge and near the interior supports. The girders were subjected to forces vertically as well as radially. This bidirectional translation confirmed that the displacement of girders does not follow a particular path.

- From the FEA, it was confirmed that the load within the top chord of the cross-frame varies significantly at the two ends of each connection. The cross-frames in the interior bays were found to carry higher forces than those in the exterior bays. The observations from the FEAs led the research team to identify the cross-frames that are critical for instrumentation. In addition, considering all the contributing load combinations, it was concluded that attention is required for the design of top chords of the cross-frames, especially at the support locations.

- From the long-term monitoring data, the maximum compressive stress level, 11 ksi, was found in the diagonal strut during the minimum temperature period. As also determined from the FEA, a stress difference of about 6 to 8 ksi is present within the top chord member in the cross-frame located near the middle of the span. Top chords and their connections may become vulnerable to higher stress differences during extreme sustained and fluctuating temperatures.

- From the field tests carried out for this analysis, the girder flange's maximum response was as follows: In the longitudinal direction, the maximum response was 80 microstrain (2.4 ksi), measured in the bottom flange of Girder 5 during LC 12 (i.e., one semi-truck). In the transverse direction, the maximum response was -20 microstrain (-0.6 ksi), measured in the bottom flange of Girder 5 during LC 12. As for the cross-frames' responses, for the interior bay, both diagonal members and the bottom chord showed higher response values than the other members, with maximum stresses of 0.6 ksi; for the exterior bay, the two diagonal members showed higher response values than the top and bottom chords. The maximum stresses were recorded during LC 12, with values of 0.9 ksi (tension) and -0.9 ksi (compression).

- No distress or anomaly was found in the field. The maximum stresses (estimated from the strain gauge readings) in the top chord and all of the other members were found to be small and consistently less than 36 ksi.

Overall, the research results suggest that the cross-frames close to supports may experience high stress levels, and therefore special attention is required for their design compared to the other cross-frames. The cross-frames within the interior bays were also found to carry higher forces than those in the outer bays. This situation requires additional analysis during design to ensure the safety and performance of curved girder bridges.

REFERENCES

AASHTO. 2017. *AASHTO LRFD Bridge Design Specifications*. American Association of State and Highway Transportation Officials, Washington, DC.

AASHTO and NSBA. 2014. *G13.1 Guidelines for Steel Girder Bridge Analysis*. American Association of State and Highway Transportation Officials and National Steel Bridge Alliance Steel Bridge Collaboration, Washington, DC.

Beckett, C. L. 2013. Response of Continuous Steel I-Girder Bridges Subject to Temperature Variation. PhD dissertation. Statler College of Engineering and Mineral Resources, West Virginia University, Morgantown, WV.

Computers & Structures, Inc. 2017. CSIBridge. Walnut Creek, CA.

Davidson, J. S., M. A. Keller, and C. H. Yoo. 1996. Cross-Frame Spacing and Parametric Effects in Horizontally Curved I-Girder Bridges. *Journal of Structural Engineering*, Vol. 122, No. 9, pp. 1089–1096.

Fiechtl, A. L., G. L. Fenves, and K. H. Frank. 1987. *Approximate Analysis of Horizontally Curved Bridges*. Center for Transportation Research, University of Texas at Austin, TX.

Geokon. 2017. *Spot-Weldable Strain Gauges*.

Greimann, L., B. M. Phares, Y. Deng, G. Shryack, and J. Hoffman. 2014. *Field Monitoring of Curved Girder Bridges with Integral Abutments*. Bridge Engineering Center, Iowa State University, Ames, IA.

Grubb, M. A. and D. H. Hall. 2019. *Curved Steel Bridge Research Project: I-Girder Bending Component Test – Philosophy and Design of the I-Girder Bending Component Tests*. Federal Highway Administration Office of Bridges and Structures, Washington DC.

Hall, D., M. A. Grubb, and C. H. Yoo. 1999. *NCHRP Report 424: Improved Design Specifications for Horizontally Curved Steel Girder Highway Bridges*. National Cooperative Highway Research Program, Washington, DC.

Helwig, T. and L. Wang. 2003. *Cross-Frame and Diaphragm Behavior for Steel Bridges with Skewed Supports*. Texas Department of Transportation, Austin, TX.

Hoffman, J. J. 2013. Analytical and Field Investigation of Horizontally Curved Girder Bridges. MS thesis. Iowa State University, Ames, IA.

Itani, A. M.,and M. L. Reno. 2000. Chapter 15: Horizontally Curved Bridges. In *Bridge Engineering Handbook*. CRC Press, Boca Raton, FL

Keating, P. B., K. C. Saindon, and D. S. Wilson. 1997. *Cross-Frame Diaphragm Fatigue and Load Distribution Behavior in Steel Highway Bridges*. Texas Transportation Institute, Texas A&M University System, College Station, TX.

Maneetes, H. and D. G. Linzell. 2003. Cross-Frame and Lateral Bracing Influence on Curved Steel Bridge Free Vibration Response. *Journal of Constructional Steel Research*, Vol. 59, No. 9, pp. 1101–1117.

McConell, J., M. Radovic, and K. Ambrose. 2014. *Cross-Frame Forces in Skewed Steel I-Girder Bridges: Field Measurements and Finite Element Analysis*. Center for Innovative Bridge Engineering, Delaware Center for Transportation, University of Delaware, Newark, DE.

Moorty, S. and C. W. Roeder. 1992. Temperature-Dependent Bridge Movements. *Journal of Structural Engineering*, Vol. 118, No. 4, pp. 1090–1105.

Nakai, H. and C. Hong Yoo. 1988. *Analysis and Design of Curved Steel Bridges*. McGraw-Hill, Inc., New York, NY.

Reynolds, J. C. 1972. Thermal Stresses and Movements in Bridges. MS thesis. University of Missouri-Rolla, MO.

Sharafbayani, M., and D. G. Linzell. 2014. Optimizing Horizontally Curved, Steel Bridge, Cross-Frame Arrangements to Enhance Construction Performance. *Journal of Bridge Engineering*, Vol. 19, No. 7.

U.S. Steel. 1984. Chapter 12 – V-Load Analysis. In *Highway Structures Design Handbook, Volume I*. United State Steel Corporation, Pittsburgh, PA.

White, D. W., D. Coletti, B. W. Chavel, A. Sanchez, C. Ozgur, J. M. J. Chong, R. T. Leon, R. D. Medlock, R. A. Cisneros, T. V. Galambos, J. M. Yadlosky, W. J. Gatti, and G. T. Kowatch. 2012a. *NCHRP Report 725: Guidelines for Analysis Methods and Construction Engineering of Curved and Skewed Steel Girder Bridges*. National Cooperative Highway Research Program, Washington, DC.

White, D., A. Sanchez, C. Ozgur, and J. M. J. Chong. 2012b. *NCHRP Project 12-79 Task 8 Report: Evaluation of Analytical Methods for Construction Engineering of Curved and Skewed Steel Girder Bridges*. National Cooperative Highway Research Program, Washington, DC.

Yoo, C. H. and P. C. Littrell. 1986. Cross-Bracing Effects in Curved Stringer Bridges. *Journal of Structural Engineering*, Vol. 112, No. 9, pp. 2127–2140.

THE INSTITUTE FOR TRANSPORTATION IS THE FOCAL POINT FOR TRANSPORTATION AT IOWA STATE UNIVERSITY.

InTrans centers and programs perform transportation research and provide technology transfer services for government agencies and private companies;

InTrans contributes to Iowa State University and the College of Engineering's educational programs for transportation students and provides K–12 outreach; and

InTrans conducts local, regional, and national transportation services and continuing education programs.

IOWA STATE UNIVERSITY

Visit **InTrans.iastate.edu** for color pdfs of this and other research reports.